Crystallization and Morphology of Poly(butylene succinate-*ran*-butylene azelate) Random Isodimorphic Copolymers

Idoia Arandia Ariño

PhD Thesis

Polymer Science and Technology Department,

Donostia, 2018

eman ta zabal zazu

Universidad del País Vasco

Euskal Herriko Unibertsitatea

Crystallization and Morphology of Poly(butylene succinate-*ran*-butylene azelate) Random Isodimorphic Copolymers

by

Idoia Arandia Ariño

Advisors

Prof. Alejandro Jesús Müller Sánchez

and

Prof. Agurtzane Mugica Iztueta

Polymer Science and Technology Department,

Donostia, 2018

I would like to acknowledge the fellowship from the University of the Basque Country UPV/EHU.

Index

Chapter 5

Chapter 6

Chapter 7

Chapter 8

Summary

List of abbreviations

AFM	Atomic force microscopy
Cp	Heat capacity
DI	Domain I
DII	Domain II
DIII	Domain III
DSC	Differential scanning calorimetry
FTIR	Infrared spectroscopy
G	Isothermal spherulite growth rate
K	Overall crystallization rate constant
M_n	Number average molecular weight
M_w	Weight average molecular weight
PBAz	Poly(butylene azelate)
PBS	Poly(butylene succinate)
PBS-*ran*-PBAz	Poly(butylene succinate-*ran*- butylene azelate)
PCL	(Poly(ε-caprolactone)
PE	Polyethylene
PET	Polyethyleneterephthalate
PLLA	Poly(L-lactide)
PLOM	Polarized light optical microscopy
PP	Polypropylene
SAXS	Small angle X-ray scattering
SEM	Scanning electron microscopy
SN	Self-nucleation
SSA	Successive self-nucleation and annealing
T_c	Crystallization temperature
TEM	Transmission electron microscopy

T_g	Glass transition temperature
TGA	Thermogravimetry analysis
T_m	Melting temperature
T_s	Self-nucleation temperature
WAXS	Wide angle X-ray scattering
wt%	Weight percentage
$1/\tau_{50\%}$	Inverse of the half of the crystallization time
ΔG	Free energy barrier
ΔH_c	Crystallization enthalpy
ΔH_m	Melting enthalpy
ΔT	Supercooling
n	Avrami index
t_0	Induction time for the beginning of the crystallization
$\tau_{1/2}$	Time needed to achieve 50% of the overall crystallization
X_c	Crystallinity degree

Chapter 1

General Introduction and Objectives

1.1 Introduction

With the aim of reducing the dependence on oil, avoiding plastic waste accumulation and taking into account the large increase in single use plastics in many areas like packaging, the development of new greener alternatives have intensified. The objective of these alternatives is to use materials that cover all the needs according to the application required, and at the same time may suffer degradation by environmental stimuli after their useful life, such as bioplastics.[1, 2]

The term bioplastic is used for those plastics that are biobased, biodegradable, or both, and they are commonly differentiated in three main groups. Biobased or partially biobased non-biodegradable plastics such as biobased PE, PP, or PET, plastics that are both biobased and biodegradable, such as PLA and PHA or PBS, and plastics that are based on fossil resources and are biodegradable, such as PBAT.[3]

Among these group, the family of aliphatic polyesters is one of the most attractive because of their biodegradability and biocompatibility. They have attracted considerable attention and numerous research works have been published dealing with biodegradable aliphatic polyesters.[4-6] Unfortunately, these kinds of biopolymers do not usually fulfill all the mechanical requirements needed and they are also characterized by a high crystallinity which limits their biodegradation rate. Therefore, in order to tailor these properties, the synthesis of random copolyesters with bio-based comonomers has been done to obtain versatile random copolymers. Copolymerization has been used to limit their degree of crystallization and improve their physical properties to extend their applications in the biodegradable polymer market. Additionally, some works showed that through the variation of the copolymer composition thermal properties could be controlled without significant loss of crystalline properties.

Several random copolyesters, such as poly(butylene succinate-*ran*-hexamethylene succinate),[7] poly(butylene succinate-*ran*-adipate),[8, 9] poly(butylene succinate-*ran*-

diethylene glycol succinate),[10] poly(butylene succinate-*ran*-butylene fumarate),[11] poly(butylene succinate-*ran*-ethylene succinate),[12, 13] poly(butylene succinate-*ran*-propylene succinate)[15] and poly(butylene succinate-*ran*-butylene azelate)[14, 15] have been synthesized and studied obtaining promising results for the future of green polymers.

Therefore, the study of the crystallization behavior of random copolymers is very important because of its strong correlation with biodegradation rates, mechanical properties and applications.[16, 17] For this purpose, the research project entitled: Crystallization and Morphology of Poly(butylene succinate-*ran*-butylene azelate) Random Isodimorphic Copolymers, has been developed in the University of the Basque Country (UPV / EHU) in the Polymer Science and Technology department of the Chemistry Faculty.

1.2 Objectives

This work is focused on the study of crystallization and morphology of poly(butylene succinate-*ran*-butylene azelate) random isodimorphic copolymers. For that next specific objectives are followed:

- Study the nonisothermal and isothermal crystallization by Differential Scanning Calorimetry (DSC).
- Study the crystallization structure by wide angle X-ray scattering (WAXS) and small angle X-ray scattering (SAXS).
- Study the isodimorphic behavior of copolymers by analyzing the experimental diffraction spacings (*d*) and lamellar thicknesses by WAXS and SAXS techniques.
- Analyze the crystallization morphology of copolymers by polarized light optical microscopy (PLOM), and atomic force microscopy (AFM) techniques.
- Perform detailed isothermal studies of the nucleation kinetics, spherulitic growth rates and overall crystallization kinetics by DSC and PLOM techniques.
- Perform self-nucleation and successive self-nucleation and annealing (SSA) studies.

- Study the complex development of the amorphous phase, especially at compositions around the eutectic point by broadband dielectric spectroscopy (BDS).

1.3 Structure

This PhD work has been reported in eight chapters. In Chapter 1 a general introduction is given and the research objectives presented. After that, a general scheme of how the work is organized, the background and bibliographical review of most significant results about polyesters and more exactly about isodimorphism are shown.

In Chapter 2, in order to better understand the present research the main crystallization theories are showed in relation to the morphology and crystallization kinetics.

In Chapter 3, the homopolymers and copolymers used in this work are presented, as well as a brief explanation of their synthesis. Furthermore, the main experimental techniques and the conditions used are also included.

All results obtained are presented in the following four independent chapters; Chapters 4, 5, 6 and 7. In the chapter 4, the structure, non-isothermal crystallization and morphology of the PBS-*ran*-PBAz copolymers previously synthesized by Mincheva et al.[18] are studied. For this purpose, DSC, WAXS and SAXS techniques have been used and the obtained results correlated with those obtained from PLOM and AFM.

In chapter 5, self-nucleation and SSA techniques have been used to corroborate the isodimorphic behavior due to these techniques promote segregation of molecular defects that interrupt crystallizable sequences.

Chapter 6 shows the dielectric spectroscopy measurements in PBS-*ran*-PBAz copolymers. As well as the rate dependence crystallization studies employing combined DSC and Dielectric spectroscopy techniques.

Chapter 7 shows the detailed isothermal studies of the nucleation kinetics, spherulitic growth rates and overall crystallization kinetics studied by DSC and PLOM techniques.

Finally, Chapter 8 presents the general conclusions reached after the development of the present investigation. And in this chapter we also include the scientific articles published in correlation with this PhD work.

1.4 Background

This Ph.D. thesis is focused on the study of Poly(butylene succinate-*ran*-butylene azelate) (PBAz) random isodimorphic copolyesters, therefore in this bibliographical review most significant results about polyesters and more exactly about isodimorphism are shown in relation to the work that has been done.

1.4.1 Bioplastics

From the first synthetic polymers, such as Bakelite, which were discovered at the beginning of the twentieth century, the study of new polymer varieties, as well as new techniques for their synthesis and processing has never stopped. Currently, plastics have managed to occupy an important place in all aspects of our daily life, as well as in industry,[19] in addition, it is estimated that the consumption of polymers increases approximately 4% every year.[20]

However, the raw material from which the vast majority of commercialized plastics are obtained is the crude oil. Even though oil does not come from a renewable source, the biggest problem of most plastics derived from the petrochemical industry is their resistance to degradation by microorganisms which are in the environment.[21] The lack of degradability is considered a very advantageous property for some applications such as construction or automotive, but at same time it contributes to the accumulation of undesirable plastic waste which not only are found in landfills or any other waste management facilities, but also in all types of environments. Among the urban solid waste, the most common polymers are those obtained from petroleum, Polypropylene (PP) and Polyethylene (PE) already represent 60% of the waste, nearly followed by Polystyrene (PS) and Polyvinyl Chloride (PVC).[20] Therefore, due to these disadvantages with traditional polymers, considerable efforts have been made in the last decades in search of alternative ma-

terials which can be synthesized from renewable sources, or that can easily be degraded in the environment or in the best cases, polymers that are both biobased and biodegradable.[19]

Since the 1970s, the search for biopolymers has been ongoing. They are obtained from different sources such as vegetable fats and oils, corn starch, straw, wood chips, and food waste. The most common biobased polymers among others are Poly(lactic acid) (PLA), Polyhydroxybutyrate (PHB), cellulose derivatives (CA, CAB) and starch derivatives. Biodegradability studies have also been carried out in polymers which are not necessarily obtained from renewable sources. This means that biodegradability depends on the chemical structure of the polymer and not on the raw material. Examples of biodegradable polymers are the Poly(lactic acids) (PLA), polyhydroxyalkanoate (PHA), cellulose derivatives, starch and also polybutylene adipate-terephthalate (PBAT) and Polybutylene succinate (PBS) or Poly(ε-caprolactone) which can be obtained from petroleum and from biomass.[22]

Most of biodegradable polymers belong to the group of polyesters, due to the ester bond, which can be easily hydrolyzed by microbial enzymes. Polyesters are normally synthesized from a reaction of a diol chemical compound and one or more dicarboxylic acids group. The diol groups used may be based on renewable resources. In the case of the acid group they can also come from renewable sources such as succinic or adipic acid, or even come from the petrochemical industry such as terephthalic acid or dimethyl terephthalate (DMT). [23, 24]

1.4.2 Polyesters

Polyesters are defined as polymers containing at least one ester linking group per repeating unit (-COO-). They can be obtained by a wide range of reactions but the most important one, as explained before, is the polyesterification between dibasic acids and diols or their derivatives (see Figure 1.1). Especially the aliphatic ones are the most extensively studied class of polyesters.[25]

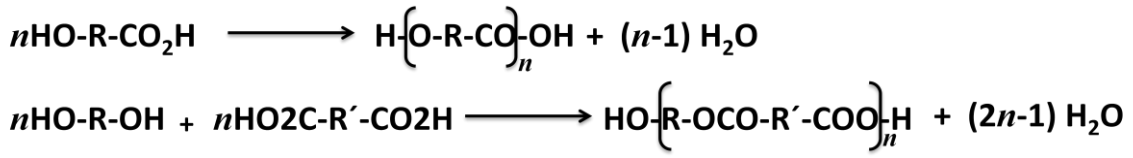

Figure 1. 1 *Polyesterification reactions.*

Polyesters were first developed in the years 1939-1941 by British chemists at Calico Printers Association, Ltd., based on the work of W.H. Carothers in 1926. After that DuPont bought the rights in 1946 to produce polyester fibers in the United States, and by 1951 DuPont begun to market the fiber under the name Dacron. Polyesters are nowadays one of the most important classes of polymers in use; there are hundreds of polyesters due to the large number of combinations of diols and diacids, although only a few are of commercial importance.[25]

They can be classified into two groups according to the bonding of the constituent monomers.

- The first group consists of the poly(hydroxyl acid)s, which are polyesters synthesized from hydroxyl acids (hydroxyl-carboxylic acids), HO-R-COOH, or by ring-opening polymerization of cyclic monomers, –R-COO-. The most common poly(hydroxyl acid)s are Poly(lactic acid) (PLA), Polyglycolide (PGA), the Polyhyroxyalkanoates (PHAs), Polyhydroxybutyrate (PHB) and Poly(ε-caprolactone) (PCL).
- The second group consist of the poly(alkylene dicarboxylate)s. These are prepared by polycondensation of diols and dicarboxylic acids. They are also classified into two groups: aliphatic polyesters such as Poly(ethylene succinate) (PES) and Poly(butylene succinate) (PBS), Poly(butylene adipate) (PBA), Poly(propylene fumarate) (PPF) and polyesters containing aromatic units such as Poly(ethylene terephtalate) PET, Poly(buthylene terephtalate) PBT and Poly(ethylene furanoate) (PEF).

In general, aliphatic polyesters have relatively poor mechanical and thermal properties and the applicability of this type of polymer is sometimes limited. On the contrary,

polyesters with aromatic units have better physical and mechanical properties, but they are so resistant to the attack of bacteria and fungi under environmental conditions that they have a very low biodegradation rate. For those reasons, the use of polymer combinations and their study has become important in order to compensate the low properties and obtain materials with improved behavior as compared to pure homopolymers. Many of these polyesters are also mixed in different proportions with another class of polymers, or with other polyesters in order to reduce the cost of the final product, produce plastics with modified properties or increase their biodegradability. As an example among them, aliphatic / aromatic copolymers which are designed to combine the biodegradability of the aliphatic unit with the beneficial physical properties of the aromatic unit have attracted increasing interest.[5, 26] In this case, the properties and biodegradable behavior depends on the proportion of the polyesters, obtaining a lower rate of degradation with a higher fraction of the aromatic polyester.

1.4.2.1 Aliphatic Polyesters

As both polymers used in this work, aliphatic polyesters are known to be the most promising category of biodegradable polymers and environmentally benign materials. The properties of these type of polymers depend on the presence of branches in the aliphatic chain that produce changes in the chemical structure and influence the geometric regularity, polarity and mobility of the molecular chains. The aliphatic and cycloaliphatic polyesters are fairly resistant to the oxidation by the air or ozone under normal conditions, but are rapidly degraded by ammonia, hydrazine, hot alkaline solutions and primary or secondary amines, which divide the ester bond by forming hydroxyl groups and salts or amid derivatives of the carboxyl functionality. Theoretically they are also potentially degradable in the presence of water, which by hydrolysis causes the breaking of the ester bonds in the main chain.

The melting points of the linear aliphatic polyesters increase with the increase of the methylene / ester group ratio in the repeating unit. In addition, in has been reported that polyesters with an even number of methylene groups have higher melting points than those containing an odd number of methylene groups.[27] Due to their combination of low

melting point, solubility and limited hydrolytic stability, most aliphatic polyesters are not used as structural materials, but their low glass transition temperatures allow them to be used as plasticizers and as components in other polymers such as polyurethanes. Despite aliphatic polyesters are considered the most economical alternative between biodegradable polymers to replace the plastics currently used in packaging, bottles and others (PE, PET, PVC) in order to protect the environment, the widespread application of the aliphatic polyesters is limited by several physical drawbacks associated with the polymer, such as poor mechanical strength and low melting points. To overcome these limitations, studies have concentrated on the development of new materials. As explained before, polyesters have the advantage of being modified according to the user requirements. Their crystallinity degree, thermal transitions, mechanical strength, and degradation can be altered based on molecular weight, composition (when used in copolymers), or addition of substituents to the polymer backbones.[28]

Aliphatic polyesters are often blended with other resins to improve their processing and end use properties. For example, they can be blended with starch to lower cost and to increase the biodegradability. They are also used as the matrix resin for mostly unidirectional bio-composite materials. Often natural fibers like flax, hemp, jute, bamboo, elephant grass, and kenaf are used as reinforcing fibers. Thanks to the versatility they provide, they have been used in a wide variety of biomedical applications, such as drug delivery and tissue engineering.[29]

1.4.3 Poly(butylene succinate) (PBS)

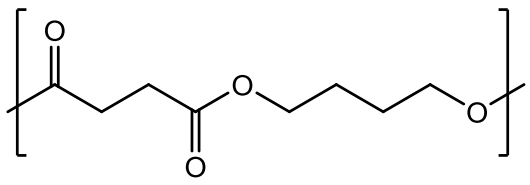

Figure 1. 2. *Chemical Structure of Poly(butylene succinate) (PBS).*

Poly (butylene succinate) (PBS) is an aliphatic polyester obtained from succinic acid and 1,4-butanediol. The synthesis of both monomers can be carried out from fossil-based or renewable resources; from fermentation of microorganisms on renewable feedstocks, such as glucose and starch.[30] It is also a promising biodegradable polyester because of its good mechanical properties that are comparable with those of such widely used polymers as low-density polyethylene and other polyolefins.[22, 31]

The glass transition temperature of this semycrystalline thermoplastic is remarkably low (being around -30 ºC), and the melting temperature is around 115ºC. With respect to its mechanical properties, it generally shows excellent mechanical and processability properties but not always a high enough biodegradability rate. The tensile yield strength of unoriented samples reaches up to 30-35 MPa, which is comparable to that of polypropylene. Additionally, PBS is flexible with Young's modulus in the range of 300–500 MPa depending on the degree of crystallinity.[32]

Through copolymerization with different types and different monomer contents the variation on physical properties and the rate of biodegradation of the PBS materials over a wide range is achieved. PBS has a wide temperature window for the processing of thermoplastics, which makes it suitable for extrusion, injection molding, thermoforming and film blowing. Among its applications PBS is usually used to produce fast food packages, bottles, supermarket bags, flushable hygiene products, mulch film and compost bags. In addition, PBS and PBS-based copolymers have been used in biomedical application,[33] most commonly in tissue engineering where these polymers have been employed in films[31, 34, 35] and as scaffolds.[36, 37] In some other cases, they have been also used as drug delivery systems.[38-40]

Although its production is based mainly on fossil resources, there are several companies (BASF, Myriant, Reverdia etc.) that are making great efforts to achieve the synthesis of PBS only from renewable sources. The objective is to reach a level of production that allows serving the large industrial demand with a material obtained entirely from green origin. PBS is commercially available since 1993 and is now produced under the trade name BionolleTM by Showa-Denko[41] and by Mitsubishi Chemical Corporation under the trade name GS PlaTM.[42]

The synthesis of PBS can be performed by a two-stage polycondensation reaction: the first one, esterification at atmospheric pressure of succinic acid with1,4-butanediol (BD) or transesterification of dimethyl succinate with BD to obtain oligomers. And the second one, polycondensation at reduced pressure of the oligomers removing BD to form high-molecular weight PBS (Figure 1.3). Different catalysts are traditionally employed for the synthesis of PBS, one of the most common is the titanium(IV) butoxide (TBT). Other types of catalysts such as organometallic or metal-oxide compounds were also tested and the results obtained reported by Jacquel et al.[43]

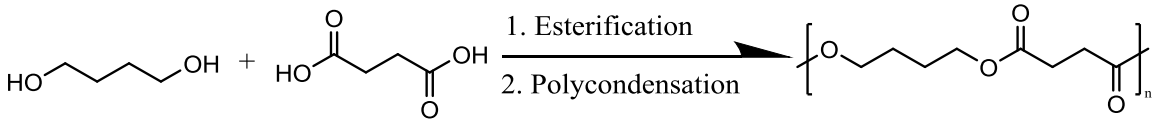

Figure 1. 3. *Chemical synthesis of PBS by means of a two-stage process: esterification of succinic acid with 1,4-butanediol or transesterification of dimethyl succinate with 1,4-butanediol.*

The semicrystalline PBS is a polymorphic material that depending on the conditions of preparation can crystallize in two different ways. Two polymorphs, i.e., α and β form, have been reported for PBS.[44] Under the usual conditions such as cooling from the melt or solution crystallization, the common modification, α form, is produced. Ichikawa et al.[45] proposed a monoclinic unit cell with dimensions (a = 0.523 nm, b = 0.912 nm, c = 1.090 nm, and β= 123.9°). The most intense reflections for PBS appeared at Bragg distances of 0.452, 0.404, and 0.392 nm, and they can be indexed to (020), (021) and (110) planes, (Figure 1.4(a)).

The β form of PBS, obtained by the stretching of the conventional α form crystals, was also reported by Ichikawa et al.[46] This β-form is characterized by chains in an all-*trans* conformation packed in a monoclinic unit cell with lattice dimensions of a = 0.584 nm, b = 0.832 nm, c (fiber axis) = 1.186 nm, and β=131.6◦, according to a space group of $P2_1/n$, Figure 1.4(b). The difference between the fiber repeat periods of the α- and β-form crystals are mainly attributed to the conformational difference of the tetramethylene units.

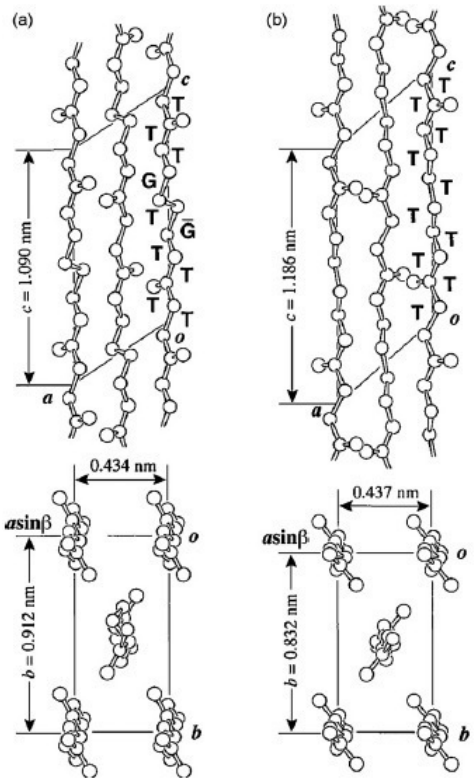

Figure 1. 4 *Crystal structures of PBS (a) α- and (b) β-form on the a´−b (bottom) and b–c (top) base planes. All hydrogen atoms are omitted. (From reference[45]).*

As explained before the PBS-based copolymers have been prepared in order to modify the PBS properties such as thermal and mechanical behavior or biodegradability rate. The two main synthetic strategies adopted to obtain PBS-based copolymers are copolycondensation and reactive blending.

By copolycondensation the synthesis of random copolymers is obtained where different comonomeric units have been introduced along the PBS macromolecular chain. Typical examples include: another aliphatic polyester Poly(butylene adipate) PBA which has been widely estudied,[8, 9, 32, 34, 47, 48] an aromatic polyester Poly(butylene terephtalate) PBT and quite recently a novel polyester Poly(neopenthyl succinate) PNS.

Xu and Guo[32] reported the physical properties of poly(butylene succinate-co-butylene adipate) (PBSA) copolyesters which varied with comonomer content. Results showed an interesting behavior when PBSA compositions with between 5 and 15 mol percent of BA content possessed a higher crystallinity degree and tensile strength than

PBS homopolymer. The biodegradation rate of PBSA film was also improved with the increase of BA content from 0 to 20 mol%. This could be due to the cocrystallization of BA units in the crystal lattice of PBS. These results are in good agreement with other examples of random copolymers[15], whose crystallinity does not decrease with the minor comonomer content. There are other examples of systems where this does not happen,[9] as even with smaller comonomer contents the crystallinity degree decreases.

Nagata et al.[49] and Guo et al.[26] also copolymerized succinic acid with terephthalic acid to produce the aliphatic/aromatic polyester poly(butylene succinate-co-butylene terephthalate) (PBST). In this case, as much comonomer content both melting point and crystallinity degree decreased showing the lowest values at 30–40 mol% of butylene terephthalate (BT) units. The tensile strength and elongation at break of PBST depended on the degree of crystallinity (X_c), since PBST with highest X_c demonstrated higher tensile strength and lower elongation at break. In this case, the biodegradation of samples did not improve and the increase in aromatic comonomer content made the biodegradation rate slower.

Guidotti et al.[50] have recently synthesized novel random PBS-based copolymers containing aliphatic side chains in order to obtain sustainable flexible food packaging. In this work Poly(butylene/2-butyl,2-ethyl-propylene succinate) ($P(BS_mBEPS_n)$) and Poly(butylene/neopenthyl succinate) ($P(BS_{70}NS_{30})$) random copolymers were prepared. Results showed that the presence of the side alkyl groups did not alter the thermal stability, whereas it significantly reduced the sample crystallinity degree, making these materials more flexible. The barrier performances to O_2, CO_2 and N_2 gases were also evaluated, envisioning for these new materials an application in food packaging and were found to be worse than in PBS homopolymer. However, some of them were comparable to or even better than those of Low Density Polyethylene (LDPE), widely employed for flexible food packaging.

On the other hand, by reactive blending, it has been possible to obtain multiblock copolymers with different block lengths by simply varying the mixing time. To this purpose, PBS has been copolymerised with other aliphatic polyesters such as Poly(lactic acid) (PLA). PLA is usually obtained in the amorphous state after being processed, and due

to its slow crystallization rate in comparison to the cooling rates employed during processing; the use of PLA in some applications is limited. In order to enhance the physical properties of PLA, PLA and PBS multi-blocks within the PLA-mb-PBS copolymers were prepared by D'Ambrosio et al.[51] According to their results PBS had a dilution effect on PLA blocks, increasing the PLA chain mobility, thus lowering the crystallization and melting temperature and increasing the undercooling during isothermal crystallization. The decrease of both the melting temperature and the crystallinity degree with PBS content, indicated that the PBS blocks perturb the PLA blocks stereocomplexation. However, the PBS blocks could retard or increase the crystallization kinetics, depending on the PBS amount in the blend.

Other authors realized PBS-based composites by blending the polyester with organic materials like collagen[40] and chestnut fibres (CSF)[52] or inorganic ones such as calcium phosphate,[53] fluoroapatite[54] and hydroxyapatite (HA),[55, 56] where a decrease in the melting point and a slight increase of the crystallinity were observed for PBS blend. Grigoriadou et al.[57] prepared PBS composites containing silica nanotubes or strontium hydroxyapatite nanorods. And in this case melting point did not decrease with the addition of a small amount of nanofiller, in the contrary, crystallinity degree increased due to the nanoparticles acted as nucleating agents.

1.4.4 Poly(butylene azelate) PBAz

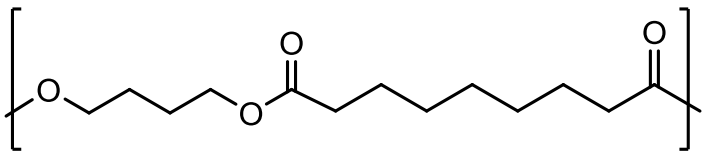

Figure 1. 5. *Chemical Structure of Poly(butylene azelate) (PBAz).*

Poly (butylene azelate) (PBAz) is an aliphatic polyester obtained from azelaic acid and 1,4-butanediol. Azelaic acid is industrially produced from the oxidation of oleic acid through ozonolysis,[58] and can be directly extracted from barley, rye, sorghum, or wheat through an adequate biocatalysis-based process.[59]

Polyesters based on azelaic acid had not been studied till recently. Papageorgiu et al.[60] analyzed the crystallization and enzymatic degradation of poly(butylene azelate) in comparison with poly(ethylene azelate) (PEAz) and poly(propylene azelate) (PPAz) wich were synthesized by the two-stage melt polycondensation method.

The glass transition temperature of this semycrystalline thermoplastic is lower than the T_g of PBS (being around -63 ºC), and the melting temperature is around 41ºC.

In the case of PBAz, the crystalline unit cell had not been reported in the literature. Diaz et al.[61] reported that fiber patterns from the melt drawn homopolymer were consistent with an orthorhombic unit cell with the following dimensions: a = 0.496 nm, b = 0.746 nm, and c = 3.65 nm. Following these results the most intense reflections (at 0.416 and 0.377 nm) for PBAz were indexed as (110) and (020) planes.

1.4.5 Random isodimorphic copolymers

As explained before, copolymers are versatile materials that have been attracting academic and industrial interest for decades. There are several types of copolymers including block, graft and random amongst others.[62] Specially random copolymerization is a simple synthetic method of combining the properties of two distinct homopolymers. It provides random covalent links between different comonomers, therefore ensuring in most cases total melt miscibility, a fact that sets random copolymers apart from the typical immiscible polymer blends. Their thermal and mechanical properties can be tailored by changing the composition of the copolymer.

Random copolymers constituted by two crystallizable units may show different crystallization behavior depending on their miscibility and ability to share crystal lattices.[44, 63, 64] Provided that the two crystallizable repeating units meet strict molecular requirements, the copolymers can crystallize in the same crystal lattice, in the entire composition range. In other words, the two comonomeric units along the chain can cocrystallize regardless of the composition. Therefore, the two comonomers can be considered totally miscible in the crystalline state, and total inclusion of comonomers in a single

crystal lattice or isomorphic behavior occurs. Figure 1.6 shows a scheme of the comonomer unit arrangement inside one lamella for the isomorphic case. Thermal and structural properties, such as melting temperatures and lattice parameters, typically show linear dependence on composition as it is shown in Figure 1.9 with blue triangles.

The concept of isomorphism in the polymer field was first considered by Natta et al.[65] The requirements to observe macromolecular isomorphism in random copolymers have been summarized by Allegra and Bassi,[63] who highlighted that: (i) the different monomer units must have approximately the same shape, occupy the same volume, and acquire a compatible chain conformation, (ii) the crystalline phase of "parent homopolymers" should be analogous in chain conformation, lattice symmetry and dimensions, (iv) the comonomers must be miscible in the melt (v) and the two homopolymer must have similar rates of crystallization. As a result, a total inclusion of both comonomers in the crystalline lattice occurs, and the composition of the crystal perfectly reflects the one of the polymer chain. Because of the specific conditions to be met, only four random copolyesters have been reported to exhibit isomorphic crystallization: P(HG-*ran*-HA),[66] P(CL-*ran*-OPD),[67] P(CL-*ran*-PDL),[68] and P(BS-*ran*-SF).[11]

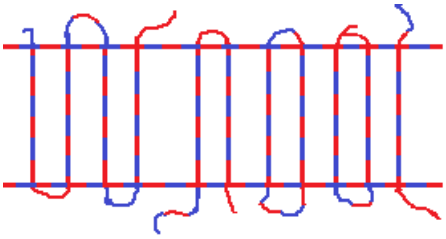

Figure 1. 6. *Scheme of the comonomer unit arrangement inside a lamellar crystal for the isomorphic case.*

The second case of cocrystallization in random copolymers, isodimorphism, occurs when the two homopolymers (A and B) do not share a common crystalline structure, but they still have similar repeating units so that two crystal structures depending on composition are formed (A-*ran*-B) constituted by the respective repeating units. A partial

inclusion of comonomer A in the unit cell of homopolymer B crystals is typically observed for copolymers with compositions rich in B units, and vice-versa. Figure 1.7 shows a scheme of the comonomer unit arrangements inside lamellae for the isodimorphic case. Comonomer inclusion is only partial, i.e., the concentration of comonomer A inside the B crystals can be lower than its exclusion to the amorphous phase. Since both comonomers can be hosted in the crystals of the majority component (comonomer A in the B crystals, and vice-versa), a pseudo-eutectic trend of the thermal properties (melting and crystallization temperatures, as well as their enthalpies) is obtained. Figure 1.9 shows (in red and green squares and circles) two examples of how these thermal properties could behave in this case.

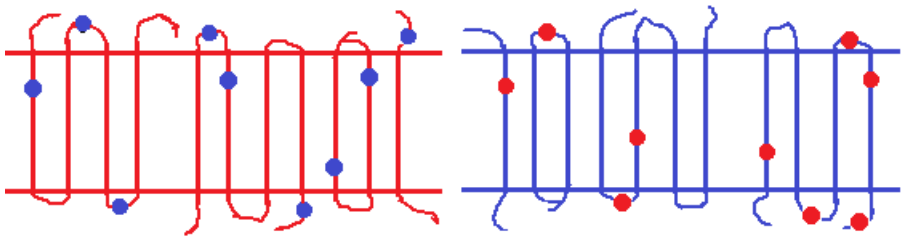

Figure 1. 7. *Scheme of the comonomer unit arrangement in lamellae for isodimorphism case.*

Isodimorphic copolymers are characterized by a homopolymer-A-rich crystalline phase on one side of the pseudo-eutectic region and a homopolymer-B-rich crystalline phase on the other side of the eutectic region. Furthermore, some copolymers can display double crystalline superstructural morphologies at the pseudo-eutectic region.

There are no general rules that can unambiguously predict if a copolymer will display isodimorphism or not. In fact, even in those cases where the comonomers have similar chemical structures and are miscible in the amorphous phase, the possibility of forming a mixed crystalline unit cell, or in other words the efficiency of comonomer inclusion, is not easily determined. In spite of this, some features affecting isodimorphic behavior have been highlighted in the literature. For instance, a homopolymer with a large unit cell is expected to include more easily a comonomer whose respective homopolymer presents a smaller unit cell.[69] Also, a comonomer with an even number of methylene groups in the repeating unit will most likely include similar even CH_2 comonomers in its unit cell, and exclude those with odd number of carbon atoms in their

chemical structure.[66, 70] These empirical rules, related to the miscibility of the comonomers in the crystalline state are not always strictly obeyed.

In Figure 1.9, two curves for the isodimorphic case are shown (cases (b) and (c)), representing different degrees of inclusion of the comonomers in the homopolymer crystal lattice. With a higher degree of inclusion, the crystallization/melting behavior deviates less from the isomorphic case (b). In contrast, when the comonomer units are largely excluded from the crystals, even though the copolymer may still able to crystallize in all compositions (c), the thermal response will be closer to that of a copolymer characterized by a complete rejection of the co-units to the amorphous phase (see Figure 1.9(d)).

The third behavior studied in random copolymers is the total exclusion of minor comonomer. When cocrystallization cannot occur and comonomer A is completely rejected from the crystalline structure of the major component (comonomer B), the transition temperatures and enthalpies are strongly depressed as the content of comonomer A increases in the random copolymer, and there exists a range of copolymer compositions where the copolymer remains completely amorphous. This case is shown in Figure 1.8 and an example of the thermal properties plotted as orange and pink stars in Figure 1.9. In those cases, 20 % of co-units randomly distributed along the chains is enough to completely inhibit the crystallization. A clear example of this behavior is given by statistical ethylene/1-octene or propene/1-octene synthesized with metallocene catalysts.[71, 72]

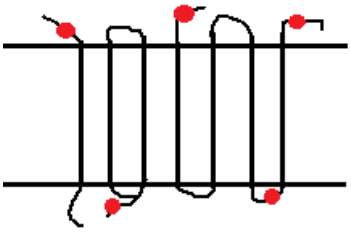

Figure 1. 8. *Scheme of the comonomer unit arrangement inside a lamella for the full exclusion case.*

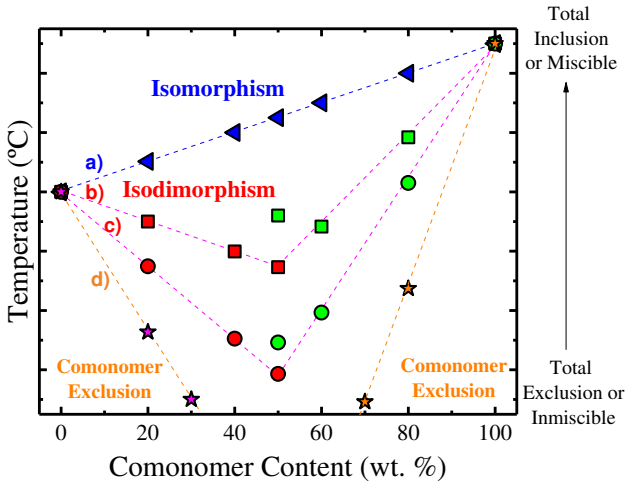

Figure 1. 9. *Melting (or crystallization) temperature as a function of comonomer content for different possible copolymers. From top to bottom four cases are represented: (a) isomorphic behavior, (b) isodimorphic behavior for copolymers with small amount of comonomer exclusion, (c) isodimorphic behavior with a large amount of comonomer exclusion, (d) copolymers with total exclusion of second comonomer.*

In this work, isodimorphism of PBSAz random copolymers has been studied in great detail. In the literature, other isodimorphic cases have also been studied in different copolyestres, most frequently in aliphatic copolyesters[9, 12, 13, 18, 47, 61, 66, 70, 73-89] and also in aromatic/aliphatic coplyesters.[48, 85, 90-97]

1.4.5.1 Characterization of isodimorphic copolymers

The isodimorphic character of random copolyesters is reflected in various aspects of their crystallization. On the one hand, isodimorphism studies have been focus on the pseudo-eutectic feature of the thermal transitions which can be analyzed by different Differential scanning calorimetry (DSC). On the other hand, it has been also studied the partial inclusion of the minority co-unit in the crystalline unit cell by techniques such as Wide and Small Angle X-Ray Scattering (WAXS/SAXS) and Infrared Spectroscopy (FT-IR). In addition, the experimental estimations of the equilibrium melting points have been compared with theoretical models which account for the effect of partial inclusion of the comonomer in the crystal on this thermodynamic value.

1.4.5.1.1 The pseudo-eutectic feature of the thermal transitions in isodimorphism

The isodimorphic behavior in random copolymers is clearly manifested in non-isothermal heating and cooling experiments, since the transition temperatures show a strong and characteristic dependence on copolymer composition. Despite being random, these copolymers can crystallize in the entire composition range. With the increase of minor comonomer concentration the melting point and crystallinity of the copolymers decreases, as it has been shown in Figure 1.9 part b. Therefore, despite the interruption of the comonomer sequences that crystallizes by the minor comonomer repeating units, major component phase can still crystallize in these copolymers, even when the content of comonomer is as high as 40-60 %. This indicates that co-crystallization (or minor comonomer inclusion within the major crystal phase) of the two comonomers in the same crystal lattice is possible to some extent.

The pseudo-eutectic behavior of isodimorphic polymers is manifested by a decrease in the transition temperatures with composition departing from those of the two homopolyesters, until a minimum value is reached. The comonomer concentration at which this minimum is found is generally located around the equimolar composition,[79, 80] however, some systems show pseudo-eutectic points in significantly different concentration intervals (e.g., 60:40, 80:20).[9, 15, 66, 74, 76, 82, 97, 98] For instance, in poly (hexamethylene dicarboxilate) copolymers the eutectic composition shifts from a co-unit concentration of 50 to 20 %, with increasing the length of aliphatic diacids from 4 to 8 CH_2 units.[74] In most studies,[9, 15, 66, 74, 80, 97] the minimum of crystallization/melting temperature is located at compositions shifted towards higher contents of the comonomer whose respective homopolyester has a lower melting point.

1.4.5.1.2 Study of co-units cocrystallization by Wide Angle X-ray Scattering (WAXS)

In many cases,[12, 66, 70, 76, 79, 80, 82, 97, 99-101] the partial inclusion of the minor comonomer into the crystalline structure of the major component of a random copolymer has been revealed by X-ray diffraction. As explained before, in isodimorphic materials WAXS results usually show that all compositions contain only one type of crystal. On one side of the pseudo-eutectic point, the samples only display reflections that are consistent with the type of unit cell of the phase which crystallized in this case. And in the other side, the samples only display reflections that are consistent with the type of unit cell of the phase which crystallized in the other case. The WAXS analysis can also reveal the (partial) inclusion of a co-unit in a given structure. Indeed, when the crystal hosts a repeating unit different from that which constitutes the homopolymer, several different situations can arise, depending on the specific crystallographic features of the considered systems. In particular, upon inclusion of a comonomer, a crystalline unit cell can: a) increase in size to accommodate the bulkier co-unit; b) shrink in certain directions, as a result of a lower volume occupied by the defect; c) remain unchanged in size.

Yu et al.[66] reported both increasing and decreasing crystal lattice size studying the case of poly (hexamethylene dicarboxilate) copolyesters, where the chain length of the aliphatic diacid was varied. In WAXS results little or no variations in the spacings was observed when comonomers with lower number of methylene units were included in the crystals of the homopolymer with longer aliphatic sequences, i.e., as in the case of glutaric acid substituting pimelic acid (3 and 5 methylene units, respectively), Figure 1.10a, or pimelic acid (5 methylene) copolymerized with azelaic acid (7 CH_2), Figure 1.10b. On the other hand, accommodating a diacid with higher number of CH_2 in the unit cell of a polyester with a shorter diacid led to both an increase or decrease in the distance between a given family of planes (P(HG-*ran*-HP) and P(HP-*ran*-HAz) plotted in Figure 1.10a and b, respectively). The difference may depend on the details of the specific structure, i.e., on the volume occupied by the co-unit in the acquired conformation along the considered crystallographic direction.

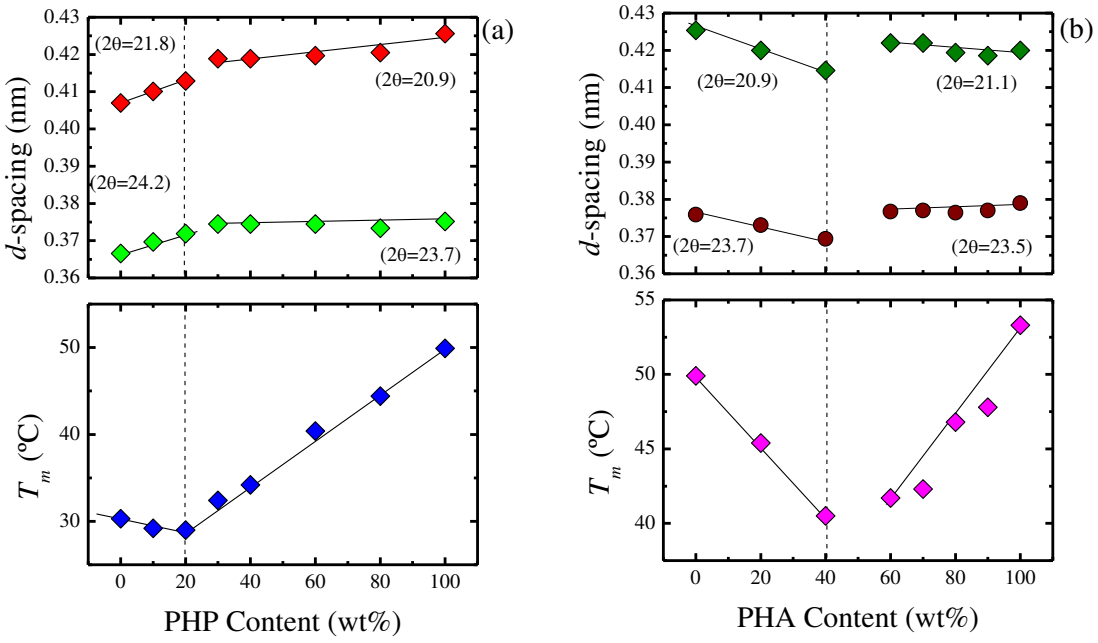

Figure 1. 10 *d-spacings values of characteristic planes and T_m as a function of (co)monomer content of (a) poly (hexamethylene glutarate-co-hexamethylene pimelate) P(HG-co-HP) and (b) poly (hexamethylene pimelate-co-hexamethylene azelate) P(HP-co-HAz) . (From reference [66])*

1.4.5.1.3 Study of co-units cocrystallization by FT infrared spectroscopy (FT-IR)

A more direct evidence of co-crystallization of the co-units can be obtained by FT infrared spectroscopy (FT-IR). Inoue et al. [76, 79, 80] and Li et al.[75, 77] studied the crystallization behavior of several aliphatic random copolyesters with this technique. In those works, some IR absorption bands were assigned specifically to a given co-unit in the crystalline state of the isodimorphic copolymers. The intensities of these characteristic bands of both comonomers simultaneously increased with time during crystallization and decreased with temperature upon melting. This result proved the co-existence of the two units in the crystalline lattice of the different homopolymers. Furthermore, by applying Lambert-Beer's law Inoue et al.[76] and Swinehart et al. [102] estimated the content of co-unit included in the crystals.

1.4.5.1.4 Study of co-units cocrystallization by comparing the equilibrium melting point with theoretical exclusion-inclusion models

Some works[12, 66, 70, 74, 78, 97, 99, 103] have reported an indirect way to derive information on the partitioning of co-units between the crystalline and amorphous phase by comparing the experimental estimations of the equilibrium melting points with theoretical exclusion-inclusion models[64], which account for the effect of partial inclusion of the comonomer in the crystal on this thermodynamic value. With these equations also percentage of the minor comonomer units which were practically incorporated in the crystals are also estimated.

When minor comonomer units were totally rejected from the crystal into the amorphous phase, Flory [104, 105] and Baur [106] exclusion models could be applied. In comonomer inclusion two models were used in order to analyze the partial inclusion of the comonomer B in crystals of the A repeating unit; the Sanchez and Eby model,[107, 108] and the Wendling and Suter theory.[109, 110] The latter provided the best fit for the experimental results using as fitting parameter the defect free energy (ε),[109-111] and from this equation information about which comonomer incorporates easier was also obtained by calculating the value of (ε). In addition, percentages of the minor comonomer units which incorporate in the crystals were also estimated.

Jeong et al.[99] studied the poly(butylene terephthalate-*ran*-butylene 2,6-naphthalate) (P(BT-*ran*-BN)) copolymer. When the defect free energy was calculated by using the Wendling and Suter equilibrium inclusion model, the defect free energy in the case of incorporation of BN units in the PBT type crystal was higher than in the opposite case, concluding that the incorporation of bulkier BN units in the PBT type crystal was more sterically hindered than the opposite case. The percentage of inclusion was bigger when introducing PBT units in PBN crystals than in the opposite case and that in both respective PBT and PBN crystal structure, the comonomer concentration in cocrystals increased with increasing the comonomer composition in bulk. However, in both cases, the comonomer concentration in each crystal was lower than the copolymer concentration in

a total inclusion model suggesting that a fraction of the comonomer unit was rejected in the amorphous phase.

Yu et al.[74] analyzed different random aliphatic copolyesters derived from 1,6-hexanediol with different diacids with chain length of 4, 6, 8 and 10 to investigate the effect of chain length of aliphatic diacids on miscibility and competition of cocrystallization behavior. By quantifying the defect free energy parameter (ε) calculated from Wendling-Suter method, they concluded that when HS unit (hexamethylene succinate) incorporated into the crystal type of the different chain length diacids, the one with longer chain length had better miscibility with the inserted HS unit. Furthermore, the comonomer concentration in crystal increased not lineally with the comonomer content, deducing that it was easier to create the excess volume necessary for a comonomer unit in an already imperfect crystal lattice.

1.4.5.2 Other studies in isodimorphic copolymers

1.4.5.2.1 Isothermal study in isodimorphic copolymers

For isodimorphic random copolyesters there are several literature reports dealing with DSC isothermal crystallization kinetics, however, they typically cover a limited range of compositions, i.e., close to the major components [14, 83, 85, 99]. This limitation is related to the widely different crystallization temperature range or kinetics observed when changing from one type of crystalline phase to the other.

In all reported cases the crystallization rate, expressed as the reciprocal of the half-crystallization time ($1/\tau_{50\%}$), decreases with increasing T_c, a common trend in the temperature range close to the melting point of the sample, where crystallization is dominated by nucleation control (in this case both primary and secondary nucleation, as the experiments are performed by DSC). In addition, due to the differences in T_c of the different compositions of the same system, the half-crystallization times curves shifts to lower temperatures as the second comonomer is incorporated in the copolymers, indicating a large change in supercooling. This behavior is attributed to a diluting effect of the comonomer, which is preferentially not included in the crystals, and to the decrease of the equilibrium melting point with increasing comonomer content. Secondary nucleation constants were also cal-

culated by these studies, and results showed that the value increased with the comonomer content.

1.4.5.2.2 Rate dependence calorimetric data

In the majority of reported works about isodimorphic systems only a single melting point was found for all compositions which belonged to each rich phase. Only in some few cases in compositions near the pseudo-eutectic point two crystalline phases could be found. Rate-dependent experiments provided an efficient strategy to detect the formation of two co-existing crystalline phases around the pseudo-eutectic point, and also managed to facilitate the crystallization of one of the rich phases making more hindering the crystallization of the other.

Diaz et al.[14] applied different cooling rates (followed by heating at a constant heating rate) in order to generate different thermal histories. They found that at a very slow cooling rate of 5 ºC/min, the crystallization of the phase which crystallized at lower temperatures was inhibited. During subsequent heating, both rich phases could crystallize, and at faster cooling rates the phase which crystallized at lower temperature could also crystallize more, but they never found a cooling rate at which the rich phase that crystallized at higher temperatures could be inhibited. In another reported case, Pérez-Camargo et al.[9] found that at a very high cooling rate of 50 ºC/min, it was possible to inhibit the crystallization of both phases. And when the copolymer was cooled at a very slow rate (i.e., at 1 °C/min), only the phase which crystallizes at higher temperature is able to crystallize as in the case of Diaz et al.

1.4.5.2.3 Mechanical and degradation studies

As explained at the beginning of this bibliography part, one of the most important reasons why copolymerization has been carried out was in order to improve some properties of its parent homopolymers. Therefore several works have studied the impact of copolymerization on mechanical properties.[12, 48, 70, 78, 91, 93, 98] On the other hand, as many of the studied polyesters tend to crystallize very quickly, as a consequence they show very low degradation rates. With the help of copolymerization this problem has been tried to solve and many studies on degradation such as biodegradation, hydrolytic and enzymatic

degradation have been reported.[12, 13, 47, 61, 70, 81, 83, 86, 89, 91, 94-96] Furthermore, studies of biocompatibility have been done obtaining promising results focused on biomedical chemistry.[70]

Tan et al.[78] synthetized and analyzed the poly(butylene succinate-co-hexamethylene succinate) (P(BS-co-HS)) copolyesters. When they studied the mechanical properties of the copolymers, results showed that the incorporation of HS altered the tensile failure mechanism from brittle failure for neat PBS to ductile for P(BS-co-HS) copolyesters with HS content higher than 30 mol%. Young's modulus and yield stress show a compositional dependence of both, decreasing as the composition becomes more equimolar. By contrast, the elongation at break increases with increasing comonomer content. In this system, copolymerization provided a tunable solubility, thermal and mechanical properties of the copolymers, making them an attractive option for a wide range of applications in biodegradable packaging and coatings.

Papageorgiou et al.[12] also studied the mechanical properties of a random copolymer, poly(butylene-*ran*-propylene succinate) (PBPSu). Results showed that there was a direct dependence of the mechanical properties on the copolymer composition, and that with the amount of BSu units increased in the copolymers the tensile strength at break as well as the Young's modulus increased. On the other hand, since PPSu is a soft material, tensile properties decreased with increasing propylene succinate (PSu) content and at high PSu amounts the tensile strength and Young's modulus were very low and almost identical to those of the neat PPSu.

In another work Papageorgiou et al.[91] analyzed aromatic/aliphatic poly(propylene terephthalate-*co*-succinate) (PPTSu) random copolyesters of high molecular weight. Neat PPSu showed fast biodegradation rates, however by the introduction of terephthalate units in the macromolecular chains of the aliphatic polyester PPSu, a decrease of the biodegradation rates of the PPTSu copolymers resulted. Although copolymers with up to 60 mol% terephthalate content showed significant biodegradation rates, copolymers with more than 70 mol % terephthalate units and PPT practically did not hydrolyze. In conclusion, by the

increasing of the terephthalate content in this copolymer hydrolytic degradation rates could be limited.

Hong et al.[86] reported the copolymerization of γ-butyrolactone (γ-BL) with ε-caprolactone (ε-CL). The hydrolytic degradation behavior of ε-CL/γ-BL copolymers with different levels of γ-BL incorporation as well as the control PCL and PBL homopolymers was studied by monitoring the weight variation of the polymer film samples immersed in neutral, acidic, and basic aqueous solutions. The study of hydrolytic stability showed that incorporation of γ-BL into PCL accelerated the hydrolytic degradation rate of PCL, which could be modulated by changing the copolyester composition. Comparing PCL with and PBL-co-PCL copolymers, the hydrolytic degradation of PBL was relatively fast, especially in the basic aqueous solution. In a study of 1 month only 4.7% of weight remained for PBL while PCL still had 87% weight remained. Despite this it was also noteworthy that the copolymer even with a high level of γ-BL incorporation (76 mol %) still exhibited relatively strong resistance toward hydrolytic degradation, rendering its degradation behavior resembling more closely to PCL than to PBL.

Papageorgiou et al.[70] studied the biodegradability and biocompatibility of Poly[propyleneco-(ethylene succinate)] random copolymers in comparison with poly(L-lactic acid) (PLA) which is a polymer of high biocompatibility and widely used in biomedical applications. The biocompatibility of PPSu and its PPESu copolymers was evaluated by measuring the viability of HUVEC cells in the presence of different concentrations of the polymers. The results showed that the biocompatibility of PPSu was comparable to that of PLA, and also the synthetized PPESu copolymers had also similar cytotoxicity with PPSu, and thus they were also considered as biocompatible polymers.

1.4.6 Poly(butylene succinate-*ran*-butylene azelate) (PBS-*ran*-PBAz) copolymers

Poly(butylene succinate-*ran*-butylene azelate) (PBS-*ran*-PBAz) copolymers, were firstly synthesized by Ravi et al.[59] by melt polycondensation. In this work only a 50/50 mol% copolymer was synthesized and also they analyzed its enzymatic biodegradation, obtaining as results that the copolymer exhibited a low biodegradation rate due to its high crystallinity degree. Later, Mincheva et al.[18] synthetized random PBS-*ran*-PBAz copolyesters with SuA/AzA molar ratio varied in the whole range via an adapted two-step melt polycondensation. They also analyzed the thermal properties, crystallinity and mechanical properties by differential scanning calorimetry (DSC) and dynamic mechanical thermal analyses (DMTA).

Very similar PBS-*ran*-PBAz random copolymers were synthesized by Diaz et al.[14, 61] with parallel results. They studied the structure of the copolymers by wide angle X-ray scattering (WAXS) and performed nonisothermal and isothermal crystallization. In their work, there were results that indicate possible isodimorphic behavior, like a systematic variation of the crystalline unit cell density with copolymer composition and composition dependent changes of Lauritzen and Hoffman parameters for the overall isothermal crystallization. However, since the equilibrium melting points (obtained by Hoffman−Weeks extrapolations) were found to decrease according to the Baur exclusion model, they finally concluded that monomer exclusion was predominant during crystallization.

In the present PhD work, we make use of the previously synthesized PBS-*ran*-PBAz copolymers by Mincheva et al.[18] to study their structure, nonisothermal and isothermal crystallization and morphology. We have performed small angle X-ray scattering (SAXS), and have correlated the results with data obtained from WAXS, polarized light optical microscopy (PLOM), and Atomic Force Microscopy (AFM). Self-nucleation and Successive Self-nucleation and Annealing (SSA) studies have also been performed as well as the study of the dielectric relaxation of PBS-*ran*-PBAz for the first time in this type of random copolymers.

1.5 References

1. Siracusa, V.; Rocculi, P.; Romani, S.; Rosa, M. D., Biodegradable polymers for food packaging: a review. *Trends in Food Science & Technology* **2008,** *19*, 634-643.
2. http://en.european-bioplastics.org/bioplastics/.
3. A. Calmon-Decriaud, V. Bellon-Maurel and F. Silvestre, A*dvances in Polymer Science,* **1998**, *135***,** 206-226.
4. Gross, R. A.; Kalra, B., Biodegradable Polymers for the Environment. *Science* **2002,** *297*, 803.
5. Díaz, A.; Katsarava, R.; Puiggalí, J., Synthesis, Properties and Applications of Biodegradable Polymers Derived from Diols and Dicarboxylic Acids: From Polyesters to Poly(ester amide)s. *International Journal of Molecular Sciences* **2014,** *15*, 7064−7123.
6. Vilela, C.; Sousa, A. F.; Fonseca, A. C.; Serra, A. C.; Coelho, J. F. J.; Freire, C. S. R.; Silvestre, A. J. D., The quest for sustainable polyesters – insights into the future. *Polymer Chemistry* **2014,** *5*, 3119-3141.
7. Wang, G.; Qiu, Z., Synthesis, Crystallization Kinetics, and Morphology of Novel Biodegradable Poly(butylene succinate-co-hexamethylene succinate) Copolyesters. *Industrial & Engineering Chemistry Research* **2012,** *51*, 16369-16376.
8. Ren, M.; Song, J.; Song, C.; Zhang, H.; Sun, X.; Chen, Q.; Zhang, H.; Mo, Z., Crystallization kinetics and morphology of poly(butylene succinate-co-adipate). *Journal of Polymer Science Part B: Polymer Physics* **2005,** *43*, 3231-3241.
9. Pérez-Camargo, R. A.; Fernández-d'Arlas, B.; Cavallo, D.; Debuissy, T.; Pollet, E.; Avérous, L.; Müller, A. J., Tailoring the Structure, Morphology, and Crystallization of Isodimorphic Poly(butylene succinate-ran-butylene adipate) Random Copolymers by Changing Composition and Thermal History. *Macromolecules* **2017,** *50*, 597-608.
10. Zeng, J. B.; Huang, C. L.; Jiao, L.; Lu, X.; Wang, Y.-Z.; Wang, X.-L., Synthesis and Properties of Biodegradable Poly(butylene succinate-co-diethylene glycol succinate) Copolymers. *Industrial & Engineering Chemistry Research* **2012,** *51*, 12258-12265.
11. Ye, H. M.; Wang, R. D.; Liu, J.; Xu, J.; Guo, B.-H., Isomorphism in Poly(butylene succinate-co-butylene fumarate) and Its Application as Polymeric Nucleating Agent for Poly(butylene succinate). *Macromolecules* **2012,** *45*, 5667-5675.

12. Papageorgiou, G. Z.; Bikiaris, D. N., Synthesis, cocrystallization, and enzymatic degradation of novel poly(butylene-co-propylene succinate) copolymers. *Biomacromolecules* **2007,** *8*, 2437-2449.
13. Mochizuki, M.; Mukai, K.; Yamada, K.; Ichise, N.; Murase, S.; Iwaya, Y., Structural effects upon enzymatic hydrolysis of poly(butylene succinate-co-ethylene succinate)s. *Macromolecules* **1997,** *30*, 7403-7407.
14. Diaz, A.; Franco, L.; Puiggali, J., Study on the crystallization of poly(butylene azelate-co-butylene succinate) copolymers. *Thermochimica Acta* **2014,** *575*, 45-54.
15. Arandia, I.; Mugica, A.; Zubitur, M.; Arbe, A.; Liu, G.; Wang, D.; Mincheva, R.; Dubois, P.; Müller, A. J., How Composition Determines the Properties of Isodimorphic Poly(butylene succinate-ran-butylene azelate) Random Biobased Copolymers: From Single to Double Crystalline Random Copolymers. *Macromolecules* **2015,** *48*, 43-57.
16. Iwata, T.; Doi, Y., Crystal structure and biodegradation of aliphatic polyester crystals. *Macromolecular Chemistry and Physics* **1999,** *200* (11), 2429-2442.
17. L. Sheng, R. A. Register, *Crystallization in Copolymers* . In Handbook of Polymer Crystallization, E. Piorkowska, G. C. Rutkedge, Eds.; Wiley: Hoboken, NJ, **2013**, 327–346.
18. Mincheva, R.; Delangre, A.; Raquez, J. M.; Narayan, R.; Dubois, P., Biobased Polyesters with Composition-Dependent Thermomechanical Properties: Synthesis and Characterization of Poly(butylene succinate-co-butylene azelate). *Biomacromolecules* **2013,** *14*, 890-899.
19. Tokiwa, Y.; Calabia, P. B.; Ugwu, U. C.; Aiba, S., Biodegradability of Plastics. *International Journal of Molecular Sciences* **2009,** *10,* 3722-42.
20. Arandes, J. M.; Bilbao, J.; López-Valerio, D., Reciclado de residuos plásticos. *Revista Iberoamericana de Polímeros*, **2004**, *5*, 28-45.
21. Vroman, I.; Tighzert, L., Biodegradable Polymers. *Materials* **2009,** *2*, 307-344.
22. Yokohara, T.; Yamaguchi, M., Structure and properties for biomass-based polyester blends of PLA and PBS. *European Polymer Journal* **2008,** *44*, 677-685.
23. Nofar, M.; Heuzey, M. C.; Carreau, P. J.; Kamal, M. R., Effects of nanoclay and its localization on the morphology stabilization of PLA/PBAT blends under shear flow. *Polymer* **2016,** *98*, 353-364.
24. Zhou, J. H.; Shen, G. Z.; Zhu, J.; Yuan, W. K., Terephthalic Acid Hydropurification over Pd/C Catalyst. *Studies in Surface Science and Catalysis*, **2006**,*159*, 293-296.

25. Niaounakis, M., Introduction to Biopolymers. *Biopolymers Reuse, Recycling, and Disposal*, **2013**, 1-75.
26. Guo, B.; Ding, H. G.; Xu, X. L.; Xu, J.; Sun, Y. B., Studies on the sequence structure and crystallinity of poly(butylene succinate) copolymers with terephthalic acid. **2003**, *24*, 2312-2316.
27. Mecham, J., Synthesis and Characterization of Cycloaliphatic and Aromatic Polyester/Poly(dimethylsiloxane) Segmented Copolymers. Blacksburg, **1997**.
28. Xiong, X. B.; Falamarzian, A.; Garg, S. M.; Lavasanifar, A., Engineering of amphiphilic block copolymers for polymeric micellar drug and gene delivery. *Journal of Controlled Release* **2011,** *155*, 248-261.
29. Amass, W.; Amass, A.; Tighe, B., A review of biodegradable polymers: uses, current developments in the synthesis and characterization of biodegradable polyesters, blends of biodegradable polymers and recent advances in biodegradation studies. *Polymer International* **1999,** *47*, 89-144.
30. Song, H.; Lee, S. Y., Production of succinic acid by bacterial fermentation. *Enzyme and Microbial Technology* **2006,** *39*, 352-361.
31. Fujimaki, T., Processability and properties of aliphatic polyesters, 'BIONOLLE', synthesized by polycondensation reaction. *Polymer Degradation and Stability* **1998,** *59*, 209-214.
32. Xu, J.; Guo, B. H., Poly(butylene succinate) and its copolymers: Research, development and industrialization. *Biotechnology Journal* **2010,** *5*, 1149-1163.
33. Gigli, M.; Fabbri, M.; Lotti, N.; Gamberini, R.; Rimini, B.; Munari, A., Poly(butylene succinate)-based polyesters for biomedical applications: A review. *European Polymer Journal* **2016,** *75*, 431-460.
34. Siracusa, V.; Lotti, N.; Munari, A.; Dalla Rosa, M., Poly(butylene succinate) and poly(butylene succinate-co-adipate) for food packaging applications: Gas barrier properties after stressed treatments. *Polymer Degradation and Stability* **2015,** *119*, 35-45.
35. Wang, H.; Ji, J.; Zhang, W.; Zhang, Y.; Jiang, J.; Wu, Z.; Pu, S.; Chu, P. K., Biocompatibility and bioactivity of plasma-treated biodegradable poly(butylene succinate). *Acta Biomaterialia* **2009,** *5*, 279-287.
36. Wang, L. C.; Chen, J. W.; Liu, H. L.; Chen, Z. Q.; Zhang, Y.; Wang, C. Y.; Feng, Z. G., Synthesis and evaluation of biodegradable segmented multiblock poly(ether ester) copolymers for biomaterial applications. *Polymer International* **2004,** *53*, 2145-2154.

37. Correlo, V.; Boesel, L.; Pinho, E.; Costa-Pinto, A.; Silva, M.; Bhattacharya, M.; Mano, J. F.; Neves, N.; Reis, R. L., Melt-based compression-molded scaffolds from chitosan-polyester blends and composites: Morphology and mechanical properties. *Journal of Biomedical Materials Research Part A* **2009**, *91*, 489-504.
38. Park, S. J.; Lee, Y. M.; Hong, S. K., Release behaviors of porous poly(butylene succinate)/poly(ε-caprolactone) microcapsules containing indomethacin. *Colloids and Surfaces B: Biointerfaces* **2006,** *47*, 211-215.
39. Liu, J.; Jiang, Z.; Zhang, S.; Saltzman, W. M., Poly(ω-pentadecalactone-co-butylene-co-succinate) nanoparticles as biodegradable carriers for camptothecin delivery. *Biomaterials* **2009,** *30*, 5707-5719.
40. Meesap, P.; Uppanan, P.; Thavornyutikarn, B.; Kosorn, W.; Janvikul, W., Surface Hydrolyzed Poly(Butylene Succinate) Microsphere Incorporated Carboxymethylchitosan Scaffolds for Cartilage Tissue Engineering. J*ournal of Metals, Materials and Minerals* **2018**, *20*, 107-111.
41. http://www.showa-denko.com.
42. https://www.m-chemical.co.jp.
43. Jacquel, N.; Freyermouth, F.; Fenouillot, F.; Rousseau, A.; Pascault, J. P.; Fuertes, P.; Saint-Loup, R., Synthesis and properties of poly(butylene succinate): Efficiency of different transesterification catalysts. *Journal of Polymer Science Part A: Polymer Chemistry* **2011,** *49*, 5301-5312.
44. Pan, P.; Inoue, Y., Polymorphism and isomorphism in biodegradable polyesters. *Progress in Polymer Science* **2009,** *34*, 605-640.
45. Ichikawa, Y.; Kondo, H.; Igarashi, Y.; Noguchi, K.; Okuyama, K.; Washiyama, J., Crystal structures of α and β forms of poly(tetramethylene succinate). *Polymer* **2000**, *41*, 4719-4727.
46. Ichikawa, Y.; Suzuki, J.; Washiyama, J.; Moteki, Y.; Noguchi, K.; Okuyama, K., Strain-induced crystal modification in poly(tetramethylene succinate). *Polymer* **1994,** *35*, 3338-3339.
47. Nikolic, M. S.; Djonlagic, J., Synthesis and characterization of biodegradable poly(butylene succinate-co-butylene adipate)s. *Polymer Degradation and Stability* **2001,** *74*, 263-270.
48. Shi, X. Q.; Aimi, K.; Ito, H.; Ando, S.; Kikutani, T., Characterization on mixed-crystal structure of poly(butylene terephthalate/succinate/adipate) biodegradable copolymer fibers. *Polymer* **2005,** *46*, 751-760.

49. Nagata, M.; Goto, H.; Sakai, W.; Tsutsumi, N., Synthesis and enzymatic degradation of poly(tetramethylene succinate) copolymers with terephthalic acid. *Polymer* **2000**, *41*, 4373-4376.
50. Guidotti, G.; Soccio, M.; Siracusa, V.; Gazzano, M.; Salatelli, E.; Munari, A.; Lotti, N., Novel Random PBS-Based Copolymers Containing Aliphatic Side Chains for Sustainable Flexible Food Packaging. *Polymers* **2017,** *9*, 724.
51. D'Ambrosio, M. R.; Michell, M. R.; Mincheva, R.; Hernández, R.; Mijangos, C.; Dubois, P.; Müller, J. A., Crystallization and Stereocomplexation of PLA-mb-PBS Multi-Block Copolymers. *Polymers* **2018,** *10*, 8.
52. Wu, C. S.; Hsu, Y. C.; Liao, H. T.; Yen, F. S.; Wang, C. Y.; Hsu, C. T., Characterization and biocompatibility of chestnut shell fiber–based composites with polyester. *Journal of Applied Polymer Science* **2014,** *131*, 40730.
53. Suphakit Arphavasin and Weerachai Singhatanadgit and Patcharee Ngamviriyavong and Wanida Janvikul and Preeyapan Meesap and Somying, P., Enhanced osteogenic activity of a poly(butylene succinate)/calcium phosphate composite by simple alkaline hydrolysis. *Biomedical Materials* **2013,** *8*, 055008.
54. Niu, Y.; Cao, L.; Wei, J.; Ma, Y.; Song, S.; Weng, W.; Li, H.; Liu, C.; Su, J., Development of a bioactive composite of nano fluorapatite and poly(butylene succinate) for bone tissue regeneration. *Journal of Materials Chemistry B* **2014,** *2*, 1174-1181.
55. Correlo, V. M.; Boesel, L. F.; Bhattacharya, M.; Mano, J. F.; Neves, N. M.; Reis, R. L., Hydroxyapatite Reinforced Chitosan and Polyester Blends for Biomedical Applications. *Macromolecular Materials and Engineering* **2005,** *290*, 1157-1165.
56. Guo, W.; Zhang, Y.; Zhang, W., Mechanical properties and crystallization behavior of hydroxyapatite/poly(butylenes succinate) composites. *Journal of Biomedical Materials Research Part A* **2013,** *101*, 2500-2506.
57. Grigoriadou, I.; Nianias, N.; Hoppe, A.; Terzopoulou, Z.; Bikiaris, D.; Will, J.; Hum, J.; Roether, J. A.; Detsch, R.; Boccaccini, A. R., Evaluation of silica-nanotubes and strontium hydroxyapatite nanorods as appropriate nanoadditives for poly(butylene succinate) biodegradable polyester for biomedical applications. *Composites Part B: Engineering* **2014,** *60*, 49-59.
58. Höfer, R.; Daute, P.; Grützmacher, R.; Westfechtel, A., Oleochemical polyols — A new raw material source for polyurethane coatings and floorings. *Journal of Coatings Technology* **1997,** *69*, 65-72.

59. Ravi, A.; Nanthini, R.; Karunanidhi, M.; Jaisankar, V., Synthesis and Characterization of Certain Biodegradable Random Aliphatic Copolyesters. *Asian Journal of Chemistry* **2011**, *23*, 556-560.
60. Papageorgiou, G. Z.; Bikiaris, D. N.; Achilias, D. S.; Papastergiadis, E.; Docoslis, A., Crystallization and biodegradation of poly(butylene azelate): Comparison with poly(ethylene azelate) and poly(propylene azelate). *Thermochimica Acta* **2011,** *515*, 13-23.
61. Diaz, A.; Franco, L.; Estrany, F.; del Valle, L. J.; Puiggali, J., Poly(butylene azelate-co-butylene succinate) copolymers: Crystalline morphologies and degradation. *Polymer Degradation and Stability* **2014,** *99*, 80-91.
62. Hiemenz, P. C.; Lodge, T. P., *Polymer Chemistry, Second Edition*. Taylor & Francis: **2007**.
63. Allegra, G.; Bassi, I. W., Isomorphism in synthetic macromolecular systems. *Advances in Polymer Science* **1969**, *6*, 549−574.
64. Pérez-Camargo, R. A.; Arandia, I.; Safari, M.; Cavallo, D.; Lotti, N.; Soccio, M.; Müller, A. J., Crystallization of isodimorphic aliphatic random copolyesters: Pseudo-eutectic behavior and double-crystalline materials. *European Polymer Journal* **2018,** *101*, 233-247.
65. Natta, G.; Corradini, P.; Sianesi, D.; Morero, D., Isomorphism phenomena in macromolecules. *Journal of Polymer Science* **1961,** *51*, 527-539.
66. Yu, Y.; Sang, L.; Wei, Z.; Leng, X.; Li, Y., Unique isodimorphism and isomorphism behaviors of even-odd poly(hexamethylene dicarboxylate) aliphatic copolyesters. *Polymer* **2017,** *115*, 106-117.
67. Latere Dwan'Isa, J. P.; Lecomte, P.; Dubois, P.; Jérôme, R., Synthesis and Characterization of Random Copolyesters of ε-Caprolactone and 2-Oxepane-1,5-dione. *Macromolecules* **2003,** *36*, 2609-2615.
68. Ceccorulli, G.; Scandola, M.; Kumar, A.; Kalra, B.; Gross, R. A., Cocrystallization of Random Copolymers of ω-Pentadecalactone and ε-Caprolactone Synthesized by Lipase Catalysis. *Biomacromolecules* **2005,** *6*, 902-907.
69. Siracusa, V.; Gazzano, M.; Finelli, L.; Lotti, N.; Munari, A., Cocrystallization phenomena in novel poly(diethylene terephthalate-co-thiodiethylene terephthalate) copolyesters. *Journal of Polymer Science Part B: Polymer Physics* **2006,** *44*, 1562-1571.

70. Papageorgiou, G. Z.; Bikiaris, D. N., Synthesis and Properties of Novel Biodegradable/Biocompatible Poly[propylene-co-(ethylene succinate)] Random Copolyesters. *Macromolecular Chemistry and Physics* **2009,** *210*, 1408-1421.
71. Eynde, S. V.; Mathot, V. B. F.; Koch, M. H. J.; Reynaers, H., Thermal behaviour and morphology of homogeneous ethylene–1-octene copolymers with high comonomer contents. *Polymer* **2000,** *41*, 4889-4900.
72. Poon, B.; Rogunova, M.; Chum, S. P.; Hiltner, A.; Baer, E., Classification of homogeneous copolymers of propylene and 1-octene based on comonomer content. *Journal of Polymer Science Part B: Polymer Physics* **2004,** *42*, 4357-4370.
73. Howard, G. J.; Knutton, S., Isomorphism in aliphatic copolyesters. *Polymer* **1968**, *9*, 527–534.
74. Yu, Y.; Wei, Z.; Zhou, C.; Zheng, L.; Leng, X.; Li, Y., Miscibility and competition of cocrystallization behavior of poly(hexamethylene dicarboxylate)s aliphatic copolyesters: Effect of chain length of aliphatic diacids. *European Polymer Journal* **2017,** *92*, 71-85.
75. Xiangyang, L.; Zhenfei, H.; Jie, S.; Yong, G.; Youju, H.; Haining, A.; Zhe, M.; Baijin, Z.; Chunguang, S.; Yapeng, F.; Chuanlu, Y.; Liangbin, L., Identifying the phase behavior of biodegradable poly(hexamethylene succinate-co-hexamethylene adipate) copolymers with FTIR. *Journal of Physical Chemistry B* **2009,** *113*, 2695-2704.
76. Liang, Z.; Pan, P.; Zhu, B.; Dong, T.; Hua, L.; Inoue, Y., Crystalline Phase of Isomorphic Poly(hexamethylene sebacate-co-hexamethylene adipate) Copolyester: Effects of Comonomer Composition and Crystallization Temperature. *Macromolecules* **2010,** *43*, 2925-2932.
77. Li, X.; Sun, J.; Huang, Y.; Geng, Y.; Wang, X.; Ma, Z.; Shao, C.; Zhang, X.; Yang, C.; Li, L., Inducing New Crystal Structures through Random Copolymerization of Biodegradable Aliphatic Polyester. *Macromolecules* **2008,** *41*, 3162-3168.
78. Tan, B.; Bi, S.; Emery, K.; Sobkowicz, M. J., Bio-based poly(butylene succinate-co-hexamethylene succinate) copolyesters with tunable thermal and mechanical properties. *European Polymer Journal* **2017,** *86*, 162-172.
79. Liang, Z.; Pan, P.; Zhu, B.; Inoue, Y., Isomorphic crystallization of aliphatic copolyesters derived from 1,6-hexanediol: Effect of the chemical structure of comonomer units on the extent of cocrystallization. *Polymer* **2011,** *52*, 2667-2676.
80. Liang, Z.; Pan, P.; Zhu, B.; Inoue, Y., Isomorphic Crystallization of Poly(hexamethylene adipate-co-butylene adipate): Regulating Crystal Modification of Polymorphic Polyester from Internal Crystalline Lattice. *Macromolecules* **2010,** *43*, 6429-6437.

81. Debuissy, T.; Sangwan, P.; Pollet, E.; Avérous, L., Study on the structure-properties relationship of biodegradable and biobased aliphatic copolyesters based on 1,3-propanediol, 1,4-butanediol, succinic and adipic acids. *Polymer* **2017,** *122*, 105-116.
82. Tsuji, H.; Sobue, T., Cocrystallization of monomer units in lactic acid-based biodegradable copolymers, poly(l-lactic acid-co-l-2-hydroxybutanoic acid)s. *Polymer* **2015,** *72*, 202-211.
83. Lavilla, C.; Alla, A.; Martínez de Ilarduya, A.; Muñoz-Guerra, S., High Tg Bio-Based Aliphatic Polyesters from Bicyclic d-Mannitol. *Biomacromolecules* **2013,** *14*, 781-793.
84. Soccio, M.; Gazzano, M.; Lotti, N.; Finelli, L.; Munari, A., Copolymerization: A new tool to selectively induce poly(butylene naphthalate) crystal form. *Journal of Polymer Science Part B: Polymer Physics* **2009,** *47*, 1356-1367.
85. Morales-Huerta, J. C.; Martínez de Ilarduya, A.; Muñoz-Guerra, S., Sustainable Aromatic Copolyesters via Ring Opening Polymerization: Poly(butylene 2,5-furandicarboxylate-co-terephthalate)s. *ACS Sustainable Chemistry & Engineering* **2016,** *4*, 4965-4973.
86. Hong, M.; Tang, X.; Newell, B. S.; Chen, E. Y. X., "Nonstrained" γ-Butyrolactone-Based Copolyesters: Copolymerization Characteristics and Composition-Dependent (Thermal, Eutectic, Cocrystallization, and Degradation) Properties. *Macromolecules* **2017,** *50*, 8469-8479.
87. Wang, K.; Jia, Y. G.; Zhu, X. X., Two-Way Reversible Shape Memory Polymers Made of Cross-Linked Cocrystallizable Random Copolymers with Tunable Actuation Temperatures. *Macromolecules* **2017,** *50*, 8570-8579.
88. Fuller, C. S., Mixed Crystal Formation in Linear Copolyesters. *Journal of the American Chemical Society* **1948,** *70*, 421-423.
89. Feng, L.; Wang, Y.; Inagawa, Y.; Kasuya, K.; Saito, T.; Doi, Y.; Inoue, Y., Enzymatic degradation behavior of comonomer compositionally fractionated bacterial poly(3-hydroxybutyrate-co-3-hydroxyvalerate)s by poly(3-hydroxyalkanoate) depolymerases isolated from Ralstonia pickettii T1 and Acidovorax sp. TP4. *Polymer Degradation and Stability* **2004,** *84*, 95-104.
90. Shi, X. Q.; Ito, H.; Kikutani, T., Characterization on mixed-crystal structure and properties of poly(butylene adipate-co-terephthalate) biodegradable fibers. *Polymer* **2005,** *46*, 11442-11450.

91. Papageorgiou, G. Z.; Vassiliou, A. A.; Karavelidis, V. D.; Koumbis, A.; Bikiaris, D. N., Novel Poly(propylene terephthalate-co-succinate) Random Copolymers: Synthesis, Solid Structure, and Enzymatic Degradation Study. *Macromolecules* **2008,** *41*, 1675-1684.
92. Gan, Z.; Kuwabara, K.; Yamamoto, M.; Abe, H.; Doi, Y., Solid-state structures and thermal properties of aliphatic–aromatic poly(butylene adipate-co-butylene terephthalate) copolyesters. *Polymer Degradation and Stability* **2004,** *83*, 289-300.
93. Cranston, E.; Kawada, J.; Raymond, S.; Morin, F. G.; Marchessault, R. H., Cocrystallization Model for Synthetic Biodegradable Poly(butylene adipate-co-butylene terephthalate). *Biomacromolecules* **2003,** *4*, 995-999.
94. Faxue, L.; Xinjian, L.; Qinghui, H.; Qiaobo, L.; Jianyong, Y.; Amin, C., Effects of comonomer sequential structure on thermal and crystallization behaviors of biodegradable poly(butylene succinate-co-butylene terephthalate)s. *Journal of Polymer Science, Part B: Polymer Physics* **2006,** *44*, 1635-1644.
95. Berti, C.; Celli, A.; Marchese, P.; Barbiroli, G.; Di Credico, F.; Verney, V.; Commereuc, S., Novel copolyesters based on poly(alkylene dicarboxylate)s: 1. Thermal behavior and biodegradation of aliphatic–aromatic random copolymers. *European Polymer Journal* **2008,** *44*, 3650-3661.
96. Berti, C.; Celli, A.; Marchese, P.; Barbiroli, G.; Di Credico, F.; Verney, V.; Commereuc, S., Novel copolyesters based on poly(alkylene dicarboxylate)s: 2. Thermal behavior and biodegradation of fully aliphatic random copolymers containing 1,4-cyclohexylene rings. *European Polymer Journal* **2009,** *45*, 2402-2412.
97. Konstantopoulou, M.; Terzopoulou, Z.; Nerantzaki, M.; Tsagkalias, J.; Achilias, D. S.; Bikiaris, D. N.; Exarhopoulos, S.; Papageorgiou, D. G.; Papageorgiou, G. Z., Poly(ethylene furanoate-co-ethylene terephthalate) biobased copolymers: Synthesis, thermal properties and cocrystallization behavior. *European Polymer Journal* **2017,** *89*, 349-366.
98. Pepels, M. P. F.; Govaert, L. E.; Duchateau, R., Influence of the Main-Chain Configuration on the Mechanical Properties of Linear Aliphatic Polyesters. *Macromolecules* **2015,** *48*, 5845-5854.
99. Jeong, Y. G.; Jo, W. H.; Lee, S. C., Cocrystallization Behavior of Poly(butylene terephthalate-co-butylene 2,6-naphthalate) Random Copolymers. *Macromolecules* **2000,** *33*, 9705-9711.

100. Zhaobin, Q.; Ikehara, T.; Nishi, T., Miscibility and crystallization behaviour of biodegradable blends of two aliphatic polyesters. Poly(3-hydroxybutyrate-co-hydroxyvalerate) and poly(butylene succinate) blends. *Polymer* **2003,** *44*, 7519-7527.

101. Ciulik, C.; Safari, M.; Martínez de Ilarduya, A.; Morales-Huerta, J. C.; Iturrospe, A.; Arbe, A.; Müller, A. J.; Muñoz-Guerra, S., Poly(butylene succinate-ran-ε-caprolactone) copolyesters: Enzymatic synthesis and crystalline isodimorphic character. *European Polymer Journal* **2017,** *95*, 795-808.

102. Swinehart, D. F., The Beer-Lambert Law. *Journal of Chemical Education* **1962,** *39*, 333.

103. Papadimitriou, S. A.; Papageorgiou, G. Z.; Bikiaris, D. N., Crystallization and enzymatic degradation of novel poly(ε-caprolactone-co-propylene succinate) copolymers. *European Polymer Journal* **2008,** *44*, 2356-2366.

104. Flory, P. J., Theory of crystallization in copolymers. *Transactions of the Faraday Society* **1955,** *51*, 848-857.

105. Flory, P. J., Thermodynamics of Crystallization in High Polymers. IV. A Theory of Crystalline States and Fusion in Polymers, Copolymers, and Their Mixtures with Diluents. *The Journal of Chemical Physics* **1949,** *17*, 223-240.

106. Baur, V. H., Einfluß der sequenzlängenverteilung auf das schmelz-ende von copolymeren. *Die Makromolekulare Chemie* **1966,** *98*, 297-301.

107. Helfand, E.; Lauritzen, J. I., Theory of Copolymer Crystallization. *Macromolecules* **1973,** *6*, 631-638.

108. Sanchez, I. C.; Eby, R. K., Thermodynamics and Crystallization of Random Copolymers. *Macromolecules* **1975,** *8*, 638-641.

109. Wendling, J.; Suter, U. W., A New Model Describing the Cocrystallization Behavior of Random Copolymers. *Macromolecules* **1998,** *31*, 2516-2520.

110. Wendling, J.; Gusev, A. A.; Suter, U. W.; Braam, A.; Leemans, L.; Meier, R. J.; Aerts, J.; Heuvel, J. v. d.; Hottenhuis, M., Crystal Morphology and Thermodynamics of Poly(ethylene-4,4‘-biphenyl dicarboxylate) and Related Copolymers with Ethylene-2,6-naphthalene Dicarboxylate. *Macromolecules* **1999,** *32*, 7866-7878.

111. Wendling, J.; Gusev, A. A.; Suter, U. W., Predicting the Cocrystallization Behavior of Random Copolymers via Free Energy Calculations. *Macromolecules* **1998,** *31*, 2509-2515.

Chapter 2

Polymer crystallization

2.1 Introduction

The study of crystallization in polymers has attracted much attention as thermal and mechanical properties of semicrystalline materials depend on the number, dimensions and organization of their crystalline structures. Although a polymer can crystallize during its polymerization reaction or from a solution, the crystallization of the polymer from the melt state is the most significant because of its similarity to most industrial processing techniques.

The study of crystallization in relation to temperature can be carried out in an isothermal way, in which the material is rapidly cooled from the melt and left crystallizing at a constant temperature, or in a non-isothermal way, in which the material is cooled at a controlled rate. Despite the fact that during industrial processes crystallization is mostly developed in a non-isothermal way, obtaining like that a large distribution of crystals with different thickness and thermal stability, not only are non-isothermal studies done, but also many studies under isothermal conditions are carried out which are after extrapolated to dynamic or non-isothermal processes.

Crystallization is the combination between nucleation and growth processes. The crystallization of a polymer can occur only in a limited range of temperatures; the glass transition temperature (T_g) which is the lower temperature limit and the melting temperature the upper limit. Below T_g, the mobility of the polymer chains is restricted while close to T_m the nucleation process is inhibited. It is known that the nucleation rate ($\dot{N}$) and the growth rate (G) do not depend in the same way on the degree of supercooling. Generally, the maximum of $\dot{N}$ appears at higher supercooling (see Figure 2.1), at these low temperatures the segmental mobility is reduced and this favors the nucleation rate generating a greater number of crystals of small size. On the other hand, at higher temperatures crystalline growth is favored and fewer nuclei are formed generating larger spherulites.[1-5]

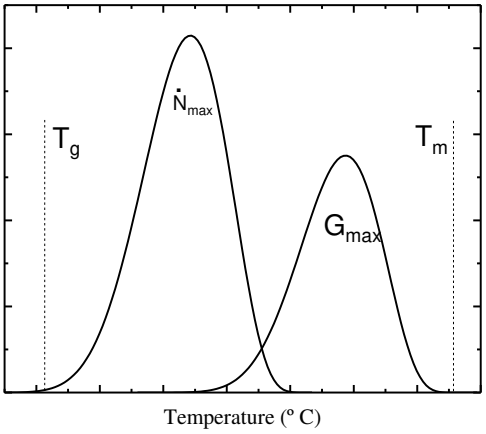

Figure 2. 1 *. Schematic representation of the nucleation rate and the crystalline growth rate (G) as a function of temperature. (Figure modified from reference [6])*

In this chapter the fundamental processes involved in polymer crystallization are briefly summarized.

2.2 Crystal Morphology

The first macromolecular structures studied by *X*-rays were the ones corresponding to different types of celluloses. In 1928 Hengstenberg and Mark estimated that crystals dimensions of cellulose were 55 Å width and 600 Å length.[7] These values are too small, as compared to macromolecules of high molecular weight which reach lengths of 1000 Å, so they wondered how these large chains were arranged in the crystals considering their small crystal size. In 1930 Herrmann reported the fringed-micelle model, which is presented schematized in Figure 2.2 and is essentially based on a double phase system characterized by crystalline and amorphous regions.[8]

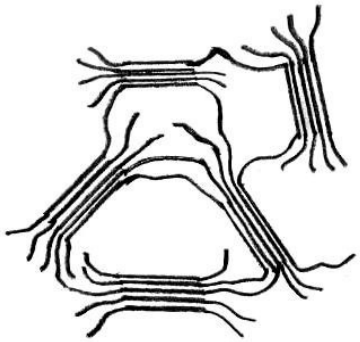

Figure 2. 2. *The fringed-micelle model scheme.*

Figure 2.2 shows that crystalline regions are composed of short-length stacks of different macromolecular chains aligned parallel to each other, and that the amorphous regions are constituted by disordered sequences which interconnect the regions of well-ordered chains. This model was able to explain, among others, the properties of hardness and flexibility based on the amorphous and crystalline percentages of the material, but it was not able to predict the optical properties. In 1938, Storks introduced the concept of "chain-folding" since he concluded that the chains of the semicrystalline trans-polyisoprene had to fold when it crystallized.[1]

Finally, in 1957 Keller[9] managed to obtain single crystals of polyethylene from a diluted xylene solution. The electron diffraction studies of the single crystals showed that the polymer chains had their axis placed perpendicularly to the single crystal base, which was explained by assuming that chains fold perpendicularly to the most extensive sides of the crystal. During the same year Fischer[10] and Till[11] also reported single polymeric crystals with very similar lamellar morphologies to those reported by Keller. Therefore, the "folded-chain model" proposed by Keller (illustrated in Figure 2.3) represented an important advance in the understanding of the organization of polymeric crystals obtained from solution.[1]

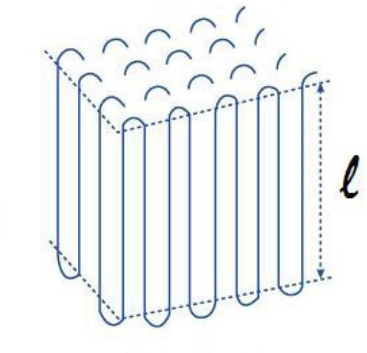

***Figure 2. 3**. Scheme of the concept of "chain-folding" proposed by Keller. (From reference [9])*

Keller reported that lamellae with folded chains are the fundamental unit of polymer morphology, which grow to form supramolecular structures such as spherulites, axialites and hedrites.[1-3] Flexible polymers capable to crystallize form spherically symmetric aggregates of radial lamellae known as spherulites. These structures appear as birefringent spheres which are observable by Polarized Light Optical Microscope (PLOM) and generally show characteristic extinction patterns called Maltese cross which are formed parallel and perpendicularly to the direction of polarization. A typical example of spherulites is shown in Figure 2.4.

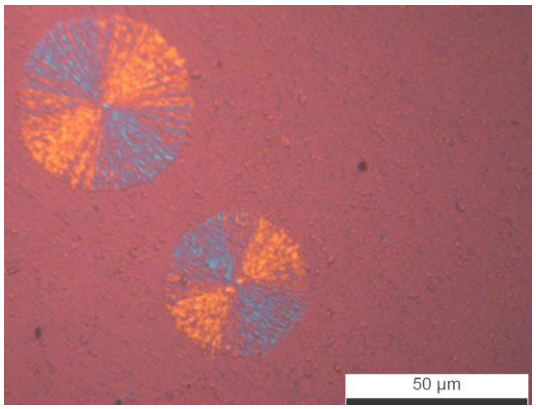

***Figure 2. 4**. Spherulites of poly(lactic acid) (PLA).*

Transmission electron microscopy measurements in the internal areas of the spherulites, showed that they are constituted by lamellae (separated by amorphous interlamellar zones) which grow radially. The chains are arranged perpendicularly to the flat horizontal surface of the lamella and are therefore tangential to the spherulite and to the direction of growth (see Figure 2.5).[1-3] The thickness of typical lamellae in polymers vary from 50 to 400 Å. The primary lamellae (or "parent lamellae") extend from the center to the end of the spherulite and along its growth axis new branches are formed by secondary lamellae (or "daughter lamellae").

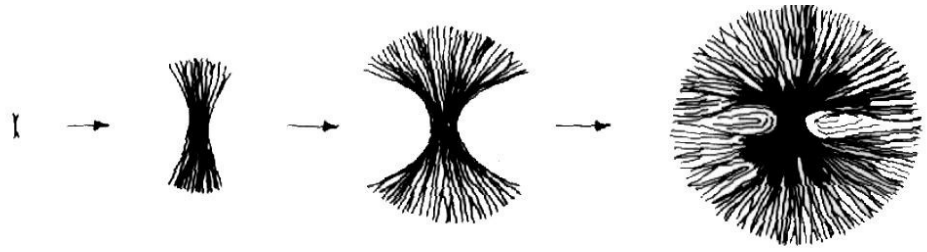

Figure 2. 5 *Scheme of development of a spherulite from a homogeneous nucleus. REF?*

From the point of view of spherulitic morphology, the model proposed by Mandelkern[2] in 1964 is currently accepted, in which three fundamental regions are defined (Figure 2.6): the first corresponds to the crystalline region formed by lamellae; the second corresponds to the amorphous region with a totally disordered conformation and similar characteristics to those of the melt; and a third, the interfacial region, formed by chains which are also part of the lamellae and are in between this interfacial region.

The difference in size and morphology between the spherulites of different polymers will depend on the chemical nature, the molecular weight and its distribution, the crystallization conditions and the density of active nuclei present in the material.

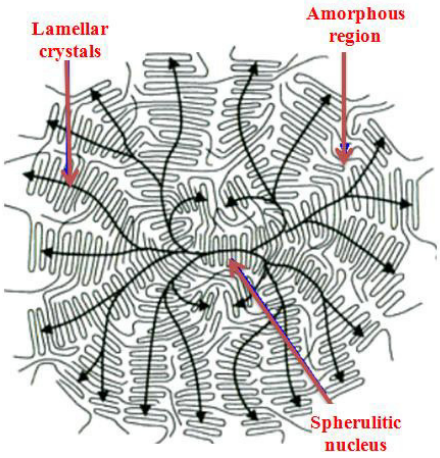

Figure 2. 6. *Radial growth of spherulite in two dimensions. Amorphous and crystalline regions.*

Different techniques such as Wide Angle and Small Angle *X*-ray Scattering, Polarized Light Optical Microscopy, Phase-contrast Microscopy and even Transmission Electron Microscopy, are used to study these crystalline superstructures. In the present work, Polarized Optical Microscopy technique (PLOM) has mostly used since it provides a simple and useful way to directly visualize crystalline morphologies while determining spherulitic growth rates and nucleation density and kinetics.

2.3 Crystallization Kinetics

2.3.1 Introduction

The crystallization in polymers can be defined as a first-order phase transformation of a supercooled liquid.[3] In the case of very low molecular weight molecules, they can crystallize almost immediately after reaching the equilibrium melting point, but in the case of polymers, they are only able to crystallize at considerable high supercoolings. As briefly explained above in the text, polymer crystallization takes place at temperatures between the melting temperature (T_m) and the glass transition temperature (T_g). Starting from the melt, as temperature decreases the crystallization rate increases as the energetic barrier needed for phase transformation decreases, but as temperature is further decrease, the diffusion of molecular segments decreases and consequently reduces the crystallization rate. The lower the crystallization temperature the thinner the lamellar formed, i.e., they

would be more metastable. This effect becomes more significant as the temperature approaches the glass transition. When polymers crystallize from the melt, as the crystallization temperature further decreases they crystallize first slowly, then more rapidly with a maximum crystallization rate, and finally slowly again following a bell shape trend.[2-3] On the other side, when they crystallize from the vitreous state, same phenomenon happens but in this case as temperature increases. Hence the high-temperature limit is controlled by the thermodynamic forces and the low-temperature limit by diffusion limitations of molecular segments.

Polymer crystallization involves primary crystallization, secondary crystallization and crystal reorganization processes. In order to better understand the kinetic analysis of the results which are presented along this PhD thesis work, below in the text some fundamental aspects of nucleation and crystal growth, will be presented and also the most important nucleation and growth theories will be discussed

2.3.2 Nucleation

Nucleation is the first step in the formation of crystals in melt polymers. The process of crystal nucleation has been extensively described in the literature and its kinetics discussed in a large number of articles and books.[2, 4, 12-16]

The first stage of primary nucleation involves both translational and rotational diffusion of crystallizable units with an appropriate orientation and position which are able to develop a stable nucleus. This step is controlled by the free enthalpy change due to the phase transformation. At a nucleus critical size r^*, the enthalpy barrier required to allow the nucleus growth is surpassed and from this point chains addition occurs irreversibly and the crystal begins the growth process.

Two nucleation mechanisms are known; homogeneous nucleation, when the formation of the nuclei occurs in the bulk phase, and heterogeneous nucleation, when the formation occurs on preexisting surfaces or heterogeneities. When nucleation goes through a homogeneous mechanism, intrinsically unstable particles (embryos) are formed in the melt because of thermal fluctuations. For those very small particles the decrease in free energy due to phase transition is exceeded by the increase in interfacial free energy.

Regarding to the critical size of these particles, as the nucleation step is an active process associated with a free energy barrier to be overcome, there is a critical size separating these particles whose free energy of formation increases during growth from those whose energy decreases. If the size of embryos surpasses this critical value, they turns into kinetically stable aggregates (nuclei) of a growing crystal, otherwise, they disappear again.[4, 17]

The critical radius of the sphere (r^*) associated with the free energy barrier is obtained following next equation[1]:

$$r^* = \frac{2\sigma T_m^\circ}{\Delta H^\circ \Delta T} \qquad 2.1$$

where ΔH^o is the enthalpy of fusion, $T_m{}^o$ is the melting temperature at the thermo-dynamic equilibrium, σ is the specific free surface energy of the nucleus at the surface and ΔT represents supercooling defined as ($T_m{}^o$- T_c). Similarly, the free energy barrier which must be overcome in order to form stable aggregates is expressed by the following equation:

$$\Delta G^* = \frac{16\pi\sigma^3 T_m^{\circ\,2}}{3\Delta H^{\circ 2}\Delta T^2} \qquad 2.2$$

Equations 2.1 and 2.2 show that nucleation occurs more easily at lower crystallization temperatures since the free energy barrier associated with the process is smaller due to the nucleus critical size needed is also smaller.

The formation rate of crystalline nuclei which overcome the critical size and are able to grow is obtained by the following equation proposed by Turnbull and Fisher.[18] In which nucleation rate ($\dot{N}$), and temperature are related.

$$\dot{N} = N_0 e^{(\frac{E_D}{kT} - \frac{\Delta G^*}{kT})} \qquad 2.3$$

$\dot{N}$ is the nucleation rate, E_D is the activation energy for the diffusion process and ΔG^* represents the free energy for the formation of an aggregate with critical dimensions.

The combination of equations 2.2 and 2.3 shows that during a controlled cooling from the molten state ΔG * progressively decreases and therefore the nucleation process increases.

At further temperature decreases the nucleation rate reaches a maximum value, and then decreases again with the approximation to the glass transition. One of the consequences of the temperature decrease is the viscosity increase which leads to a decrease of chains diffusion.

As explained before, nucleation can occur in different ways; the homogeneous nucleation, when nucleation process occurs in the bulk phase and nuclei are formed only by segments of polymer chains, and the heterogeneous nucleation, when nucleation occurs on preexisting surfaces or heterogeneities and impurities. Heterogeneous nucleation commonly occurs in polymers, since it is very difficult to produce pure polymer without any heterogeneities such as catalyst residues and solvent impurities. Furthermore, heterogeneous nucleation is thermodynamically favored due to the presence of impurities allows heterogeneous nucleation to take place at smaller supercooling temperatures since the free energy barrier to be overcome will be smaller than forming new nuclei.

2.3.3 Crystal Growth

Crystal growth occurs by secondary and tertiary nucleation. The initial step is the formation of secondary nuclei which is followed by a series of tertiary nucleation events.[1] The relationship of spherulitic growth rate (G), which involves the transport (diffusion) term and the secondary nucleation term, with temperature is similar to that of the primary nucleation. Due to both terms have an opposite temperature dependence behavior, as it is shown in Figure 2.7 the growth rate exhibits a maximum and follows a bell shape curve as function of the crystallization temperature (or supercooling). On the left side of the bell shape curve, at high supercooling the dominant term is the molecular transport (diffusion). The diffusion of the macromolecules to the growing front becomes very difficult as melt viscosity greatly increases as the temperature reaches the glass transition temperature, where growth rate decreases to zero. On the right side of the bell shape curve, at high crystallization temperatures, the growth rate is driven by thermodynamic forces of the secondary nucleation.[19]

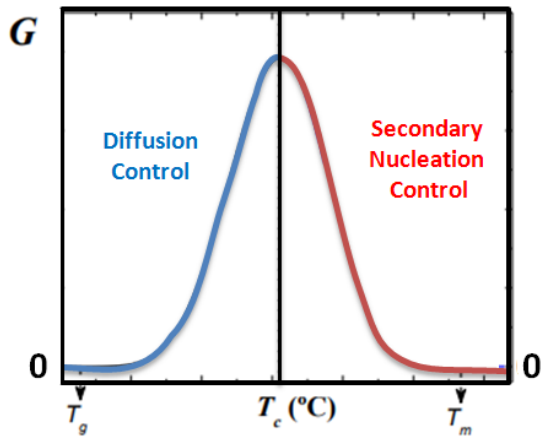

Figure 2. 7*. Crystal growth rate (G) as a function of the isothermal crystallization temperature.*

2.3.4 Polymer crystallization theories

Once nuclei are formed, their growth is affected by different factors such as structural regularity, plasticizers, molecular weight and flexibility. Several theories have been developed in order to explain polymer crystallization and the most important are divided by thermodynamic theories[20, 21] and kinetics theories.[1-4] The former explain some characteristics about semicrystalline state such as the crystal thickness, however there is a general agreement which considers that kinetic factors control the growth rate and the morphology of polymers.

Kinetic theories are able to predict the temperature dependence with the growth rate, the initial crystal thickness (l_c^*), and other important morphological parameters. These theories also explain that the final state is the kinetically most favorable state. Furthermore, the growth rate varies with crystal thickness (l_c) and therefore the result on a of different crystal thicknesses distribution will depend on the relation between the crystallization rate and the crystal thickness at each particular temperature.

Depending on the different polymer crystallization theories, they can take into consideration the overall crystallization kinetics, which includes both primary nucleation and crystal growth contributions,[17] or only the secondary nucleation (crystal growth). The most common theories among others are the Lauritzen and Hoffman (LH) model,[13-14]

which was developed to provide analytical expressions to quantify the energy barrier associated to the crystal growth, the Sadler and Gilmer theory,[1,22] the Strobl mesomorphic precursors thesis,[4] and the "free growth" theory formulated by Göler and Sachs.[2,23]

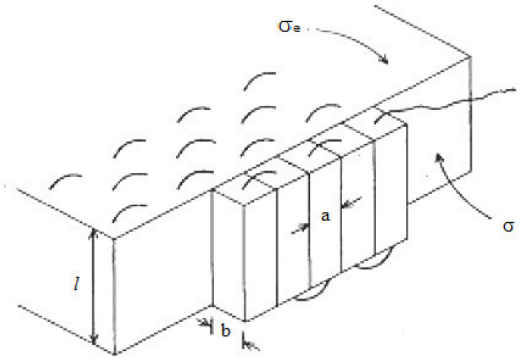

Figure 2. 8. *Growth model of a polymer lamellar crystal through the successive deposition of adjacent chain segments (Taken and modified from reference[24]).*

The last "free growth" theory formulated by Göler and Sachs is one of the first theories developed and the Avrami equation is one of its possible solutions. This theory also establishes that once a given nuclei is created, it grows unrestricted without the influence of others around that may have also been nucleated and could be growing within the same time. [2,19, 25]

2.3.5 The Avrami Equation

The Avrami equation describes how solids transform from one phase (state of matter) to another at constant temperature. The crystallization process occurs when polymers arrange into regular crystalline structures from an amorphous state, and as explained before in the text, the overall rate of crystallization involves two processes: the nucleation rate and the crystal growth rate.[26] One way to follow the crystallization kinetics has been developed through isothermal tests which are usually performed in a DSC. One of the most well-known theories used in order to study the isothermal overall crystallization kinetics is the Avrami model, which gives information about the variation of the crystalline content as a function of time at a constant crystallization temperature (T_c).

Avrami's model was proposed by Evans, Kolmogoroff and Avrami during the 1930s and 1940s, and it successfully describes the crystallization phenomenon of macromolecular chains,[27-30] however, it does not give any detail of the molecular process involved in the nucleation and growth of polymeric crystals. The development of Avrami's theory as well as its limits have been described in detail,[1,31] and it can be expressed as the following equation:[25]

$$1 - V_c = \exp(-k(t - t_0)^n) \qquad 2.4$$

where V_c is the relative volumetric transformed fraction and k the overall crystallization rate constant which includes contributions from both nucleation and growth. n is the Avrami index, whose value depends on the mechanism of nucleation and on the dimensionality of crystal growth, t is the experimental time and t_0 the induction time.

The induction time correction deals with the fact that a certain time may elapse before crystallization starts. In other words, once the isothermal crystallization temperature is reached, there is period of time in which there is not crystallization. This time is called the induction time. In mathematical terms, the Avrami equation is only defined when crystallization starts. Therefore, the experimental induction time must be subtracted from the absolute time.[32]

One way to express V_c as a funtion of mass fraction of the samples which crystallizes (W_c), is presented in equation 2.5;

$$V_c = \frac{W_c}{W_c + \left(\frac{\rho_c}{\rho_a}\right)(1 - W_c)} \qquad 2.5$$

where W_c is the mass fraction of the sample, ρ_c the density of a 100% crystalline sample and ρ_a the density of 100% amorphous sample. W_c is calculated from the following equation (equation 2.6), from the integration of the DSC experimental data measured during the isothermal crystallization;[1]

$$W_c = \frac{\Delta H\ (t)}{\Delta H_{total}} \qquad 2.6$$

where $\Delta H(t)$ is the enthalpy variation as function of the time spent at a given crystallization temperature and ΔH_{total} is the maximum enthalpy value reached at the end of the isothermal crystallization process.

The Avrami constant (k) is used to provide a quantitative evaluation of the crystallization evolution since it includes the contribution of both nucleation and crystal growth events. It is directly related with the overall crystallization rate $^1/_{t_{1/2}}$ and follows next equation:[17]

$$K = \left(\frac{1}{t_{1/2}}\right)^n ln2 \qquad 2.7$$

where $^1/_{t_{1/2}}$ is the inverse of the half of the crystallization time (that can be considered an experimental measurement of the overall crystallization rate), and $t_{1/2}$ corresponds to the time needed to achieve 50% of the overall crystallization.

On the other hand, the Avrami index also determines the nucleation type and the crystal growth geometry according to n value, which is composed of two terms: [33]

$$n = n_d + n_n \qquad 2.8$$

n_d represents the dimensionality of the growing crystals. This term only have integer values, 1, 2 or 3, corresponding to the formation of one, two and three dimensional entities. In the case of polymers the possible dimensions of the growing crystal are 2 or 3. They represent axialites (two dimensional lamellar aggregates) and spherulites (superstructural three dimensional aggregates), respectively.

The term n_n represents the time dependence of the nucleation. This term has a range of values between 0 and 1, where zero corresponds to an instantaneous nucleation, and one to a sporadic nucleation. However, there are several cases where nucleation is not purely instantaneous or purely sporadic and non-integer contributions to the Avrami index are obtained. Next table (table 2.1) represent the different combinations of both terms.

***Table 2. 1**. Avrami Index n for various types of nucleation and crystal dimensionality.* [25, 32]

Avrami index(n)	**Crystal dimensionality (n_d)**	**Nucleation dependence (n_n)**	**Description**
1	1	0	Intantaneus needle
2	1	1	Sporadic needle
2	2	0	Intantaneous Axialite
3	2	1	Sporadic Axialite
3	3	0	Intantaneous Spherulite
4	3	1	Sporadic Spherulite

The crystallization rate can be expressed as the inverse of the half of the crystallization time, which is usually close to the time at which spherulites impinged on one another and it is usually close to the time where primary crystallization ends and secondary crystallization begins. It can also be defined as the time needed to achieve 50% of the overall crystallization, and it is calculated by equation 2.9:

$$\tau_{50\%} = \left(\frac{-ln(1-V_c)}{k}\right)^{1/n}$$
$$\tau_{50\%} = \left(\frac{-ln\,0.5}{k}\right)^{1/n} = \left(\frac{0.69315}{k}\right)^{1/n} \qquad 2.9$$

In equation 2.9 it is assumed that at 50% of the conversion1-V_c is equal to 0.5. Therefore, the inverse of this time needed to achieve the 50% of the total transformation to the semi-crystalline state during the isothermal crystallization process ($1/\tau_{50\%}$) provides an experimental measure of the overall crystallization rate which includes both nucleation and growth. This value is determined experimentally from the isothermal crystallization at a given T_c, as shown in Figure 2.9 a.

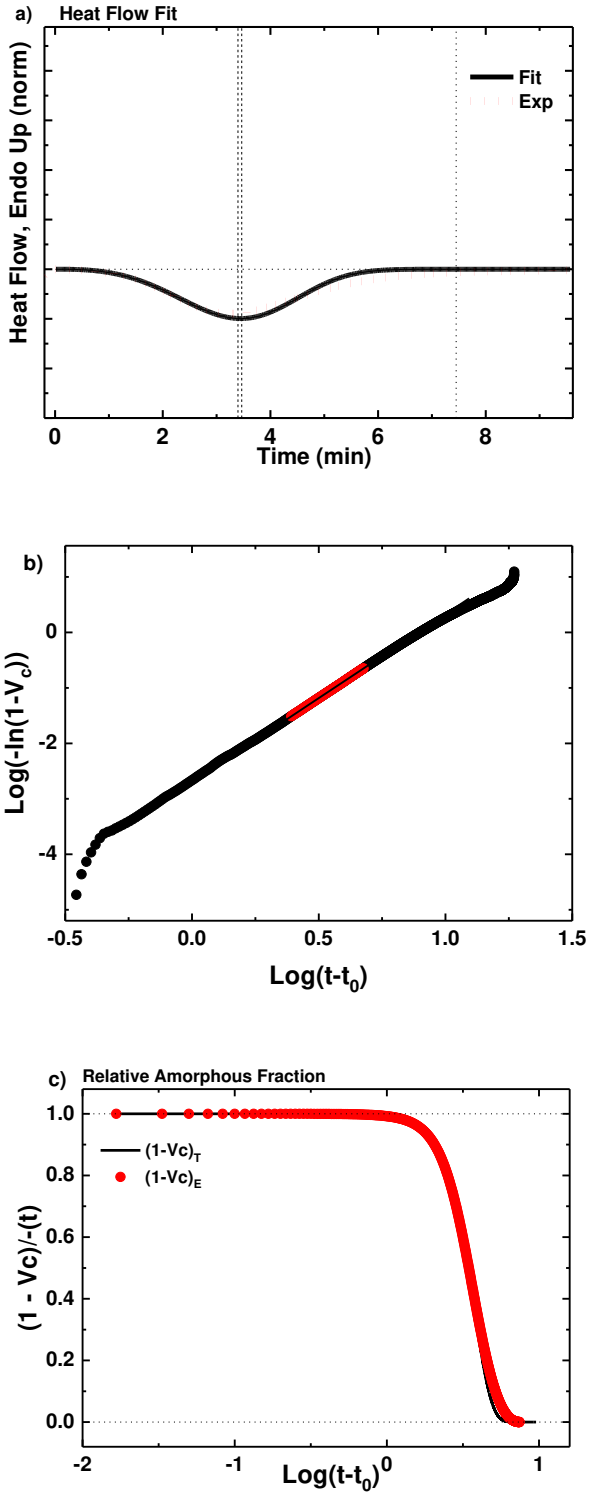

Figure 2. 9. *Avrami fits obtained by Origin: (a) Isothermal curve fit (b) Representation of the Avrami equation, (c) Untransformed relative amorphous fraction (1-V_c), as a function of time.*

After applying logarithmic properties to both sides, the following equation is obtained equation 2.10:

$$\log(-\ln[1 - V_c(t - t_o)]) = \log k + n \log(t - t_0) \quad 2.10$$

Following this equation straight lines are obtained for each studied temperature and from the slopes the Avrami index are calculated. By using the Origin plug-in developed by Lorenzo et al.[25], the Avrami fits are obtained. The Figure 2.9 shows an example of a representative fit of Avrami model and the Figure 2.9b the straight line previously mentioned in equation 2.10.

Figure 2.9a shows the Avrami fit to an isothermal crystallization curve obtained by DSC, while Figure 2.9b shows the untransformed relative amorphous fraction that indicates which percentage of transformation fits the equation. A good fit requires R2 values larger than to 0.9990 according to the recommendations of Lorenzo et al.25 while the Avrami equation must be fitted up to 50% of transformation, as it assumes free growth of the superstructural entities.

2.4 References

1. Gedde, U. W., *Polymer physics*. Chapman & Hall: London; New York, **1995**.
2. Mandelkern, L., *Crystallization of Polymers: Volume 2: Kinetics and Mechanisms*. Cambridge University Press, **2004**.
3. Schultz, J. M., *Polymer Crystallization: The Development of Crystalline Order in Thermoplastic Polymers.* Oxford: Oxford University Press, **2001**.
4. Reiter, G.; Strobl, G. R., *Progress in understanding of polymer crystallization*. Springer: Berlin, **2007**.
5. Hiemenz, P. C.; Lodge, T. P., *Polymer Chemistry, Second Edition*. Taylor & Francis: **2007**.
6. Lorenzo, A. T.; Müller, A. J., Estimation of the nucleation and crystal growth contributions to the overall crystallization energy barrier. *Journal of Polymer Science Part B: Polymer Physics* **2008,** *46*, 1478-1487.
7. Sperling, L. H., *Introduction to Physical Polymer Science: Fourth Edition*. **2005**, 1-845.
8. Gerngross, O.; Herrmann, L.; Abitz, W., *Z Physical Chemistry* **1930,** *10B*, 371.
9. Keller, A., A note on single crystals in polymers: Evidence for a folded chain configuration. *Philosophical Magazine* **1957,** *2*, 1171-1175.
10. Fischer, E. W., Step and spiral crystal growth of high polymers. *Z. Naturforch* **1957,** *12a*, 753-754.
11. Till, P. H., The growth of single crystals of linear polyethylene. *Journal of Polymer Science* **1957,** *24*, 301-306.
12. Flory, P. J., *Principles of polymer chemistry*. Ithaca : Cornell University Press, 1953.
13. Hoffman, J. D.; Davis, G. T.; Lauritzen, J. I., The Rate of Crystallization of Linear Polymers with Chain Folding. In *Treatise on Solid State Chemistry: Volume 3 Crystalline and Noncrystalline Solids*, Hannay, N. B., Ed. Springer US: Boston, **1976**, 497-614.
14. Lauritzen Jr, J. I.; Hoffman, J. D., Formation of Polymer Crystals with Folder Chains from Dilute Solution. *The Journal of Chemical Physics* **1959,** *31*, 1959.
15. Hoffman, J. D.; Miller, R. L., Kinetic of crystallization from the melt and chain folding in polyethylene fractions revisited: theory and experiment. *Polymer* **1997,** *38*, 3151-3212.
16. Sharples, A., *Introduction to polymer crystallization*. Edward Arnold: **1966.**
17. Van Krevelen, D. W.; Te Nijenhuis, K., *Calorimetric Properties*. **2009**, 109-128.

18. Turnbull, D.; Fischer, J. C., Rate of Nucleation in Condensed Systems. *Journal of Chemical Physics* **1949,** *17*, 71-73.
19. Müller, A. J.; Michel, R. M.; Lorenzo, A. T., Isothermal Crystallization Kinetics of Polymers," in Polymer Morphology: Principles, Characterization, and Processing, Q. Guo, Ed. Hoboken, NJ: John Wiley & Sons, Inc,. **2016**, 181-203.
20. Frank, F. C., I. Liquid crystals. On the theory of liquid crystals. *Discussions of the Faraday Society* **1958,** *25*, 19-28.
21. Peterlin, A.; Fischer, E. W.; Reinhold, C., Thermodynamic theory of finite thickness of polyethylene crystals. *Journal of Polymer Science* **1962,** *62*, S59-S62.
22. Sadler, D. M.; and Gilmer, G. H.; Selection of lamellar thickness in polymer crystal growth: A rate-theory model. *Physical Review B* **1988**, *38*, 5684-5693.
23. Ergoz, E.; Fatou, J. G.; and Mandelkern, L. Molecular Weight Dependence of the Crystallization Kinetics of Linear Polyethylene. I. Experimental Results. Macromolecules **1972**, *5*, 147-157.
24. Young, R. J.; Lovell, P. A., *Introduction to Polymers, Second Edition*. Taylor & Francis: **1991**.
25. Lorenzo, A. T.; Arnal, M. L.; Albuerne, J.; Müller, A. J., DSC isothermal polymer crystallization kinetics measurements and the use of the Avrami equation to fit the data: Guidelines to avoid common problems. *Polymer Testing* **2007,** *26*, 222-231.
26. Muthukumar, M., Shifting Paradigms in Polymer Crystallization. In *Progress in Understanding of Polymer Crystallization*, **2007**, 1-18.
27. Ziabicki, A., *Fundamentals of Fibre Formation: The Sciencs of Fibre Spinning and Drawing*. Wiley, London: **1976**.
28. Avrami, M., Kinetics of Phase Change. I, General Theory. *Journal of Chemical Physics* **1939,** *7*, 1103-1112.
29. Avrami, M., Kinetics of Phase Change. II, Transformation-Time Relations of Random Distribution Nuclei. *Journal of Chemical Physics* **1940,** *8*, 212-224.
30. Avrami, M., Granulation, Phase Change, and Microstructure Kinetics of Phase Change. III. *The Journal of Chemical Physics* **1941,** *9*, 177.
31. Wunderlich, B., In *Macromolecular Physics*, Academic Press, New York: **1973**.
32. Hiemenz, P. C., Lodge, T.P., *Polymer Chemistry*, **2007**.
33. Müller, A. J.; Balsamo, V.; Arnal, M. L., Nucleation and Crystallization in Diblock and Triblock Copolymers. In *Block Copolymers II*, Abetz, V., Ed. Springer Berlin Heidelberg, **2005**, 1-63.

Chapter 3

Experimental Part

3.1 Materials

Poly(butylene succinate-*ran*-butylene azelate) (PBS-*ran*-PBAz) copolymers were synthesized and characterized by the group of Professor Philippe Dubois in the University of Mons (UMONS), Belgium.[1]

The synthesis of PBS-*ran*-PBAz copolyesters was performed via a two-stage melt polycondensation. The reaction was performed in a specially designed and adapted 250 mL Inox Autoclave reactor (Autoclave-France, France) allowing high vacuum coupling with effective stirring for rapid byproduct diffusion and elimination.

1. Esterification at atmospheric pressure of SuA, DMAz, and BDO.

In the first step, 165 g of a mixture of SuA, DMAz, and BDO ([COOH]:[COOCH3] 1.0:0, 0.8:0.2, 0.6:0.4, 0.5:0.5, 0.4:0.6, 0.2:0.8 and 0:1.0 and [COOH/COOCH3]:[OH] 1:1.5, mol/mol) was directly charged into the Autoclave reactor at room temperature. The reactor was closed and purged with N_2 under stirring for 30 min. After that the temperature was increased to 190 °C under stirring and N_2 flow stopped. The reaction was conducted in the absence of catalyst at this temperature (190 °C) for 2h and at 200 °C for 2h under atmospheric pressure.

2. Polycondensation at reduced pressure.

In the second step, in order to start polycondensation stage TBT (1.4 mmol/mol diacid/ diester) was added and the pressur reduced to 20 mbar for 1 h 30 min. The reaction was further conducted at 230 °C for 1 h and at 250 °C for an extra 4 h.

When the reaction ended the product was then collected, cooled to room temperature, purified by dissolution in chloroform and washing once with 0.1 M aqueous hydrochloric acid solution. Then twice with demineralized water for catalyst extraction, and precipitated in seven-fold (v/v) excess of cold heptane. Finally the precipitate was recovered by filtering and drying until a constant weight at 40 °C under reduced pressure overnight.

Table 3. 1. *Characteristic Features of the PBS-ran-PBAz Copolyesters.*

BS/BAz, mol				13C NMR[a]			SEC[b]			
Entry	theoretical	experimental[c]	yield, %	L̄BS	L̄Baz	R	M̄n	M̄w	M̄p	Đ
1	1/0	1/0	87				25 300	59 800	49 500	2.36
2	0.8/0.2	0.82/0.18	94	7.83	1.47	0.81	22 300	39 300	37 100	1.76
3	0.6/0.4	0.61/0.39	93	7.37	1.82	0.7	31 300	161 600	62 500	5.16
4	0.5/0.5	0.58/0.42	87	2.17	1.92	0.98	36 500	125 000	77 500	3.44
5	0.4/0.6	0.45/0.55	92	1.85	2.32	0.97	38 300	124 300	80 600	3.24
6	0.2/0.8	0.25/0.75	85	1.69	3.05	0.92	39 600	136 600	73 200	3.45
7	0/1	0/1	89				42 500	102 800	79 700	2.42

[a]*Average sequence length of BS and BAz units (LBS, LBAz) and degree of randomness (R) calculated based on the expanded 13C NMR spectra.* [b]*Molecular characteristics of the P(BS-co-BAz) polyesters as obtained by SEC in chloroform using PS standards.* [c]*As obtained from 1H NMR (CDCl3, 300 MHz).*

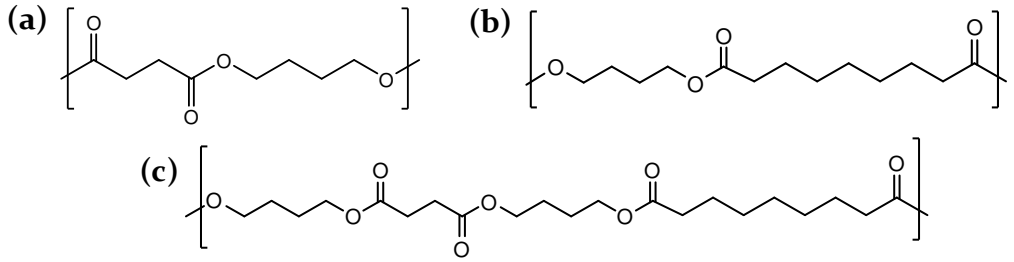

Figure 3. 1. *(a) Chemmical structure of poly(butylenesuccinate) (PBS). (b) Chemical structure of poly(butyleneazelate) (PBAz). (c) Chemical structure of the PBS-**ran-PB**Az copolymers.*

3.2 Experimental Techniques

3.2.1 Differential Scanning Calorimetry (DSC)

Differential scanning calorimetry, or DSC, is a thermoanalytical technique in which the difference in heat capacity (C_p) of a sample and a reference is recorded as a function of temperature. This technique is used to observe fusion and crystallization events as well as glass transition temperatures T_g. DSC can also be used to study oxidation, as well as other chemical reactions.

DSC is composed by two cells where in one the sample in a suitable pan and in the other the reference pan are placed. Two heating circuits control the temperature average

and the difference between the two ovens. The first circuit changes the temperature of the two ovens, both the sample and the reference, at a constant speed as indicated in the program. The second circuit compensates the temperature difference between the two ovens when any exothermic or endothermic process occurs in the sample, maintaining the temperature of the sample and the reference constant. This instrument uses a feedback loop to maintain the sample at a set temperature while measuring the power needed to do this against a reference furnace.

In polymers this technique allows to determine the changes that polymers suffer when the temperature varies, such as the melting temperature (T_m), the glass transition temperature (T_g), the crystallization temperature (T_c) or cold crystallization temperature (T_{cc}), transitions between crystalline phases, the percentage of crystallinity of a material as well as the enthalpies corresponding to the aforementioned thermal transitions. In addition, from the corresponding enthalpies the degree of crystallinity of the samples is calculated following equation;

$$W_c = \frac{\Delta H_m}{\Delta H_{(100\%)}} \qquad 3.1$$

where ΔH_m is the value of melting enthalpy and $\Delta H_{(100\%)}$ is the heat of fusion of a 100 % crystalline polymer.

DSC measurements were performed using a PerkinElmer Pyris 1 calorimeter equipped with a refrigerated cooling system Intracooler 2P, under nitrogen atmosphere flow and calibrated with indium (T_m = 156.61 ºC y ΔH_m = 28.71 J/g). The samples were weighted (~ 5mg) and sealed in aluminum pans.

The experimental conditions used according to the different studies are described in the following sections.

3.2.1.1 Nonisothermal studies

The nonisothermal measurements were performed following next steps:

a) Erasure of previous thermal history by heating the samples to 30 °C above their peak melting temperature for 3 min.

b) Cooling the molten sample to -30 °C at a controlled temperature (1, 5, 10 o 20 °C/min).
c) Hold the simple at -30 ºC for 1 minute.
d) Heating from -30 ºC to to 30 °C above their peak melting temperature at a controlled temperature (1, 5, 10 o 20 °C/min).

From these measurements the glass transition temperatures (T_g), the crystallization temperature (T_c) or the cold crystallization temperature (T_{cc}), the melting temperature (T_m) and the corresponding enthalpies of each one have been obtained.

3.2.1.2 Isothermal studies

Isothermal measurements were performed using the procedure recommended by Lorenzo et al.[2]

a) Erasure of previous thermal history by heating the samples to 30 °C above their peak melting temperature for 3 min.
b) Quenching the samples to a chosen isothermal crystallization temperature T_c at 60 °C/min.
c) Isothermal crystallization until saturation.
d) Heating from T_c to 30 °C above their peak melting temperature at 20 ºC/min.

In this case all the samples were able to crystallize during cooling; therefore before starting with the isothermal procedure, the minimum isothermal crystallization temperature was first determined. This was done by heating the sample directly from the chosen T_c temperature, after being quenched from the melt. The lowest temperature which did not show any melting enthalpy during immediate subsequent heating was the minimum isothermal crystallization temperature employed. In most cases a total of 10 or 17 isothermal temperatures were tested with variations of 1 ° C between them.

3.2.1.3 Self-nucleation (SN) Studies

Self-nucleation is a technique designed to enhance nucleation density. Crystal fragments or chain segments with residual crystal memory are the best nucleating source for any polymer.[3-5] The SN procedure applied here consists of several steps which are also plotted in Figure 3.2:

a) Erasure of previous thermal history by heating the samples to 30 °C above their peak melting temperature for 3 min (or to a temperature above the equilibrium melting point, if such temperature is known). All thermally sensitive nuclei are destroyed in this step leaving only temperature-resistant heterogeneous nuclei.
b) Creation of the initial "standard" semicrystalline state by cooling the molten polymer at 10°/min down to −30 °C. The peak crystallization temperature is recorded during cooling and identified as the "standard" crystallization temperature (or standard T_c), since it is a function of the number density of thermally stable nuclei of the polymer sample.
c) The sample is heated from −30 °C up to a selected self-nucleation temperature (denoted T_s) at 10 °C/min, and then the sample is held at this T_s temperature for 5 min. During this period of time at T_s, the sample could melt, self-nucleate or self-nucleate and anneal depending on the temperature value.
d) Subsequent cooling at 10 °C/min from Ts down to −30 °C.
e) Final melting. The sample is heated from −30 °C to above its melting point at 10 °C/min to record the full melting behavior.

The effects of the SN treatment can be assessed by examining steps d) and e) above. Fillon et al.[3] defined the so-called "domains" of self-nucleation as follows:

Domain I (complete melting domain). The polymer is in domain I when complete melting occurs and the crystalline memory of the material is erased.

Domain II (exclusive self-nucleation domain). When the T_s temperature is able to self-nucleate the material without causing annealing, T_c (the peak crystallization temperature) is shifted to higher temperatures while the subsequent melting does not show any signs of annealing. When the sample is within domain II, an increase in nuclea-

tion density is obtained as indicated by the increase in T_c values. The minimum Ts temperature within domain II is defined as the "ideal self-nucleation temperature" ($T_{c,ideal}$), since it is the temperature that causes maximum self-nucleation without annealing.

Domain III (self-nucleation and annealing domain). When Ts is too low, partial melting is produced, and the unmolten crystals anneal during the 5 min at T_s.

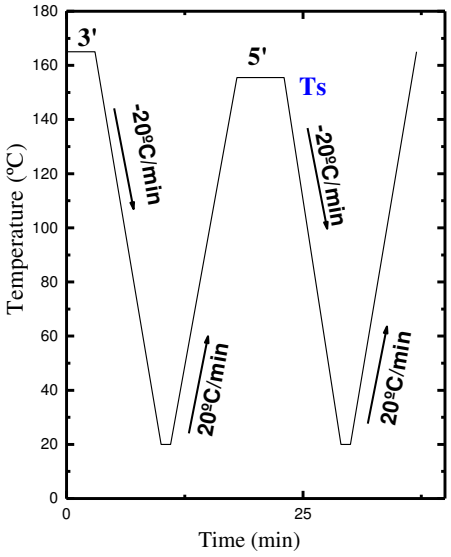

Figure 3. 2. *Self-Nucleation thermal procedure.*

3.2.1.4 Successive Self Nucleation and Annealing (SSA)

Successive self Nucleation and Annealing (SSA) thermal protocol was designed and implemented for the first time by Müller et al. in 1997 and its use has become widely spread in the past decades.[6-14] This technique is based on the molecular segregation process that occurs when polymers are isothermally crystallized from the melt.[4, 15]

Thermal fractionation exploits the molecular segregation capacity exhibited by semicrystalline polymeric systems when they are isothermally crystallized or annealed. Fractionation occurs because defects that interrupt the linear crystallizable sequences are generally segregated to the amorphous regions of the material. SSA sequentially applies a series of self-nucleation and annealing steps to a polymer sample. After the thermal conditioning is over, a final DSC heating scan shows the distribution of thermal fractions

(i.e., distribution of peak melting points) induced by the SSA treatment as a result of the heterogeneous nature of the chain structure of the polymer under analysis. SSA is capable of performing thermal fractionation with much better resolution and in faster times than previously available techniques, such as step crystallization. [15, 16]

The SSA experimental protocol is based on the sequential application of self-nucleation and annealing steps designed to perform thermal fractionation in a fast and efficient way. The procedure to apply SSA is shown schematically in Figure 3.3 and described below:

(a) Erasure of thermal history by heating the samples to 30 ºC above their peak melting temperature for 3 min.
(b) The sample is cooled at 20 ºC/min to -30 ºC to create the initial ‘‘standard’’ thermal history. Then, the sample is equilibrated at -30 ºC during 3 min.
(c) The sample is heated at 20 ºC/min to a temperature denoted T_s. At this first T_s temperature, the sample will only self-nucleate without any annealing (i.e., T_s will be high enough to almost completely melt the polymer but low enough to leave self-nuclei that can later self-seed the polymer during cooling). In fact, this first T_s temperature corresponds with the ideal self-nucleation temperature within Domain II (see ref. 16) of the sample with the highest melting point (i.e., neat PBS).
(d) The sample is held at this T_s for 5 min. The same fractionation time (i.e., 5 min) will be used in the following different SSA steps.
(e) The sample is cooled at a constant rate at 20 ºC/min from T_s to -30 ºC, so the polymer will crystallize during cooling after self-nucleation. Then, the sample is equilibrated at -30 ºC during 3 min.
(f) The sample is heated at 20 ºC/min from -30ºC to T_s (1), and it is held at this temperature for 5 min. The difference in temperature between T_s and T_s (1) is set at 5 ºC, and it is denoted as the fractionation window (ΔT_f). It determines the size of the thermal fraction and it is kept constant during all SSA experiments. The T_s (1) temperature will be within Domain III. Therefore, the unmolten part of the sample will undergo annealing and in this way the first thermal fraction is created, i.e., a fraction of lamellar crystals with melting points higher than T_s (1).

(g) The sample is cooled down from T_s (1) to -30 ºC at 20 ºC/min, and is held at this temperature for 3 min.

(h) Steps ‘‘f’’ and ‘‘g’’ are repeated until the full melting range of the samples is covered. The number of repetitions (cycles) is chosen to cover the entire melting range of the samples with a “standard” thermal histories. In the case of neat PBS the fractionation was performed with 10 cycles (from 116ºC to 71ºC) while in the case of $BS_{58}BAz_{42}$, 14 cycles (from 76ºC to 11ºC).

(i) Finally, the sample is heated at 20 ºC/min to the melt state, during this final heating run the consequences of SSA fractionation are revealed.

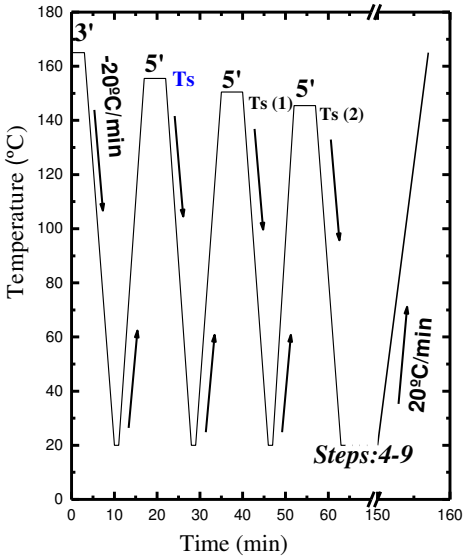

Figure 3. 3. *SSA thermal protocol schematic representation. Cooling and heating scans are performed at a constant scanning rate.*

3.2.2 Wide Angle X-ray Scattering (WAXS) and Small Angle X-ray Scattering (SAXS)

Wide-angle *X*-ray Scattering (WAXS) and Small Angle *X*-ray Scattering (SAXS) are *X*-ray-diffraction techniques that are often used to determine the crystalline structure of polymers. WAXS specifically refers to the analysis of Bragg peaks scattered to wide an-

gles, which (by Bragg's law) implies that they are caused by sub-nanometer-sized structures. When X-rays are directed in solids they will scatter in predictable patterns based upon the internal structure of the solid. The diffraction pattern generated allows researchers to determine the chemical composition or phase composition of the film, the texture of the film (preferred alignment of crystallites), the crystallite size and presence of film stress. According to this method the sample is scanned in a wide-angle X-ray goniometer, and the scattering intensity is plotted as a function of the 2θ angle. X-ray diffraction is a non destructive method of characterization of solid materials. A crystalline solid consists of regularly spaced atoms (electrons) that can be described by imaginary planes. The distance between these planes is called the d-spacing. The intensity of the d-space pattern is directly proportional to the number of electrons (atoms) that are found in the imaginary planes.

By using Small Angle *X*-ray Scaterring (SAXS) technique, nanoscale density differences in a sample can be quantified. This is achieved by analyzing the elastic scattering behaviour of X-rays when travelling through the material, recording their scattering at small angles (typically 0.1 - 10°, hence the "Small-angle" in its name). Depending on the angular range in which a clear scattering signal can be recorded, SAXS is capable of delivering structural information of dimensions between 1 and 100 nm, and of repeat distances in partially ordered systems of up to 150 nm.

Wide Angle *X*-ray scattering measurements were performed on a Bruker D8 Advance diffractometer working in parallel beam geometry. By using a Göbel mirror, the originally divergent incident X-ray beam from a line focus X-ray tube (Cu, operating at 40 kV and 40 mA) is transformed into an intense and parallel beam that is free of Kβ radiation. The parallel beam optics required in the secondary beam path is achieved by an equatorial axial Soller slit of 0.2°. The linear detector LYNXEYE used presents an active area of 14.4 mm ×16 mm. Measurements were performed in reflection (θ−2θ configuration) varying 2θ from 4 to 30° with a step of 0.05°. The measuring time employed was 10 s/point. The films were placed in an Anton Paar TTK 450 low-temperature chamber under vacuum conditions allowing variations of the sample temperature between −193 and 450 °C with 0.1 °C resolution.

SAXS was used to probe the lamellar structure within the spherulites by determining their long periods. The experiments were conducted on a Rigaku 3-pinhole PSAXS-L equipment operating at 45 kV and 0.88 mA. The MicroMax-002+ *X*-ray Generator System is composed by a microfocus sealed tube source module and an integrated *X*-ray generator unit which produces CuKα transition photons of wavelength λ = 1.54 Å. The flight path and the sample chamber in this equipment are under vacuum. The scattered *X*-rays are detected on a two dimensional multiwire *X*-ray detector (Gabriel design, 2D-200X). This gas-filled proportional type detector offers a 200 mm diameter active area with c.a. 200 μm resolution. The azimuthally averaged scattered intensities were obtained as a function of wave vector q, $q = 4\pi\lambda^{-1} \sin\theta$, where θ is half the scattering angle. Reciprocal space calibration was done using silver behenate as standard. Films were placed in a Linkam Scientific Instruments THMS 600 temperature controller (range: −196 to +600 °C, stability <0.1 °C) in transmission geometry, with a sample to detector distance of 2 m. Measuring times of 20 min were employed.

3.2.3 Polarized Light Optical Microscopy (PLOM)

The polarized light microscope is an optical microscope equipped with two polarizers located above and below the sample. The polarized light microscope is designed to observe and photograph samples that are visible primarily due to their optically anisotropic character. In order to accomplish this task, the microscope must be equipped with both a polarizer, positioned in the light path somewhere before the specimen, and an analyzer (a second polarizer), placed in the optical pathway between the objective rear aperture and the observation tubes or camera port. When the polarizers are crossed, light goes only in the orthogonal direction. This means that light is not transmitted when there is no sample or when the sample has an isotropic disordered structure, as in the case of amorphous polymers or semicrystalline molten polymers. In the case when polarizers are crossed and a semicrystalline polymer is observed, a birefringent sample, an interference phenomenon occurs allowing the light beam to pass through the microscope. Therefore, the areas of the sample with ordered anisotropic regions appear bright on a smooth and dark background, which corresponds to the fraction of amorphous or molten material.

The spherulitic morphologies were observed by two polarized light optical microscopy (PLOM). A Leitz Aristomet polarized microscope equipped with polarizers and a sensitive red tint plate (this was employed to determine the sign of the spherulites) and an Olympus BX51 polarized light optical microscope. A Linkam THMS600hot stage connected to a liquid nitrogen system was used to control the temperature. The samples were pressed on a glass slide and covered with a glass coverslip. They were heated to a temperature of 30 °C above their DSC melting peak and they were kept at this temperature for 5 min to erase previous thermal history. Samples were then quickly cooled to the selected crystallization temperature. Micrographs were taken with a Leica DC420 digital camera.

3.2.3.1 Spherulitic growth rate (*G*)

Spherulite growth rate experiments were also performed by recording their growth by PLOM (Olympus BX51), incorporating a λ plate in between the polarizers at 45° to facilitate observation and determine the sign of the birefringence. In order to determine the spherulitic growth rate (G) as a function of crystallization temperature (T_c) The dimensions of the spherulites were periodically registered with an Olympus SC50 digital camera after following procedure described below:

(a) Erasure of thermal history by heating the samples to 30 ºC above their peak melting temperature for 3 min.
(b) The sample is cooled from the melt to a selected isothermal crystallization temperature (T_c) at 60°C /min.
(c) At this temperature (*Tc*) the dimensions of the spherulites are periodically registered until they impinged on one another completely filling the microscope observation field.
(d) With DIGIMIZER program, the radius of the spherulites are measured taking into account the scale used in the measurements. Once the radio data is obtained, it is plotted as a function of time obtaining a straight line whose slope corresponds to G at that measured *T*c.
(e) The processes described from a) to d) are repeated at different crystallization temperatures (*T*c) in order to know Spherulite growth rate at different temperatures.

3.2.3.2 Nucleation density (*ρ)*

The density of nuclei as a function of time was determined counting the number of nuclei as a function of time. To do this, the steps from (a) to (c) described in the previous section are followed. In this case once T_c is reached, photographs are taken until the saturation when spherulites impinge on one another completely filling the microscope field. As the thickness of the sample is also determined, the nuclei number in a given volume, the density of nuclei (ρ) at a selected crystallization temperature (T_c) is obtained according to equation 3.2;

$$\rho_{nuclei} = N°Nuclei \cdot V \qquad 3.2$$

3.2.4 Atomic Force Microscopy (AFM)

Atomic Force Microscopy (AFM) is a type of scanning probe microscopy (SPM), with demonstrated resolution on the order of fractions of a nanometer, more than 1000 times better than the optical diffraction limit. The information is gathered by "feeling" or "touching" the surface with a mechanical probe. Though AFM polymer morphology at the nanoscale can be observed, including lamellar thickness and growth mode of the crystals.

AFM measurements were performed using a Di_Veeco Multimode scanning probe microscope equipped with a Nanoscope IIIa controller. For AFM studies, the sample BS45BAz55 (see Table 1) was spin-coated into a homogeneous thin film on a mica substrate from chloroform solution (40 mg/mL). The film was then melted to erase thermal history at 100 °C for 5 min. Then it was cooled at 10 °C/min until 35 °C. At this temperature, the sample was isothermally crystallized for 15.5 h, and then cooled to room temperature. Height and phase images of spherulites were recorded in tapping mode using silicon TESP tips having a resonance frequency of approximately 320 kHz and a cantilever spring constant about 42 N/m. The micrographs size were in a range of 1 to 3 μm.

3.2.5 Broadband Dielectric Spectroscopy (BDS)

The dielectric spectroscopy technique is used to study relaxation processes which are caused by the rotational fluctuations of molecular dipoles. This technique is based on the application of an external field ($\vec{E}$) which weakly perturb the molecular dipole system of a sample from the equilibrium.[17] Once the field is removed, the dipole system is able to return to the equilibrium supplying information about the spontaneous fluctuations in the system, and therefore through this technique information about the dynamical processes of characteristic parts of a molecules or systems is obtained. Whit this technique the dielectric properties of a medium can be measured as a function of the frequency, by an external oscillating field, and also in the time domain.

Measurements of the complex dielectric permittivity ($\varepsilon^* = \varepsilon' - i\varepsilon''$) *vs* frequency were performed in the range 10^{-1}–10^6 Hz, using a Novocontrol high resolution dielectric analyzer (alpha-A analyzer). The sample preparation consisted in forming a parallel plate capacitor filled with the sample previously melted in a hot stage under nitrogen atmosphere. An upper electrode of 20 mm was placed on the previously prepared film over the gold coated disk, and a separation of 100 μm between both electrodes was maintained by using a cross-shaped Teflon spacer of small area. The sample cell was set in a cryostat, and its temperature was controlled via a nitrogen gas jet stream coupled with the Novocontrol Quatro controller. Before the dielectric measurements, the sample capacitor was subjected to vacuum for a few hours, and once inside the BDS cell, it was heated above the melting temperature of the polymer to erase thermal history. Isothermal frequency scans were performed every fifth degree during cooling down to 130 K. Sample temperature was controlled by nitrogen gas flow with temperature stability better than ±0.1 K. In addition isochronal measurements at frequencies every decade between 10–10^6 Hz were carried out at a 3 K/min heating rate.

When analyzing the data, the ratio $\varepsilon^*/\varepsilon_\infty$ has been used trying to minimize the effect of the uncertainties in sample geometry when comparing results from different samples. Note that ε_∞, as determined from very low temperature behavior at high frequencies, is free of significant dipole reorientation contributions and therefore related mainly with the

induced polarization phenomena. Consequently, no significant differences in the actual ε_∞ values among the different samples should exist.

3.3 References

1. Mincheva, R.; Delangre, A.; Raquez, J. M.; Narayan, R.; Dubois, P., Biobased Polyesters with Composition-Dependent Thermomechanical Properties: Synthesis and Characterization of Poly(butylene succinate-co-butylene azelate). *Biomacromolecules* **2013,** *14*, 890-899.
2. Lorenzo, A.; Arnal, M.; Albuerne, J.; Müller, A., DSC isothermal polymer crystallization kinetics measurements and the use of the Avrami equation to fit the data: Guidelines to avoid common problems. *Polymer Testing* **2007**, *26*, 222-231.
3. Fillon, B.; Wittmann, J. C.; Lotz, B.; Thierry, A., Self-nucleation and recrystallization of isotactic polypropylene (alpha-phase) investigated by differential scanning calorimetry. *Journal of Polymer Science Part B-Polymer Physics* **1993,** *31*, 1383-1393.
4. Müller, A. J.; Arnal, M. L., Thermal fractionation of polymers. *Progress in Polymer Science* **2005,** *30*, 559-603.
5. Lorenzo, A. T.; Arnal, M. L.; Sanchez, J. J.; Muller, A. J., Effect of annealing time on the self-nucleation behavior of semicrystalline polymers. *Journal of Polymer Science Part B: Polymer Physics* **2006,** *44*, 1738-1750.
6. Michell, R. M.; Müller, A. J.; Deshayes, G.; Dubois, P., Effect of sequence distribution on the isothermal crystallization kinetics and successive self-nucleation and annealing (SSA) behavior of poly(ε-caprolactone-co-ε-caprolactam) copolymers. *European Polymer Journal* **2010,** *46*, 1334-1344.
7. Denisova, Y. I.; Shandryuk, G. A.; Krentsel', L. B.; Blagodatskikh, I. V.; Peregudov, A. S.; Litmanovich, A. D.; Kudryavtsev, Y. V., Thermal fractionation of vinyl acetate-vinyl alcohol copolymers. *Polymer Science Series A* **2013,** *55*, 385-392.
8. Liu, L.; Tong, Z. Z.; Xu, J. T.; Fan, Z. Q.; Yu, K. M., Composition heterogeneity of tetrafluoroethylene-hexafluoropropylene random copolymers characterized by successive self-nucleation and annealing. *Journal of Thermal Analysis and Calorimetry* **2013,** *114*, 573-579.
9. Mazzola, N.; Cáceres, C. A.; França, M. P.; Canevarolo, S. V., Correlation between thermal behavior of a sealant and heat sealing of polyolefin films. *Polymer Testing* **2012,** *31*, 870-875.

10. Franco-Urquiza E, S. O., Gámez-Pérez J, Martínez AB,; ML, M., Influence of processing on the ethylene-vinyl alcohol (EVOH) properties: Application of the successive self-nucleation and annealing (SSA) technique. *eXPRESS Polymer Letters* **2010,** *4*, 153-160.
11. Wang, S.; Yang, D., Effect of the γ-form crystal on the thermal fractionation of poly(propylene-co-ethylene). *Journal of Polymer Science Part B: Polymer Physics* **2004,** *42*, 4320-4325.
12. Villarreal, N.; Gobernado-Mitre, I.; Merino, J. C.; Pastor, J. M. Comparative study between metallocene polyolefin blends modified by Beta-Irradiation and a silane crosslinking process. **2005**, 260-264.
13. Horváth, Z.; Menyhárd, A.; Doshev, P.; Gahleitner, M.; Varga, J.; Tranninger, C.; Pukánszky, B., Chain regularity of isotactic polypropylene determined by different thermal fractionation methods. *Journal of Thermal Analysis and Calorimetry* **2014,** *118*, 235-245.
14. Liu, W.; Wang, W.-J.; Fan, H.; Yu, L.; Li, B.-G.; Zhu, S., Structure analysis of ethylene/1-octene copolymers synthesized from living coordination polymerization. *European Polymer Journal* **2014,** *54*, 160-171.
15. Müller, A. J.; Hernández, Z. H.; Arnal, M. L.; Sánchez, J. J., Successive self-nucleation/annealing (SSA): A novel technique to study molecular segregation during crystallization. *Polymer Bulletin* **1997,** *39*, 465-472.
16. Arnal, M. L.; Balsamo, V.; Ronca, G.; Sánchez, A.; Müller, A. J.; Cañizales, E.; Urbina de Navarro, C., Applications of Successive Self-Nucleation and Annealing (SSA) to Polymer Characterization. *Journal of Thermal Analysis and Calorimetry* **2000,** *59*, 451-470.
17. F. Kremer and A. Schönhals, (eds.) Broadband Dielectric Spectroscopy, *Springer-Verlag, Berlín* **2003**.

Chapter 4

Crystallization and Morphology of PBS-ran-PBAz Copolymers

4.1 Introduction

As explained before in Chapter 1, the copolymerization is an interesting way to modify the crystallization behavior of homopolymers, introducing new monomers and sequences inside the macromolecular architectures. In this chapter, we make use of the previously synthesized PBS-*ran*-PBAz copolymers by Mincheva et al.[1] in order to study their structure, nonisothermal crystallization and morphology, as well as analyze their properties which can be tailored by composition and thermal history. We also studied if comonomer inclusion is present during nonisothermal crystallization and if copolymers can be considered isodimorphic under such conditions; for that, results obtained from small angle X-ray scattering (SAXS) measurements have been correlated with data obtained from DSC, WAXS, PLOM, and AFM.

4.2 Differential scanning calorimetry

4.2.1 Nonisothermal DSC measurements

The standard nonisothermal behavior of neat PBS and PBAz homopolymers and PBS-*ran*-PBAz copolymers are presented in Figure 4.1. Table 4.1 lists all the relevant transition temperatures and enthalpies. The copolymers exhibited a single glass transition temperature (T_g) (see Table 4.1) in between the T_g values of the homopolymers, as expected for random copolymers that form a miscible amorphous phase.

Even though the prepared copolymers are random, as demonstrated previously by ^{13}C NMR,[1] all samples were able to crystallize, and their crystallization and melting temperatures were found to be a strong function of composition. The results are consistent with previous works.[1-3]

Table 4. 1. *Molar Composition Determined by 1 H NMR and Thermal Transitions Determined by DSC (at 10°C/min) of the Materials Employed in This Work*[a].

	Code	Composition (PBS/PBAz), mol[1]		Data DSC						
		Theoretical	Exp. (^{1}H NMR)	$T_{g,\text{onset}}$ (ºC)	T_{m1} (ºC)	T_{m2} (ºC)	ΔH_{m1} (J/g)	ΔH_{m2} (J/g)	T_c (ºC)	ΔH_c (J/g)
1	BS	1/0	1/0	-36	114.7	--	66	--	75	69
2	$BS_{82}BAz_{18}$	0.8/0.2	0.82/0.18	-50	98	--	70	--	59	72
3	$BS_{61}BAz_{39}$	0.6/0.4	0.61/0.39	-56	72.3	--	70	--	12	79
4	$BS_{58}BAz_{42}$	0.5/0.5	0.58/0.42	-57	60.3	--	74	--	3.2	77
5	$BS_{45}BAz_{55}$	0.4/0.6	0.45/0.55	-61	46.3	26.4	72	57	9.4	57
6	$BS_{25}BAz_{75}$	0.2/0.8	0.25/0.75	-62	--	34.4	--	80	16	67
7	BAz	0/1	0/1	-63	--	41.2	--	65	22	58

[a]The melting enthalpies are normalized by composition in all cases. The crystallization enthalpies are also normalized by composition, except for the coincident crystallization case in sample $BS_{45}BAz_{55}$. Estimation of errors is based on the repetition of DSC experiments; calibration and baseline drifts indicate that transition temperatures are valid within 0.5 °C (except for T_g measurements which are within 1 °C) and enthalpy values within 1 J/g.

One way to explain why the copolymers can crystallize in the entire composition range is to consider that the PBS-*ran*-PBAz copolymers are isodimorphic and therefore can crystallize in crystalline unit cells that resemble those of the homopolymers, but with inclusions of the second component repeating units.

Figure 4.1a shows that all materials exhibit a main sharp crystallization peak during cooling from the melt that in some cases contains a high temperature shoulder or tail, like in $BS_{61}BAz_{39}$ and $BS_{45}BAz_{55}$.

The subsequent heating scans, after cooling from the melt (Figure 4.1a), are presented in Figure 4.1b. PBS exhibits cold crystallization during the scan followed by a double melting peak. The presence of two melting peaks could be due to a partial melting and recrystallization process during the heating scan or to the melting of two populations with different mean lamellar thickness (one lamellar population formed during the cool-

ing scan in Figure 4.1a and the second during the cold crystallization process in Figure 4.1b). PBAz displays a single sharp melting endotherm that is consistent with its previous comparably sharp crystallization exotherm (Figure 4.1a).

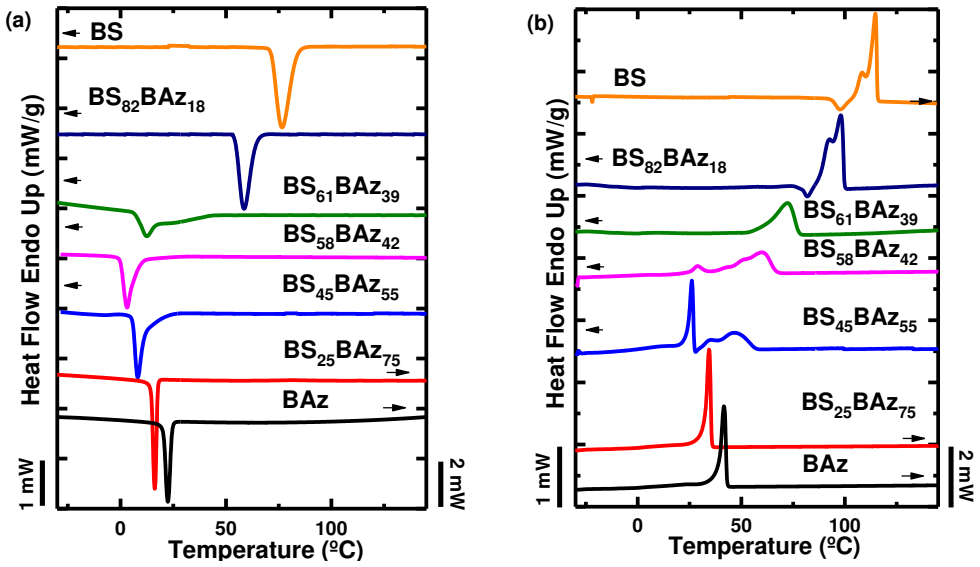

Figure 4. 1. *(a) Cooling DSC scans from the melt and (b) subsequent heating scans for the indicated homopolymers and random copolymers samples. Scanning rates: 10 ºC/min.*

When BAz is incorporated in the copolymer, the melting of the crystalline PBS phase is depressed to lower temperatures because PBS linear sequences are frequently interrupted by PBAz repeating units. However, since at high PBAz incorporation (for copolymers where PBAz content is between 39 and 55%), the PBS phase is still undergoing crystallization (according to WAXS measurements to be presented below), it is possible that PBS crystals incorporate some randomly distributed repeating units of BAz. WAXS results to be presented below confirm the inclusion of PBAz into PBS-rich crystalline phase. We will refer to those copolymeric PBS crystals (that contain PBAz moieties in their unit cells) as PBS-rich crystalline phase.

WAXS results (to be presented below) indicate that only PBS-rich crystals are formed in the samples with 58% or more PBS content. On the other hand, both WAXS

and DSC show that $BS_{45}BAz_{55}$ is the only copolymer that is able to form both PBS-rich and PBAz-rich phase crystals. Finally, the copolymer with 75% PBAz contains only PBAz-rich crystals.

Figure 4.2 shows plots of crystallization (Figure 4.2a) and melting (Figure 4.2b) temperatures as a function of composition, with legends identifying the crystalline phases in accordance with parallel WAXS experiments (presented below). The presence of a eutectic point is readily apparent and has been reported for several iso-dimorphic copolyesters.[4]

Figure 4.2 illustrates the tremendous potential of the thermal properties of isodimorphic copolymers. By a careful choice of composition, the melting point and therefore the applications of these biobased copolymers can be tailored from room temperature to 100 °C.

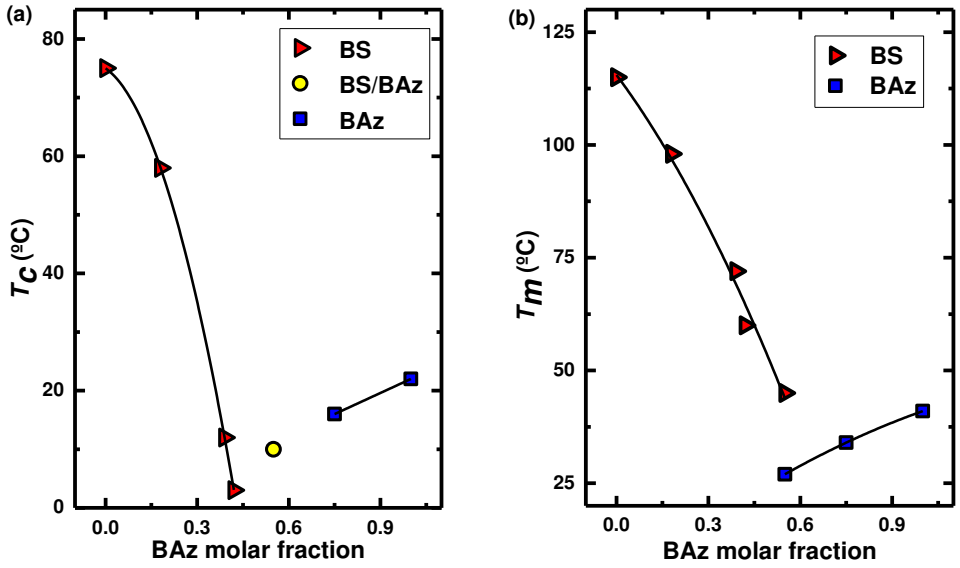

Figure 4. 2. *Peak crystallization (a) and melting (b) temperatures as a function of copolymer composition.*

According to the thermal behavior presented in Figure 4.2, the eutectic point should be very close to 55% BAz content. For copolymers where the random copolymer chains contain a majority of BS repeating units (i.e., whose composition is lower or equal

to 42% BAz), PBS dominates the copolymer structural behavior. In these cases, the crystals with a large amount of BS repeating units (and a small amount of BAz "impurities" within their unit cells) will be thermodynamically favored and in fact, only PBS type crystals are formed according to WAXS (see below). On the other hand, for compositions with more than 55% BAz, only PBAz like crystals can form. For compositions near the eutectic point both crystalline phases can be produced in double crystalline random copolymers.

For the $BS_{45}BAz_{55}$ copolymer, whose composition is near the eutectic point, coincident crystallization of both phases occurs. This means that the crystallization exotherms of the PBS and the PBAz-rich phase overlap (see Figure 4.1a) and as a result a single point is plotted in Figure 4.2a, since only one sharp crystallization peak is observed (the exotherm is broad and asymmetric). During the heating scan (Figure 4.1b) fully separate melting of PBAz and PBS-rich crystalline phases is clearly seen and two melting points were plotted in Figure 4.2b at the corresponding composition for 55% BAz. This is the only copolymer that is able to develop a double crystalline structure because it is close to the eutectic point where both phases have similar chances for crystallization. It would be highly unlikely that a random copolymer with an almost symmetric composition exhibits the crystallization of its two components without isodimorphic behavior (i.e., some comonomer inclusion must be present in both phases as confirmed by WAXS below).

A closer look at the coincident crystallization of both phases within $BS_{45}BAz_{55}$ is presented in Figure 4.3. Figure 4.3a shows cooling scans from the melt at 10 °C/min that are stopped at specific temperatures followed by immediate reheat scans (also at 10 °C/min) to record the melting behavior, see Figure 4.3b.

When $BS_{45}BAz_{55}$ is cooled down to −30 °C, both phases crystallize until saturation (at 10 °C/min). The cooling DSC scan in Figure 4.3a shows a wide crystallization exotherm with a high temperature shoulder (between 25 and 12.5 °C), a sharp peak at approximately 9 °C, and a broad weak crystallization exotherm between 0 and −25 °C

(seen only in a close-up indicated with an arrow). The subsequent heating scan shown in Figure 4.3b clearly demonstrates the melting of both PBAz-rich crystalline phase (in a broad bimodal melting range, with a low intensity first peak between −10 and 20 °C, hence a closeup is provided, and a sharp second peak at 26 °C approximately) and PBS-rich crystalline phase (with a broad bimodal melting peak between 27 and 56 °C).

The complex thermal behavior of $BS_{45}BAz_{55}$ can be understood by comparing Figure 4.3a and Figure 4.3b:

a) Upon cooling from the melt, only PBS-rich phase crystallizes as long as the sample is cooled down to 20 °C (see data for cooling and subsequent heating scans from the melt down to 20 and 15 °C, the first two traces at the top of parts a and b of Figure 4.3 and their corresponding enthalpy values). Notice the total absence of a melting peak for the PBAz-rich phase for the top DSC trace corresponding to 20 °C in Figure 4.3b. In the case of 15 °C, a very small melting peak corresponding to the PBAz-rich phase crystals fusion was detected.
b) The PBAz-rich phase can only start its crystallization from the melt when cooled down to temperatures of at least 15 °C (see above) and below, in a coincident fashion with the PBS-rich phase (see the corresponding DSC traces labeled with 15 and 12.5 °C in Figure 4.3a). Upon subsequent heating from 12.5 °C, note the small but clear melting peak at approximately 26 °C that corresponds to the PBAz-rich crystals fusion in Figure 4.3b.
c) The PBS-rich phase achieves its maximum degree of crystallinity when cooled down to 10 °C according to Figure 4.3b. The enthalpy values reported in Figure 4.3b for the melting of the PBS-rich phase increase as the sample is cooled to progressively lower temperatures and then become constant within the error of the measurements at temperatures of 10 °C or below (25−27 J/g).
d) The PBAz-rich phase keeps crystallizing all the way down to −30 °C, although most of the crystallization had already occurred at 0 °C.
e) The main crystallization peak at 9 °C in Figure 4.3a occurs in a temperature range where both phases crystallize simultaneously or coincidentally.

Coincident crystallization processes have also been found in double crystalline diblock copolymers that are either miscible in the melt or in the weak segregation regime.[5-8] Following these previous works, we decided to employ the self-nucleation technique[9, 10] to try to separate the individual crystallization process for each phase.

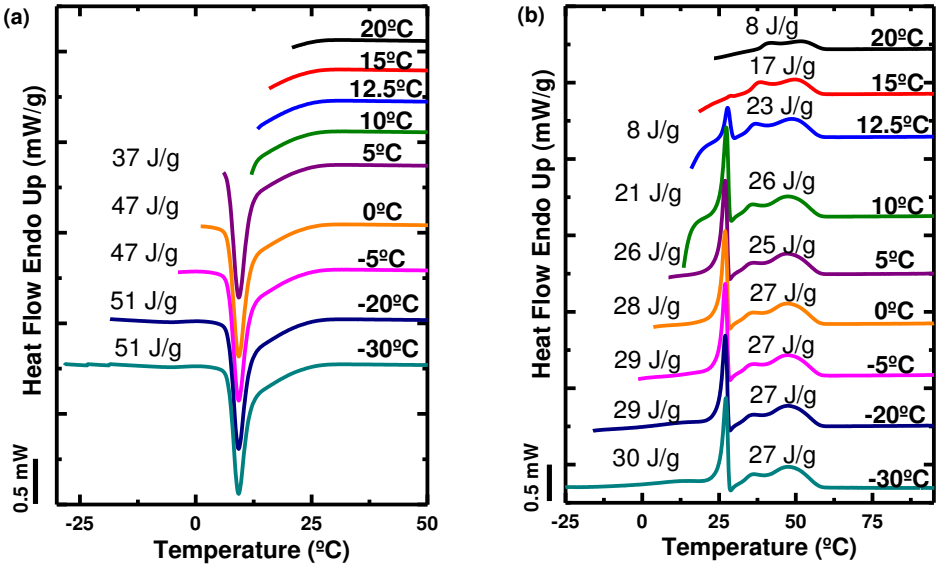

Figure 4. 3. *(a) DSC cooling scans for the double crystalline $BS_{45}BAz_{55}$ that exhibits coincident crystallization. The legend contains the total crystallization enthalpy (left-hand side) and the final temperature of the scan (right-hand side). (b) Subsequent DSC heating scans. The legend contains the melting enthalpy of the PBAz-rich phase (low temperature melting peak at approximately 26 °C) and the PBS-rich phase (bimodal melting peak in the range 29−60 °C) without normalizing by composition. The legend also includes (right-hand side) the starting temperature for the scan. Scanning rate: 10 °C/min.*

4.3 X-ray Scattering

4.3.1 Wide Angle X-ray Scattering (WAXS)

Samples for WAXS were prepared by melting films in a hot stage at identical conditions to the thermal protocol applied to the samples for the DSC measurements shown in Figure 4.1, except that they were cooled initially to 25 °C at 10 °C/min. Then they were

loaded in the diffractometer chamber at 25 °C and the WAXS patterns were measured, as shown in Figure 4.4.

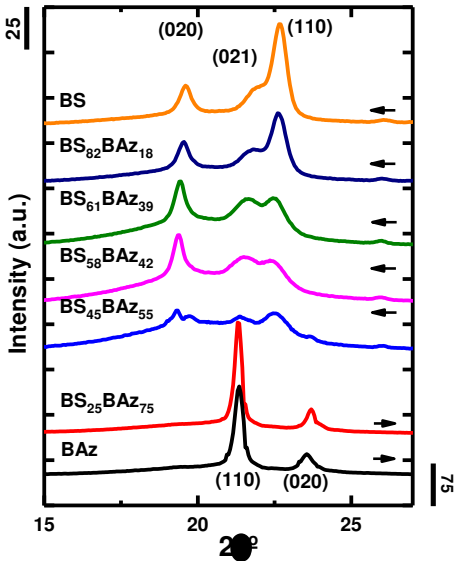

Figure 4. 4. *WAXS diffraction patterns for samples cooled from the melt at 10 °C/min to 25 °C. Measurements performed at 25 °C. See text.*

Table 4.2 lists all the reflections and the d spacings calculated by employing Braggs law. The data reported in Table 4.2 for poly(butylene succinate) is consistent with the most common α form whose monoclinic unit cell dimensions are reported to be[11-13] a = 0.523 nm, b = 0.908−0.912 nm, c = 1.079−1.090, nm and β = 123.9°. The most intense reflections for PBS appeared at 0.452, 0.404, and 0.392, and they can be indexed to (020), (021) and (110) planes,[3, 11-13] as indicated in Figure 4.4. In the case of PBAz, the crystalline unit cell has not been reported in the literature yet. A recent publication[3] has reported that fiber patterns from the melt drawn homopolymer are consistent with an orthorhombic unit cell with the following dimensions: a = 0.496 nm, b = 0.746 nm, and c = 3.65 nm. Following their results,[3] the most intense reflections (at 0.416 and 0.377 nm) for PBAz have been tentatively indexed in Figure 4.4 as (110) and (020).

A careful examination of the WAXS patterns of Figure 4.4 indicates that at 25 °C, almost all samples contain only one type of crystal. The samples with more than 58% BS only display reflections that are consistent with a PBS type unit cell. BAz and $BS_{25}BAz_{75}$ display a WAXS pattern that is characteristic of neat PBAz.

Table 4. 2. *Calculated Diffraction Spacings (d) According to Bragg's Law for the Indicated Samples at Two Different Temperatures (See Text).*

	25ºC		-30ºC	
Sample	**2θ**	***d* (nm)**	**2θ**	***d* (nm)**
BS	19.60	0.452	19.70	0.450
	21.95	0.404	22.10	0.402
	22.55	0.392	22.80	0.389
$BS_{82}BAz_{18}$	19.55	0.454	19.65	0.451
	21.80	0.407	21.95	0.404
	22.60	0.393	22.8	0.389
$BS_{61}BAz_{39}$	19.45	0.456	19.45	0.456
	21.65	0.409	21.7	0.409
	22.45	0.396	22.70	0.391
$BS_{58}BAz_{42}$	19.40	0.457	19.40	0.457
	21.50	0.413	21.63	0.410
	22.35	0.397	21.65	0.392
$BS_{45}BAz_{55}$	19.35	0.458	19.34	0.458
	19.75	0.449	20.00	0.443
	21.35	0.416	21.30	0.417
	22.45	0.396	21.75	0.390
	23.60	0.377	23.90	0.371
$BS_{25}BAz_{75}$	21.30	0.417	21.45	0.414
	23.70	0.375	23.95	0.371
BAz	21.35	0.416	21.45	0.414
	23.55	0.377	23.80	0.373

The only sample that contains characteristic reflections of both phases is $BS_{45}BAz_{55}$, but the WAXS pattern is completely dominated by PBS reflections, since the reflections of the PBAz phase that can be detected have extremely small intensity values (at 0.416 and 0.377 nm as shown in Figure 4.4), indicating that the amount of PBAz like

crystals is minimal at room temperature. This is consistent with the DSC curves presented in Figure 4.1b and the data reported in Table 4.1 that indicates a T_m value for the PBAz phase within the copolymer of 26.4 °C. Therefore, at 25 °C, the temperature at which the WAXS patterns were taken, the PBAz phase was almost completely molten, especially since the temperature control within the WAXS chamber has a precision of ±1 °C.

As the amount of PBAz increases in the copolymers from 18 to 55%, the PBS-rich phase exhibits a PBS like unit cell with d spacings that slightly increase with PBAz content. The change in d spacings with BAz content is plotted in Figure 4.5. The change is small but beyond experimental error (±0.001 nm) and the increase in diffraction spacings with composition is systematic. Presumably, the crystal unit cells have to increase slightly their volume to accommodate the extra PBAz repeating units that coexist with the PBS major component as a result of isodimorphism. Since the increase in d spacings is small, this probably indicates that comonomer incorporation is also small but finite.

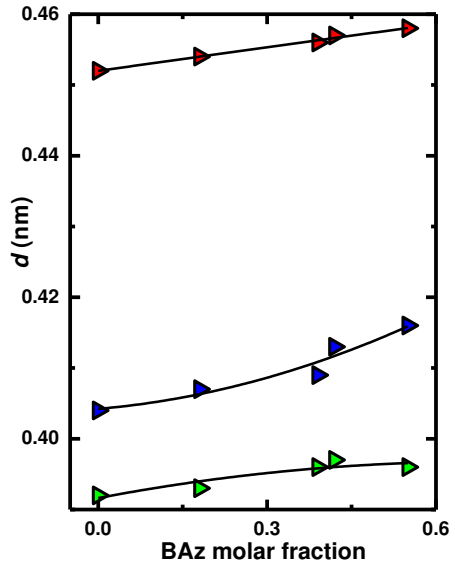

Figure 4. 5. *Experimental diffraction spacings (d) for PBS-rich crystalline phase as a function of BAz molar content. From bottom to top, the series of data points joint together by arbitrary trend lines are for (110), (021), and (020) planes respectively of PBS (or PBS-rich) crystalline unit cell (green, blue, and red symbols).*

In the other extreme of compositions, where PBAz is the major phase, the d spacings of PBAz do not exhibit a clear trend with composition, partly because of the limited number of samples (see Table 4.2).

Figure 4.6 shows WAXS patterns that were measured for the same samples of Figure 4.4 after they were cooled down to −30 °C in order to promote the crystallization of the PBAz phase within the copolymers. As expected, in all samples, most d spacings decreased (see Table 4.2) as compared to those measured at 25 °C, because of the effect of temperature on the unit cell volume. Besides these small changes in d spacings, only one sample experienced a significant and large change in its WAXS pattern. This is the double crystalline $BS_{45}BAz_{55}$ copolymer, for which the PBAz-rich phase was able to crystallize upon cooling to −30 °C and now exhibits much more intense reflections (i.e., the (110) reflection appearing at 0.417 nm and the (200) reflection at 0.371 nm) corresponding to the PBAz like unit cell, as compared to the WAXS pattern in Figure 4.4 (taken at 25 °C).

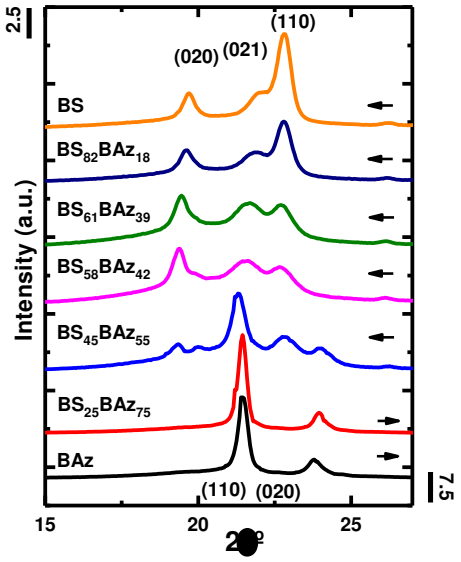

Figure 4. 6. *WAXS diffraction patterns taken at −30 °C for the indicated samples.*

4.3.2 Small Angle X-ray Scattering (SAXS)

Analogous experiments to those performed by WAXS were conducted employing SAXS. The results for the measurements at +25 °C and −30 °C are presented in Figure 4.7a and Figure 4.7b respectively, where the intensity is plotted as a function of the scattering vector q. Most samples exhibit a clear intense maximum that can be interpreted as the scattering caused by lamellar stacks.

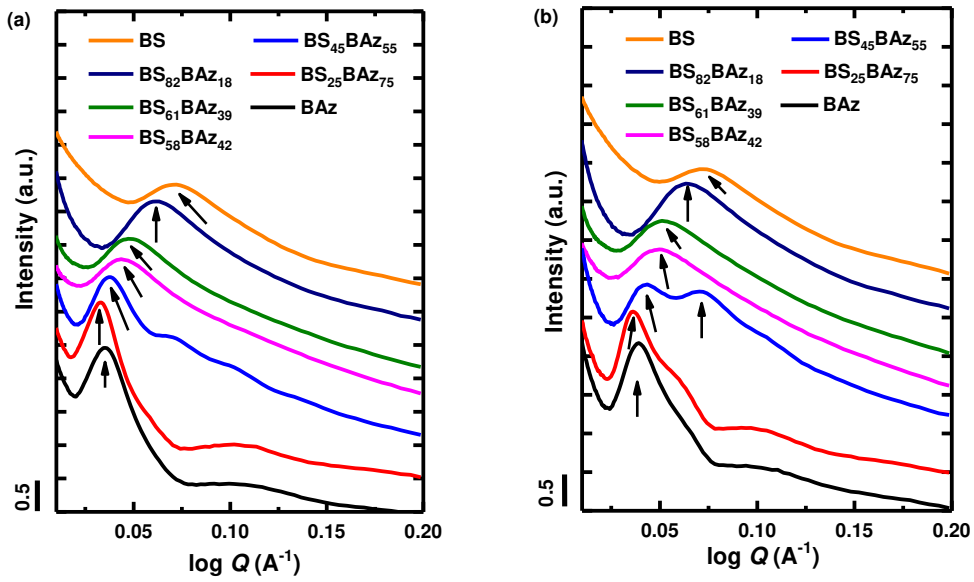

Figure 4. 7. *Intensity as a function of scattering vector for the indicated homopolymers and copolymers. Data taken at the following temperatures: (a) +25 °C and (b) −30 °C.*

The long periods (d^*) were estimated by equation 4.1 from Lorentz corrected plots (Iq^2 versus q):

$$d^* = {}^{2\pi}/_{q_{max}} \qquad 4.1$$

At 25 °C our WAXS results have shown that only one type of crystal is present in the materials, i.e., either the PBS-rich phase or the PBAz-rich phase. Therefore, any subsidiary low intensity maxima located at higher q values in Figure 4.7a as compared to the highest intensity peak can be explained as second or third order reflections arising from

the lamellar structure, since their positions correspond to approximately 2qmax and 3qmax and the intensities are much lower compared to their first order peaks.

When the SAXS patterns are measured at −30 °C (Figure 4.7b), the $BS_{45}BAz_{55}$ copolymer exhibits a remarkable change as a result of the crystallization of both PBS-rich and PBAz-rich phases. The SAXS pattern taken at −30 °C exhibits two scattering peaks with almost equivalent intensity indicating that the material is constituted by two types of lamellar stacks with enough density contrast to be able to individually produce small angle scattering at discrete q values. The peak located at lower q values can be assigned to the long period of the PBS-rich lamellar stacks (see Figure 4.8 below) while that at higher q values to the PBAz-rich phase lamellar long period. No significant changes were observed for the other samples at −30 °C (when compared with 25 °C) except relatively small changes in *d* values.

Figure 4.8 shows a plot of the measured long periods as a function of copolymer composition. The long periods were obtained from the data presented in Figure 4.7 and also from one additional experiment that was performed to evaluate reversibility and reproducibility. After the samples were cooled to −30 °C, they were heated back to 25 °C and remeasured, and both data sets obtained at 25 °C were equivalent within experimental errors as shown in Figure 4.8 (labeled 25 and 25 °C, second heating).

SAXS data for this type of copolymers had not been reported in the literature as far as the authors are aware. It is interesting to note that *d** spacings strongly depend on composition (Figure 4.8). A vertical line has been drawn at the composition corresponding to the $BS_{45}BAz_{55}$ copolymer (dash line in Figure 4.8), which should be very close to the eutectic point of the system. To the left of the eutectic all data points correspond to *d** spacings of the PBS-rich phase. To the right of the eutectic the data points correspond to the *d** spacings of the PBAz-rich phase. The lines that go through the data points have been drawn arbitrarily to guide the eye.

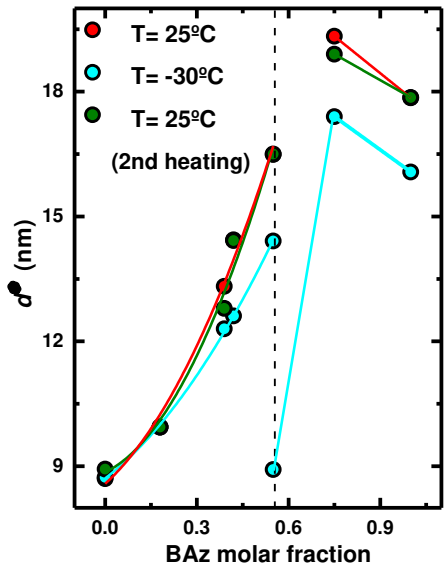

Figure 4. 8. *Long periods (d*) obtained by SAXS as a function of copolymer composition (expressed as BAz molar fraction). Arbitrary lines have been drawn joining the data points to guide the eye.*

Let us consider in Figure 4.8 the long period values to the left of the eutectic point, i.e., for PBS and PBS-rich crystalline phases. PBS crystallizes forming spherulites that contain lamellar stacks with an average long period of approximately 8.5 nm. For the PBS-rich phase, both at +25 °C and at −30 °C, spherulites are also formed (see below) and the lamellar long period increases with BAz content in the copolymers to values as high as 13.5−16.3 nm. This is a remarkable behavior indicating that the incorporation of PBAz both in the crystalline unit cell (Figure 4.4) and in the amorphous regions of the PBS-rich interlamellar zones has a synergistic effect on the morphology at the lamellar level. Increases in long period can indicate changes in lamellar thickness and/or interlamellar regions (amorphous intervening layer). The changes in the lamellar thickness are estimated below.

In the case of the PBAz-rich phase, the behavior shown in Figure 4.8 is very peculiar in two aspects: (a) *d** increases when 25% BS is included in the copolymer, a behavior that may be related to the incorporation of some BS repeating units in the PBAz-rich phase lamellae (a similar case to that described above for the PBS-rich copolymers). (b) At −30 °C, the long period of the PBAz-rich phase experiences a dramatic decrease when

45% BS is incorporated in the copolymer. This reduction in long period is caused by the previous crystallization of the PBS-rich phase within the $BS_{45}BAz_{55}$ copolymer. When the sample was originally cooled from the melt, the PBS phase crystallized forming space filling spherulites (see Figure 4.11) that constitute a template for the copolymer morphology. Upon further cooling to −30 °C, the PBAz-rich phase had to crystallize within the confined interlamellar regions of the previously obtained PBS-rich phase spherulites.

The changes in the SAXS pattern of the $BS_{45}BAz_{55}$ copolymer while it transforms from a single semicrystalline material (i.e., containing only of PBS-rich phase lamellae) to a double crystalline material (i.e., containing both PBS-rich and PBAz-rich phase lamellae) can be clearly observed in Figure 4.9a. In this figure, the sample was first heated from −30 to 40 °C in order to fully melt the PBAz-rich crystalline phase. Then SAXS patterns were taken at increasingly lower temperatures, as the sample was cooled down as shown in Figure 4.9a.

The SAXS patterns at 40, 30, and 20 °C do not exhibit significant changes (see Figure 4.9a) since only the PBS-rich crystalline lamellar stacks are present (as confirmed by WAXS). At 10 °C, the PBAz-rich phase starts to crystallize and the SAXS patterns progressively evolve. Such evolution can be seen in Figure 4.9b where the change in long periods as a function of temperature is represented. The first SAXS maxima correspond to the long period of the PBS-rich phase, which remains approximately constant until 20 °C. However, as the PBAz-rich phase starts to crystallize at temperatures below 20 °C (and a second maximum develops at higher q values), the long spacing of the PBS-rich phase decreases (see Figure 4.9b, first SAXS maximum data). Such a decrease indicates that extensive lamellar rearrangement occurs within the spherulites (together with the density increase that accompanies crystallization) for the two types of lamellae to coexist inside the mixed spherulites formed by this isodimorphic random copolymer.

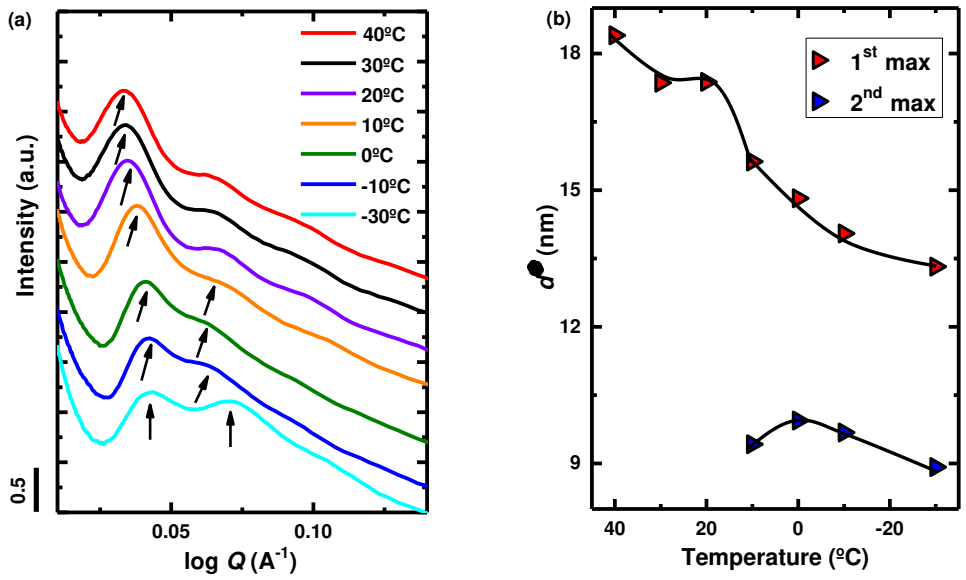

Figure 4. 9. *(a) Intensity versus scattering vector for the $BS_{45}BAz_{55}$ copolymer as it is cooled from +40 °C down to −30 °C. (b) Long spacings (d*) calculated from SAXS data presented in (a) as a function of temperature. Arbitrary lines have been drawn joining the data points to guide the eye.*

Perfect interlamellar stacking (or interdigitation, where alternating lamellae of each phase are stack on one another) would not be consistent with the values obtained at −30 °C for the two characteristic long periods of each crystalline phase: approximately 13.3 and 8.5 nm (Figure 4.9b). The results may stem from average long periods of a complicated interfibrillar structure that could be schematically represented in the model shown in Figure 4.10. Similar structures have been observed in crystalline/crystalline binary blends.[14-21]

Calculation of the lamellar thickness requires the knowledge of the crystallinity degree of each phase. The calculation of the lamellar thickness, l, could be performed employing the following approximation:

$$l = d^* x_v \qquad 4.2$$

where x_v is the crystalline volume fraction that can be estimated from the following equations:

$$x_v = (x_m \rho)/\rho_c \quad 4.3$$

$$x_m = \frac{\Delta H_m}{\Delta H_{m(100\%)} W} \quad 4.4$$

where x_m is the mass fraction of crystals, ρ is the experimentally determined density of the sample (at 25 °C), and ρ_c is the density of a 100% crystalline sample.

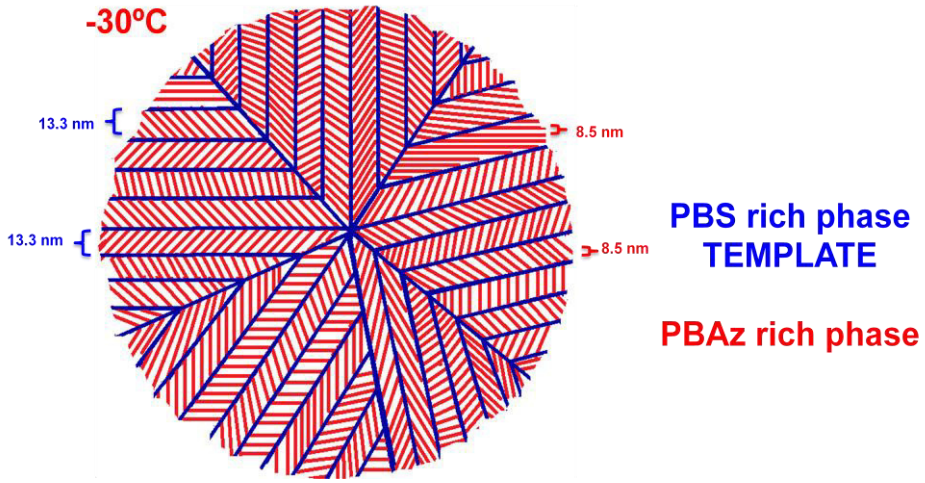

Figure 4. 10. *Schematic (not to scale) model of the possible double crystalline lamellar stacking morphology inside mixed spherulites of the $BS_{45}BAz_{55}$ copolymer at −30 °C. The blue lines indicate PBS-rich lamellae while the red lines correspond to PBAz lamellae.*

The mass fraction of crystals can be calculated from the enthalpy of fusion of the phase under consideration (ΔH_m), the enthalpy of fusion of a 100% crystalline sample and the weight fraction of the phase under consideration (W) employing eq 4. The density of the samples at 25 °C was determined experimentally and the results are listed in Table 4.3. The crystalline density of PBS can be found in the literature as well as its $\Delta H_{m(100\%)}$ value: $\Delta H_{m(100\%)}$ = 210 J/g[22] and ρ_c= 1.26 g/ cm^3.[23] A value for $\Delta H_{m(100\%)}$ of 150 J/g has been reported[24] for PBAz. However, since the crystalline structure of PBAz has not been solved, its crystalline density is unknown.

Table 4.3 reports the calculations of the lamellar thickness based on DSC and density determinations at both +25 and −30 °C. The calculated values exhibit, for the PBS phase, an increasing trend in l as the BAz content in the copolymers increase. The values increase from approximately 2.6 nm for PBS up to 5.0 nm for the PBS-rich phase within the $BS_{45}BAz_{55}$ copolymer. Since the crystallinity degrees determined by DSC do not vary much (less than 15%) with copolymer composition for the PBS-rich phase, the lamellar thickness variation follows the trend exhibited by the long period in Figure 4.8 when the amount of PBAz is increased (left side of the eutectic).

An attempt was also made to calculate the crystallinity degrees employing WAXS data taken at −30 °C. Following the method of Krimm and Tobolsky,[25] the crystallinity index was calculated by deconvolution of amorphous and crystalline scattering peaks. The values of l in that case exhibit a different trend with composition compared with those calculated by DSC (see Table 4.3). The striking results manifest the complicated structure of the PBS-*ran*-PBAz copolymers. It is possible that the thermodynamic parameters of these materials are composition dependent, such as equilibrium melting temperature, enthalpy of fusion for 100% crystallinity, and folded surface free energy. Therefore, some well-established regulations may not be applicable in these materials.

***Table 4. 3**. Density (±0.0003 g/cm3), Normalized Enthalpy of Crystallization (±1 J/g), Mass and Volume Crystalline Fractions (±0.01), Long Period, and lamellar Thickness Values (±0.1 nm).*

25ºC – 100ºC

		ρ (g/cm^3)	ΔH_m (J/g)	χ_m	χ_v	d^* (nm)	l (nm)
1	BS	1.2447	67	0.32	0.32	8.2	2.6
2	$BS_{82}BAz_{18}$	1.1973	67	0.32	0.3	9.4	2.8
3	$BS_{61}BAz_{39}$	1.1672	68	0.32	0.3	12	3.6
4	$BS_{58}BAz_{42}$	1.1399	79	0.38	0.34	12.6	4.3
5	$BS_{45}BAz_{55}$	1.1355	73	0.35	0.31	16.1	5
6	$BS_{25}BAz_{75}$	1.1224	74	0.5	--	18.3	9.1*
7	BAz	1.1087	51	0.34	--	17.4	5.9*

-30ºC – 100ºC

		ρ (g/cm^3)	ΔH_m (J/g)	χ_m	χ_v	d^* (nm)	l (νμ)	χ_c (WAXS)	l (nm) (WAXS)
1	BS	1.2447	67	0.32	0.32	8	2.6	0.61	5.3
2	$BS_{82}BAz_{18}$	1.1973	68	0.32	0.31	9.2	2.8	0.45	4.5
3	$BS_{61}BAz_{39}$	1.1672	83	0.4	0.37	10.5	3.9	0.29	3.6
4	$BS_{58}BAz_{42}$	1.1399	80	0.38	0.34	10.8	3.7	0.25	3.2
5	$BS_{45}BAz_{55}$	1.1355	79	0.38	0.34	13.3	4.5		
			41	0.27	--	8.5	2.3*		
6	$BS_{25}BAz_{75}$	1.1224	81	0.54	--	16.5	8.9*	0.62	10.7
7	BAz	1.1087	50	0.33	--	15.6	5.2*	0.57	9.2

[a]*These values were calculated using the following approximation: $l = d^*\chi_m$ because ρc is unknown for PBAz. The density of the samples was measured at 25 °C and was also used for the calculations at −30 °C (although a change in density must have occurred).*

4.4 Examination of the $BS_{45}BAz_{55}$ Copolymer

4.4.1 Polarized Light Optical Microscopy (PLOM)

$BS_{45}BAz_{55}$ is the only copolymer that developed a double crystalline morphology. This isodimorphic copolymer features a morphology that is somewhat similar to that exhibited by double crystalline diblock copolymers that are miscible or in the weak segregation regime.[6, 26, 27] Upon cooling from the melt in a PLOM hot stage at 10 °C/min, the first phase capable of crystallization is the PBS-rich phase.

Figure 4.11 shows PBS-rich phase spherulites after the sample was cooled from the melt and held at 35 °C for 38 min. This phase develops negative spherulitic superstructural aggregates that resemble those of PBS but exhibit irregular edges (not perfectly circular). At this temperature the PBAz-rich phase is in the melt. If the sample is held at this temperature for a long time (a couple of days for instance), the whole field fills with impinged PBS-rich phase spherulites that contain within them two phases: (a) A crystalline phase constituted by PBS-rich phase radial lamellae, where mostly BS repeating units are organized in stacked unit cells with their c axis tangentially arranged, and a certain proportion of BAz units that have been able to enter the PBS crystalline unit cells; and (b) an amorphous phase constituted by copolymer chains with BAz and BS repeating units in the amorphous intraspherulitic regions.

Parts b and c of Figure 4.11 show the result of quenching the sample shown in Figure 4.11a from 35 °C down to 8 °C, a temperature at which the BAz-rich phase crystallizes rapidly. The remaining PBS amorphous phase can also crystallize at 8 °C. As a result of enhanced nucleation at this lower temperature, a higher number of spherulites can be seen. Figure 4.11c is a micrograph taken after just 2 min at 8 °C and the microscope field is already filled with impinging mixed spherulites that contain lamellar crystals of both phases, as indicated schematically in Figure 4.10. Figure 4.11d shows the morphology after the sample was heated back up to 25 °C to melt the PBAz-rich phase crystals. The field remains full with PBS-rich phase spherulites as expected since the molten PBAz-rich phase is within the intraspherulitic regions of the PBS phase.

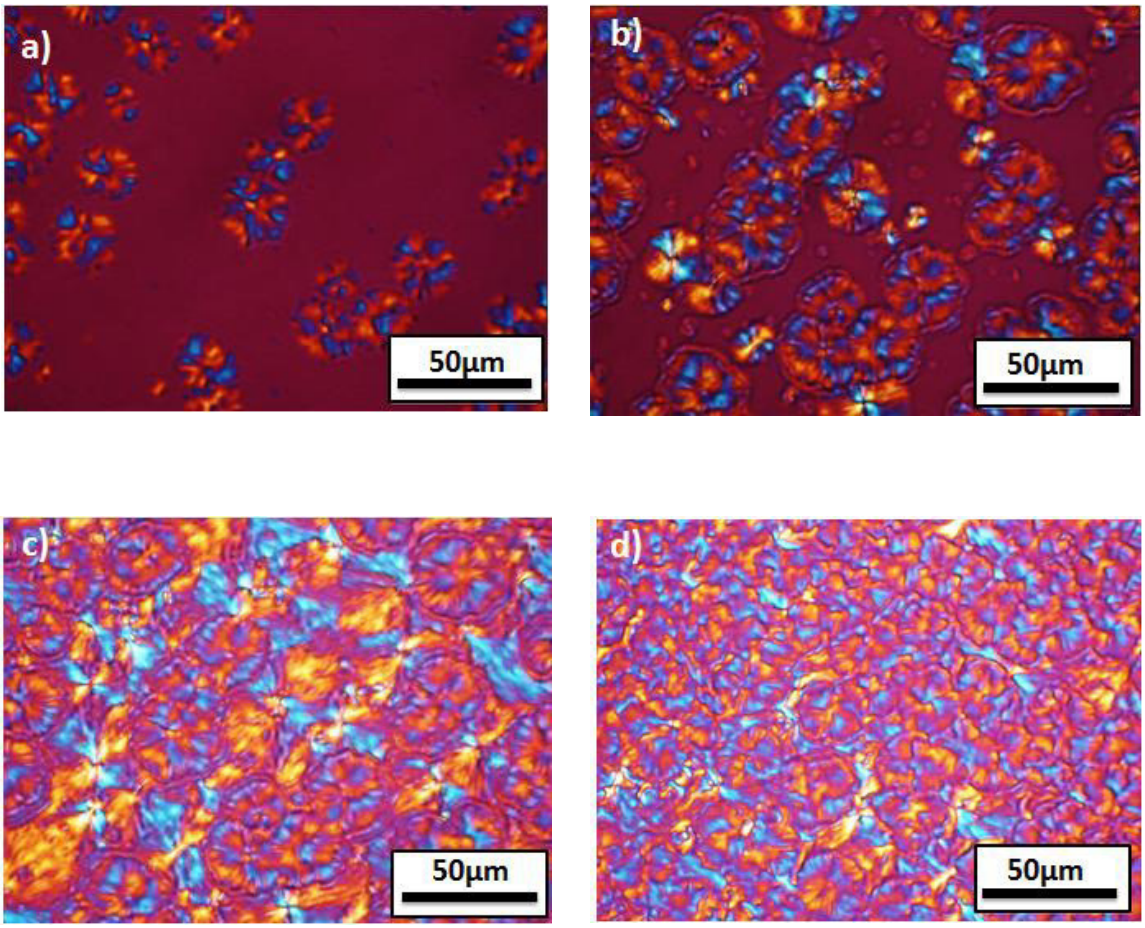

Figure 4. 11. *Polarized light optical micrographs of the $BS_{45}BAz_{55}$ copolymer: (a) the sample was cooled from the melt and held at 35 °C for 38 min, (b) micrograph taken after the sample in part a was quenched rapidly from 35 °C down to 8 °C and (c) after 2 min at 8 °C, and (d) the sample was reheated to 25 °C. See text.*

4.4.2 AFM Examination

A sample of the same $BS_{45}BAz_{55}$ copolymer was spin coated onto a mica substrate (see Experimental Section). The sample was then isothermally crystallized at 35 °C for 15.5 h and then cooled to 25 °C. The sample was observed at 25 °C under an AFM microscope. At room temperature we can consider that only the PBS-rich phase is present, since the PBAz-rich phase is mostly in the melt state. Figure 4.12a shows a panoramic view of the crystalline texture of the sample obtained in the phase contrast mode. The image shows edge on and flat on PBS-rich phase lamellae embedded in an amorphous matrix where the potentially crystallizable (at much lower temperatures) PBAz-rich phase is in the molten state. Taking advantage of the regions of the sample where many edge on lamellae are located (see Figure 4.12, parts b and c, which represents a close up of two areas within Figure 4.12a), measurements were taken of at least 50 representative lamellae and their long period and lamellar thickness were averaged. The values obtained were as follows: $d^* = 15.2 \pm 0.3$ nm and $l = 5.2 \pm 0.8$ nm. These values are in excellent agreement with the values obtained by SAXS at 25 °C where a d^* value of 16.1 nm was measured and an l value of 5.0 nm was calculated (see Table 4.3). Our AFM microscope cannot cool below room temperature and we were not able to see the crystallization of the PBAz-rich phase by AFM. However, the evidence by PLOM and SAXS are consistent with the schematic picture shown in Figure 4.10.

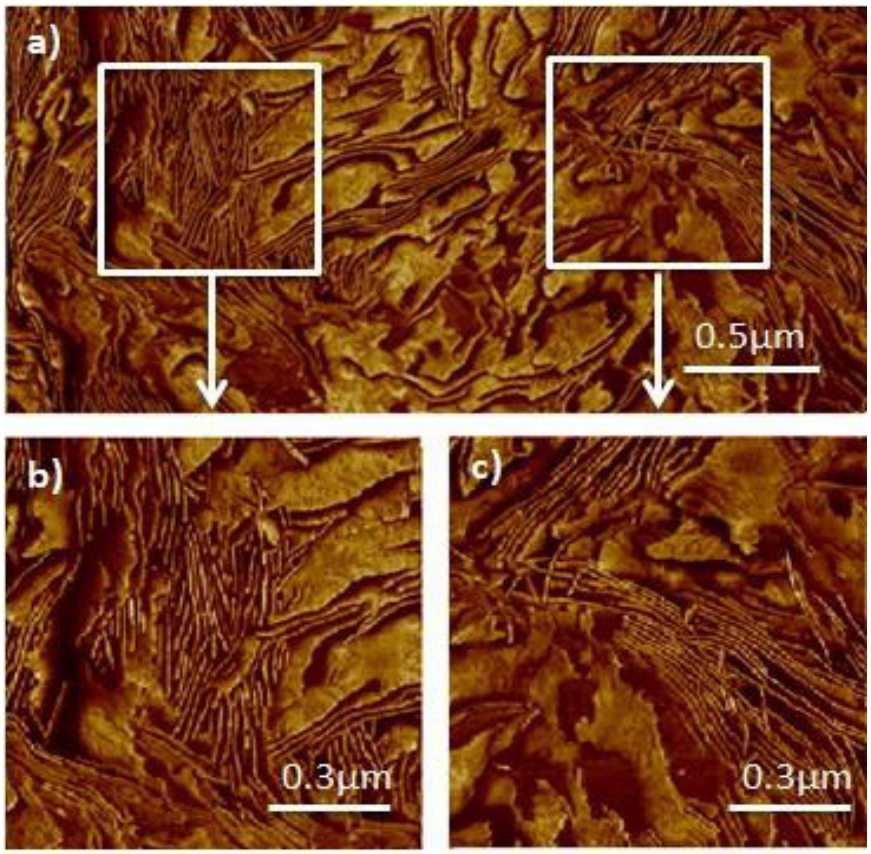

Figure 4. 12. *AFM phase contrast micrographs for a spin-coated* $BS_{45}BAz_{55}$ *copolymer sample observed at 25 °C.*

4.5 Conclusions

Regulating the composition of isodimorphic random copolymers is a valuable tool to tailor their properties in an unusually wide temperature range. The melting temperature of the materials goes through a eutectic point when plotted as a function of composition. WAXS measurements demonstrated that apart from one composition around the eutectic point, all of the other random copolyesters were characterized by the sole crystallization of the most abundant component. Our WAXS results showed that small but reproducible changes are produced in the crystalline unit cell of the dominant crystalline phase upon inclusion of comonomer units.

On the other hand, very large changes were observed in terms of crystallization and melting temperatures as well as in the superstructural and lamellar morphology when PBAz is incorporated randomly into PBS macromolecular chains. Lamellar spacings and lamellar thicknesses were found to be strongly dependent on copolymer composition by SAXS determinations.

In the interesting case of the double crystalline copolymer with a composition close to the eutectic point ($BS_{45}BAz_{55}$), coincident crystallization occurred when the material was cooled from the melt at 10 °C/min.

Considering the results from WAXS, SAXS, PLOM, and AFM for the double crystalline $BS_{45}BAz_{55}$ copolymer, a clear morphological picture emerged. When the material is cooled from the melt, PBS-rich space filling spherulites are formed and they produce a template for the copolymer morphology. These spherulites are constituted by radially growing lamellae of PBS-rich crystals with amorphous intervening layers of PBAz-rich phase. Upon further cooling from the melt, the PBAz-rich phase crystallizes forming much smaller lamellae that are stacked within the intraspherulitic regions of the large PBS-rich spherulites. The two types of lamellae coexist within these unusual mixed spherulites and have enough contrast and different spacings to produce two well-defined equally intensive SAXS maxima.

4.6 References

1. Mincheva, R.; Delangre, A.; Raquez, J. M.; Narayan, R.; Dubois, P., Biobased Polyesters with Composition-Dependent Thermomechanical Properties: Synthesis and Characterization of Poly(butylene succinate-co-butylene azelate). *Biomacromolecules* **2013,** *14*, 890-899.
2. Diaz, A.; Franco, L.; Puiggali, J., Study on the crystallization of poly(butylene azelate-co-butylene succinate) copolymers. *Thermochimica Acta* **2014,** *575*, 45-54.
3. Diaz, A.; Franco, L.; Estrany, F.; del Valle, L. J.; Puiggali, J., Poly(butylene azelate-co-butylene succinate) copolymers: Crystalline morphologies and degradation. *Polymer Degradation and Stability* **2014,** *99*, 80-91.
4. Iwata, T.; Doi, Y., Crystal structure and biodegradation of aliphatic polyester crystals. *Macromolecular Chemistry and Physics* **1999,** *200*, 2429-2442.
5. Muller, A. J.; Albuerne, J.; Marquez, L.; Raquez, J. M.; Degee, P.; Dubois, P.; Hobbs, J.; Hamley, I. W., Self-nucleation and crystallization kinetics of double crystalline poly(p-dioxanone)-b-poly(epsilon-caprolactone) diblock copolymers. *Faraday Discussions* **2005,** *128*, 231-252.
6. Castillo, R. V.; Müller, A. J., Crystallization and morphology of biodegradable or biostable single and double crystalline block copolymers. *Progress in Polymer Science* **2009,** *34*, 516-560.
7. Müller, A. J.; Arnal, M. L.; Balsamo, V., Crystallization in Block Copolymers with More than One Crystallizable Block. *Lecture Notes in Physics* **2007**, 229-259.
8. Castillo, R. V.; Müller, A. J.; Lin, M.-C.; Chen, H.-L.; Jeng, U. S.; Hillmyer, M. A., Confined Crystallization and Morphology of Melt Segregated PLLA-b-PE and PLDA-b-PE Diblock Copolymers. *Macromolecules* **2008,** *41*, 6154-6164.
9. Fillon, B.; Wittmann, J. C.; Lotz, B.; Thierry, A., Self-nucleation and recrystallization of isotactic polypropylene (alpha-phase) investigated by differential scanning calorimetry. *Journal of Polymer Science Part B: Polymer Physics* **1993,** *31*, 1383-1393.
10. Müller, A. J.; Arnal, M. L., Thermal fractionation of polymers. *Progress in Polymer Science* **2005,** *30*, 559-603.

11. 1Ihn, K. J.; Yoo, E. S.; Im, S. S., Structure and Morphology of Poly(tetramethylene succinate) Crystals. *Macromolecules* **1995,** *28*, 2460-2464.
12. Ichikawa, Y.; Kondo, H.; Igarashi, Y.; Noguchi, K.; Okuyama, K.; Washiyama, J., Crystal structures of α and β forms of poly(tetramethylene succinate). *Polymer* **2000**, *41*, 4719-4727.
13. Ichikawa, Y.; Suzuki, J.; Washiyama, J.; Moteki, Y.; Noguchi, K.; Okuyama, K., Strain-induced crystal modification in poly(tetramethylene succinate). *Polymer* **1994,** *35*, 3338-3339.
14. Schultz, J. M., The crystallization and morphology of melt-miscible polymer blends. *Frontiers of Chemistry in China* **2010,** *5*, 262-276.
15. Weng, M.; Qiu, Z., Unusual Fractional Crystallization Behavior of Novel Crystalline/Crystalline Polymer Blends of Poly(ethylene suberate) and Poly(ethylene oxide) with Similar Melting Points. *Macromolecules* **2014,** *47*, 8351-8358.
16. Qiu, Z.; Ikehara, T.; Nishi, T., Unique Morphology of Poly(ethylene succinate)/Poly(ethylene oxide) Blends. *Macromolecules* **2002,** *35*, 8251-8254.
17. He, Y.; Zhu, B.; Kai, W.; Inoue, Y., Nanoscale-Confined and Fractional Crystallization of Poly(ethylene oxide) in the Interlamellar Region of Poly(butylene succinate). *Macromolecules* **2004,** *37*, 3337-3345.
18. Ikehara, T.; Kimura, H.; Qiu, Z., Penetrating Spherulitic Growth in Poly(butylene adipate-co-butylene succinate)/Poly(ethylene oxide) Blends. *Macromolecules* **2005,** *38*, 5104-5108.
19. Lu, J.; Qiu, Z.; Yang, W., Effects of Blend Composition and Crystallization Temperature on Unique Crystalline Morphologies of Miscible Poly(ethylene succinate)/Poly(ethylene oxide) Blends. *Macromolecules* **2008,** *41*, 141-148.
20. Yang, Y.; Qiu, Z., Crystallization and Morphology in a 30/70 Poly(ethylene succinate-co-6 mol % butylene succinate)/Poly(ethylene oxide) Blend. *Industrial & Engineering Chemistry Research* **2012,** *51*, 9191-9197.
21. Weng, M.; Qiu, Z., A Spherulitic Morphology Study of Crystalline/Crystalline Polymer Blends of Poly(ethylene succinate-co-9.9 mol % ethylene adipate) and Poly(ethylene oxide). *Macromolecules* **2013,** *46*, 8744-8747.
22. Papageorgiou, G. Z.; Bikiaris, D. N., Crystallization and melting behavior of three biodegradable poly(alkylene succinates). A comparative study. *Polymer* **2005,** *46*, 12081-12092.

23. Yang, J.; Liang, J.-Z.; Li, F.-J., Melt Strength and Extensional Viscosity of Low-Density Polyethylene and Poly(butylene succinate) Blends Using a Melt-Spinning Technique. *Journal of Macromolecular Science, Part B* **2012,** *51*, 1715-1730.
24. Papageorgiou, G. Z.; Bikiaris, D. N.; Achilias, D. S.; Papastergiadis, E.; Docoslis, A., Crystallization and biodegradation of poly(butylene azelate): Comparison with poly(ethylene azelate) and poly(propylene azelate). *Thermochimica Acta* **2011,** *515*, 13-23.
25. Krimm, S.; Tobolsky, A. V., Quantitative x-ray studies of order in amorphous and crystalline polymers. Quantitative x-ray determination of crystallinity in polyethylene. *Journal of Polymer Science* **1951,** *7*, 57-76.
26. Hamley, I. W.; Castelletto, V.; Castillo, R. V.; Muller, A. J.; Martin, C. M.; Pollet, E.; Dubois, P., Crystallization in poly(L-lactide)-b-poly(epsilon-caprolactone) double crystalline diblock copolymers: A study using X-ray scattering, differential scanning calorimetry, and polarized optical microscopy. *Macromolecules* **2005,** *38*, 463-472.
27. Hamley, I. W.; Parras, P.; Castelletto, V.; Castillo, R. V.; Müller, A. J.; Pollet, E.; Dubois, P.; Martin, C. M., Melt Structure and its Transformation by Sequential Crystallization of the Two Blocks within Poly(L-lactide)-block-Poly(ε-caprolactone) Double Crystalline Diblock Copolymers. *Macromolecular Chemistry and Physics* **2006,** *207*, 941-953.

Chapter 5

Self-nucleation and Successive Self-nucleation and Annealing (SSA) studies

5.1 Introduction

In this chapter we make use of self-nucleation and successive self-nucleation and annealing SSA techniques to corroborate the isodimorphic behavior of PBS-*ran*-PBAz samples. Self-nucleation is a technique designed to enhance nucleation density and gives information about self-nucleation domains. In the other hand, SSA technique promotes segregation of molecular defects that interrupt crystallizable sequences, and together with the SAXS and WAXS analysis before and after SSA fractionation, it allows an examination of the isodimorphic nature of the copolymers.

5.2 Standard DSC

Melting and crystallization characteristics of neat PBS and PBAz homopolymers and PBS-*ran*-PBAz copolymers derived from standard DSC are presented in Table 5.1. The melting and crystallization enthalpies reported in Table 5.1 have been normalized to take into account the weight fraction of the crystallizable phase. All copolymers were semicrystalline despite being random as demonstrated previously by ^{13}C NMR.[1] Crystallization and melting temperatures decrease with respect to those of the homopolymers when the percentage of the minority comonomer increases, showing an eutectic point at intermediate compositions (see Figures 4.1 and 4.2 in chapter 4, which correspond to the same materials). In a previous investigation of these materials, in Charter 4,[2] it was concluded that these copolymers are isodimorphic. The results indicated that an inclusion of a small amount of repeating units of the minor comonomer in the crystalline cell of major component occurs.[2]

Table 5. 1. *Molar composition determined by ^1H NMR, number-average molecular weight determined by SEC[1] and thermal transitions determined by DSC (at 20 °C min^{-1}) of the materials employed in this work.*[a]

	Code	Composition (PBS/PBAz), mol ^{1}H NMR	*Mn* (g/mol)^{SEC}	Data DSC					
				T_{m1} (ºC)	T_{m2} (ºC)	ΔH_{m1} (J/g)	ΔH_{m2} (J/g)	T_c (ºC)	ΔH_c (J/g)
1	BS	1/0	25.3	116.2	--	65		71.9	69
2	$BS_{82}BAz_{18}$	0.82/0.18	22.3	98.3	--	69	--	60.6	77
3	$BS_{61}BAz_{39}$	0.61/0.39	31.3	74.3	--	68	--	17.2	77
4	$BS_{58}BAz_{42}$	0.58/0.42	36.5	60.9	--	90		1.8	84
5	$BS_{45}BAz_{55}$	0.45/0.55	38.3	46.9	28.3	66	61	9.9	59
6	$BS_{25}BAz_{75}$	0.25/0.75	39.6	--	39.2	--	73	15.9	74
7	BAZ	0/1	42.5	--	44.2	--	60	22.1	60

[a]*The melting enthalpies are normalized by composition in all cases. The crystallization enthalpies are also normalized by composition, except for the coincident crystallization case in sample $BS_{45}BAz_{55}$. Estimation of errors based on the repetition of DSC experiments, calibration and baseline drifts indicate that transition temperatures are valid within 0.5 ºC and enthalpy values within 1 J/g.*

In addition, $BS_{45}BAz_{55}$, whose composition is near the eutectic point, is the only copolymer that shows two melting points (see Table 5.1) that corresponds to PBAz and PBS-rich crystalline phases, respectively. These results confirm that this random copolymer exhibits an isodimorphic behavior (i.e., some comonomer inclusion must be present in both phases as confirmed by WAXS below) as it would be highly unlikely that the two components of a random copolymer with an almost symmetric composition could crystallize.

5.3 Self-nucleation behavior of PBS, PBAz and $BS_{45}BAz_{55}$ Copolymer

5.3.1 DSC results and PLOM results

In order to illustrate the self-nucleation process with a simple case, this technique was first applied (as described in Chapter 3, Experimental Part) to PBS. Figure 5.1a shows cooling scans from selected T_s temperatures. At temperatures of 134ºC and above, crystalline memory is completely erased and only high temperature resistant

heterogeneities capable of nucleating the polymer during cooling remain. As a consequence, the peak crystallization temperature is constant in Figure 5.1 for these T_s temperatures and the melting traces are invariant upon subsequent heating, as seen in Figure 5.1b. The described behavior occurs for Ts values equal or larger than 134ºC, when the sample is within the complete melting domain (Domain I).

When T_s temperatures lower than 134ºC (but higher than or equal to 116ºC) are employed, PBS experiences only self-nucleation, and its crystallization temperature increases (Figure 5.1a). The corresponding maximum peak melting point in Figure 5.1b does not show signs of annealing. Therefore, the sample falls under the exclusive self-nucleation domain (Domain II). For higher T_s values within Domain II, like 133ºC, the melting process of the sample upon subsequent heating (after the cooling from T_s shown in Figure 5.1a) does not change significantly, since cold crystallization is still observed in Figure 5.1b. However, at further decrease in T_s values within Domain II, cold crystallization disappears from the heating DSC trace and the double melting process is more pronounced (see for example the DSC traces corresponding to T_s =117 or 116ºC in Figure 5.1b). This is a consequence of an increase in the crystallization enthalpy produced during cooling from these lower T_s values as a result of the self-nucleation effect (compare the crystallization exotherms in Figure 5.1a for the samples cooled from T_s values 133ºC and 117ºC for example).

Finally when the T_s temperature is lower or equal to 115ºC, partial melting occurs and the unmelted crystals experience annealing during the 5 min holding time at T_s, the sample is then in the self-nucleating and annealing domain (Domain III). This is easily distinguished by the appearance of a high temperature additional melting peak, signaled with an arrow in Figure 5.1b.

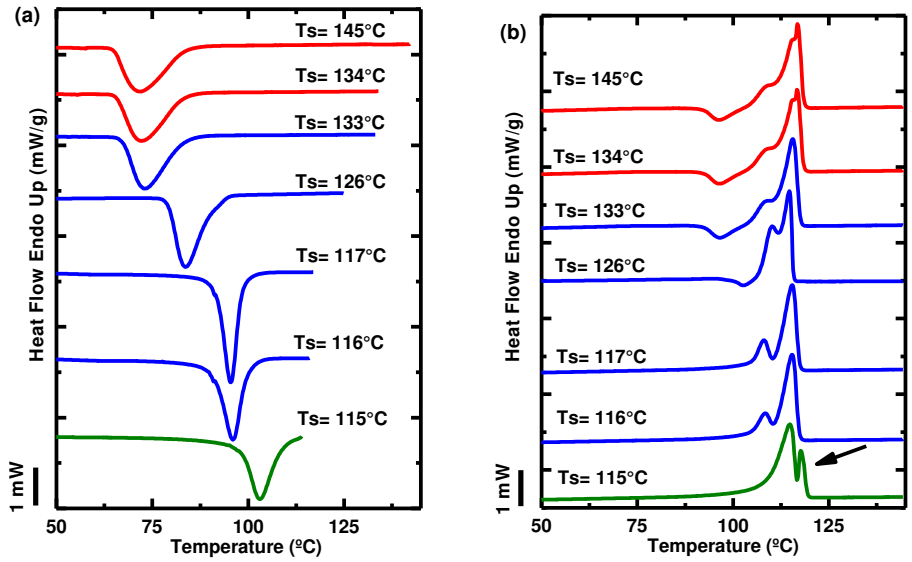

Figure 5. 1. *Self-nucleation of PBS homopolymer: (a) DSC cooling scans from the indicated self-nucleation (Ts) temperatures and (b) subsequent heating scans at 10ºC/min.*

Figure 5.2 shows the standard DSC melting trace of the PBS homopolymer employed in this work where the different self-nucleation domains have been indicated by color codes (red for domain I, blue for domain II and green for domain III, the same color codes are employed in Figure 5.1) while the domain transitions are marked by vertical lines. It is remarkable how domain II extends to temperatures well above the end of PBS melting. The self-nuclei in the temperature region between 120 and 133 °C cannot be crystalline in nature and must be produced by residual chain segmental orientation in the melt as a result of a crystalline memory phenomenon.[3]

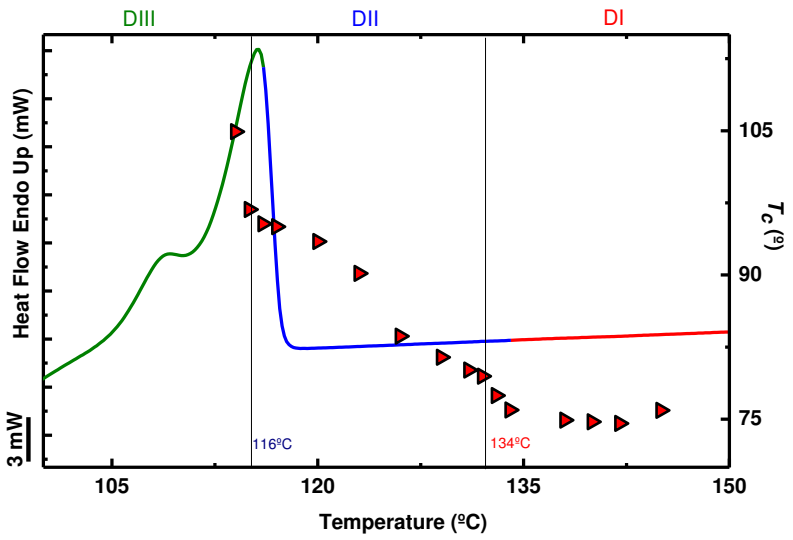

Figure 5. 2. *Representation of the self-nucleation domains for PBS homopolymer on top of the standard DSC melting trace. Insets include PLOM micrographs taken during cooling from T_s = 145 °C (domain I) and T_s = 116 °C (domain II). The data points represent peak crystallization temperatures (plotted on the right-hand side y axis) as a function of T_s values (plotted on the x axis).*

Figure 5.2 illustrates the changes in peak crystallization temperatures as a function of T_s values (see right-hand side y axis for T_c values and x axis for T_s values). Crossing from domain I to domain II causes a large increase in T_c that is proportional to the exponential increase in nucleation density that occurs during self-nucleation.[4, 5] When the sample enters domain III, T_c values increase further while the unmelted crystal population is annealed.

Two representative polarized light optical microscopy (PLOM) micrographs are floted in Figure 5.3 to illustrate the enhancement in nucleation density. The micrographs were taken during cooling from 145 °C (domain I) or from 116 °C (domain II) at the same cooling rate of 10 °C/min. The superstructural aggregates are clear negative spherulites partially or totally impinged with one another in domain II. The much higher number of spherulites in the self-nucleated sample is readily seen, as the number of spherulites is proportional to the number of active nuclei (i.e., each spherulite is nucleated by one active heterogeneous nuclei). The T_s value of 116 °C is the lowest T_s value within domain II or the ideal self-nucleation temperature, i.e., the T_s temperature that causes

maximum self-nucleation without annealing. Therefore, it is not surprising that very small spherulites were produced upon cooling after self-nucleation at 116 °C.

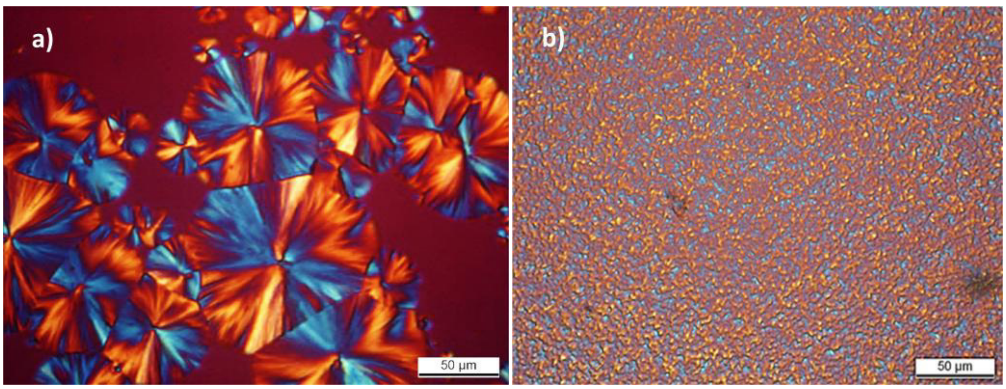

Figure 5. 3. *Polarized optical micrographs of PBS. (a) The sample was cooled from the 145ºC (domain I), (b) Sample cooled from the 116ºC (domain II).*

Similar self-nucleation experiments were performed to the PBS-rich phase of the $BS_{45}BAz_{55}$ copolymer and are presented in Figure 5.4 with similar color codes as those employed to indicate the self-nucleation domains in Figure 5.2.

Figure 5.4a shows that when the PBS-rich phase is self-nucleated, within domain II (blue curves in Figure 5.4a the complex crystallization peak changes as T_s decreases. The high temperature shoulder progressively shifts to higher temperature provoking a separation of the original peak that contained a shoulder into two peaks. At T_s = 59 °C, the peak crystallization temperature of the PBS-rich phase is above 25 °C. At the same time a low temperature crystallization exotherm develops at temperatures below 0 °C that corresponds to the crystallization of the PBAz-rich phase. Upon comparing in Figure 5.4a the DSC cooling curves from T_s = 100 °C (domain I) and T_s = 59 °C (domain II), it is clear that trough self-nucleation the separate crystallization of each phase has been achieved. However, the PBS-rich phase that after self-nucleation crystallizes at much higher temperatures does not nucleate the PBAz-rich phase. On the contrary, the self-nucleated PBS-rich phase antinucleates the PBAz-rich phase, as will be also evidenced below in Figure 5.4a.

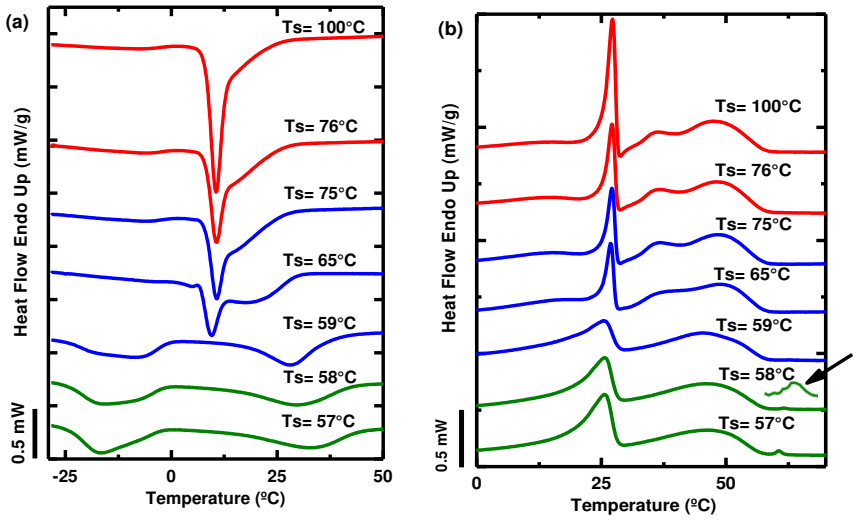

Figure 5. 4. *Self-nucleation of the PBS-rich crystalline phase within $BS_{45}BAz_{55}$: (a) DSC cooling scans from the indicated self-nucleation (T_s) temperatures and (b) subsequent heating scans at 10 °C/min.*

Figure 5.4b shows the subsequent DSC heating scans, after the cooling runs performed in Figure 5.4a. The self-nucleation process produces, besides a separate crystallization, a broadening of the PBAz-rich phase melting (i.e., the melting process occurring between 0 and 27 °C) when T_s temperatures are in the lower range of domain II (at 59 °C). The melting enthalpy of the PBS-rich phase varies as expected during the self-nucleation process.[4, 5] However, in the case of the PBAz-rich phase, the melting enthalpy sharply decreases when the sample goes from domain I to domain II. This is due to the antinucleation effect caused by the anticipated crystallization of the PBS-rich phase when it is self-nucleated.

The self-nucleation domains of the PBS-rich phase within $BS_{45}BAz_{55}$ are schematically shown by vertical lines on top of the DSC standard heating scan of the material presented in Figure 5.5. The crystallization peak temperatures corresponding to the self-nucleation of the material are also presented in Figure 5.5. In domain I coincident crystallization occurs and only one T_c value is plotted in Figure 5.5. When the material is self-nucleated, an interesting behavior is observed. As the PBSrich phase is self-nucleated, its T_c value is greatly increased as T_s decreases as expected. However, the peak

crystallization temperature of the PBAz-rich phase is seen to dramatically decrease as T_s decreases, an evidence of antinucleation.

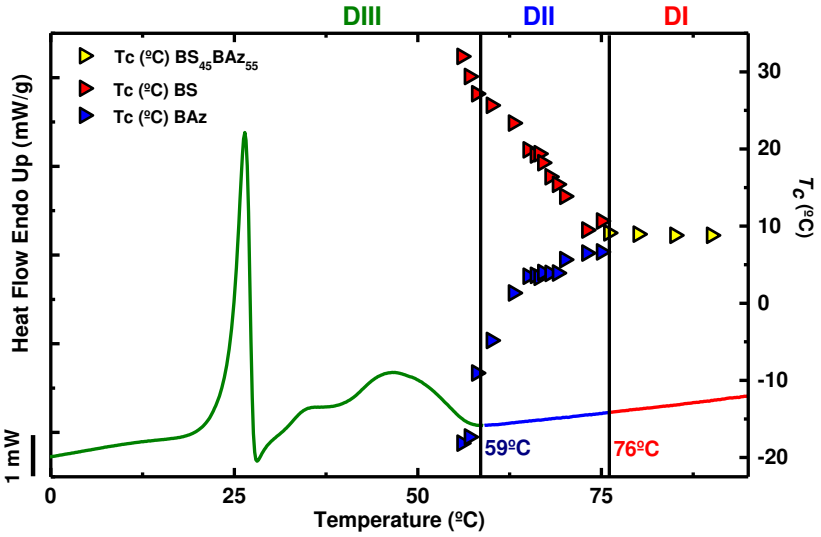

Figure 5. 5. *Representation of the self-nucleation domains for the PBS-rich crystalline phase within $BS_{45}BAz_{55}$ on top of a standard DSC melting trace for the copolymer. The data points represent peak crystallization temperatures for the indicated phases (plotted on the right-hand side y axis) as a function of T_s values (plotted on the x axis).*

The $BS_{45}BAz_{55}$ random copolymer forms a single phase melt (a fact that was also corroborated by SAXS, data not shown). Upon cooling from the melt, the PBS-rich phase crystallizes first (at higher temperatures) in space filling spherulites (see PLOM micrographs in Figure 4.11 in Chapter 4) where later (at lower temperatures) the PBAz-rich phase must accommodate inside their interlamellar spaces. If the PBS-rich phase is self-nucleated, it can crystallize to saturation at much higher temperatures well before the PBAz-rich phase starts to crystallize. The PBAz-rich phase antinucleation is therefore probably caused by topological restrictions created in the interlamellar domains of PBS-rich phase spherulites that are fully grown and impinged with one another.

On the other hand, when the $BS_{45}BAz_{55}$ is not self-nucleated, upon cooling from the melt at 10 °C/min, the PBS-rich phase cannot complete its crystallization before the PBAz-rich phase starts to crystallize and coincident crystallization or simultaneous crystallization develops.

5.4 Successive Self-nucleation and Annealing (SSA)

5.4.1 SSA in PBS-*ran*-PBAz copolymers

Figure 5.6 shows DSC heating scans of both homopolymers (PBS and PBAz) and $BS_{45}BAz_{55}$ copolymer, before and after having been subjected to SSA treatments. Vertical lines indicate the values of the T_s temperatures employed for the fractionation. All studied samples (Figure 5.6 and Figure 5.7) exhibit fractionation, and therefore a distribution of lamellar sizes that melt at distinct temperatures has been produced by SSA. The higher the melting point is, the thicker the lamellae are.

As it is clearly seen in Figure 5.6, the SSA technique is less effective in linear homopolymers, because the only possible thermal fractionation that can be achieved is due to molecular segregation based on chain length differences. Nevertheless, a certain degree of thermal fractionation is achieved in both homopolymers probably aided by their low melt viscosity. Similar behavior of linear chain polyesters has also been reported.[6-10]

In all cases, the number of expected fractions was generated by the SSA fractionation, taking into account that the ideal self-nucleation temperature causes only self-nucleation and no annealing, therefore this first T_s temperature does not generate a thermal fraction.[11] In Figure 5.6a, the standard DSC scan of PBS (after having been cooled at 20 °C/min) exhibits a cold crystallization exotherm before a large bimodal melting endotherm. After SSA, the cold crystallization disappears, as the successive self-nucleation and annealing treatments induce crystallization of the PBS sample up to saturation, as expected.

SSA is particularly sensitive to chain branches or to any molecular unit (e.g., comonomer) that interrupts the linear sequence of the crystallizable chains. This makes SSA an ideal technique to study copolymers where one of the monomers cannot crystallize and interrupts the crystallization of the other. The typical example is that of ethylene/α-olefin copolymers, where short chain branches are excluded from the crystal lattice.[11]

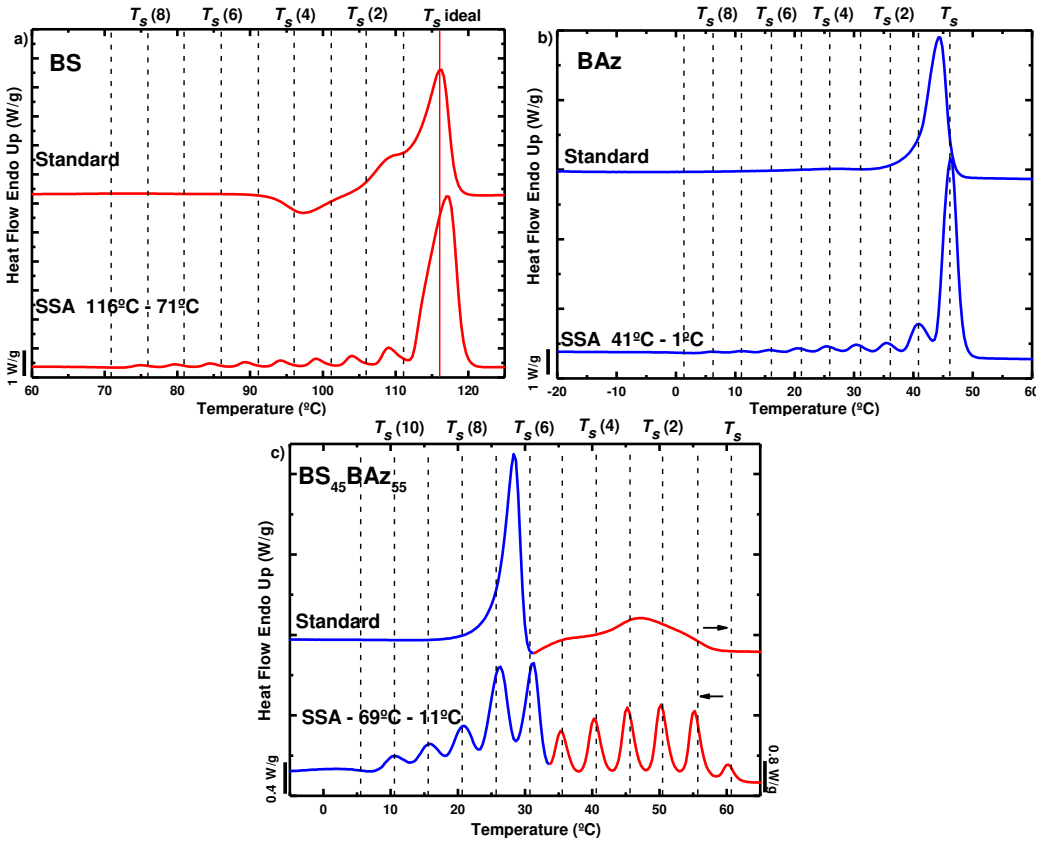

Figure 5. 6. *DSC heating scans (20ºC/min) for a) BS, b) BAz and c) $BS_{45}BAz_{55}$, before and after SSA fractionation.*

In the present case of isodimorphic copolymers, will SSA be capable of fractionating the copolymer samples up to a larger extent than their parent homopolymers? If both comonomers were equally incorporated inside the crystal lamellae, then SSA would not be able to fractionate the copolymers up to a larger extent than the homopolymers.

According to the results presented in Figures 5.6 and 5.7, SSA can fractionate PBS-*ran*-PBAz random copolymers up to a greater extent (in terms of quality of fractionation and relative amount of each fraction) than in the case of the parent homopolymers. This is an interesting result, since it indicates that the degree of isodimorphism achieved by the copolymers is limited, as anticipated from the small changes in the unit cell dimensions (see ref. 5 and below). In other words, when the PBS-rich phase crystallizes, it excludes a large number of PBAz repeating units (and vice

versa) from the growing crystals, leading to the molecular fractionation phenomenon that is the basis of thermal fractionation.

Each melting peak obtained in the final DSC heating scan after SSA corresponds to the melting of a different thermal fraction. Each thermal fraction will be formed by chains whose crystallisable chain lengths are similar. The higher the melting point, the longer the crystallisable sequence length and the larger the average lamellar thickness in the crystals belonging to the thermal fraction.

Figure 5.7 shows the evolution of the SSA fractionation profiles with composition. The blue color has been assigned to the PBAz and PBAz-rich thermal fractions, while red has been used for PBS and PBS-rich fractions.

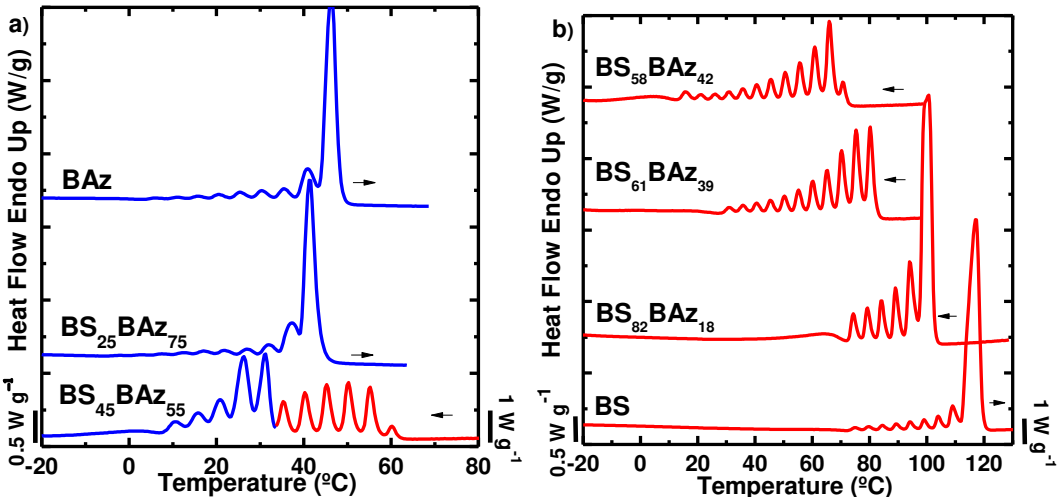

Figure 5. 7. *Final heating DSC scans after applying the SSA protocol for the indicated homopolymers and random copolymer samples.*

In the case of neat PBAz (code BAz in Table 5.1), the most important and largest thermal fraction within the material is that corresponding to the sharp highest temperature peak (at approximately 45 °C), see Figure 5.7a. The behavior changes when BAz is added in the copolymers. When 25 mol% of BS is included in the copolymer, the fractionation profile is qualitatively similar to that of neat PBAz. However, it shows a significant displacement to lower temperatures. Such melting point depression of the dominant fraction (which now peaks at 41.5 °C) is due to the interruption of the crystallizable linear BAz units by the 25 mol % BS component that is randomly distributed within the chains.

Only a small portion of such BS units can be incorporated in the PBAz-rich crystals (as indicated by WAXS below), while the rest are acting as defects that restrict PBAz crystallization. Additionally, subtle changes in the fractionation profile can be also seen. The relative proportion of the first (highest melting point) fraction with respect to the second is changing, as the first fraction decreases in height while the second slightly increases in the $BS_{25}BAz_{75}$ copolymer as compared to neat PBAz (see also Figure 5.8 below).

When the amount of BS in the copolymer increases to 45%, the PBAz component is still able to crystallize and to fractionate by SSA (see Figure 5.7a). However, the fractionation profile that corresponds to the PBAz-rich phase has greatly changed. The second highest melting point fraction is now as intense and important as the first. The results of Figure 5.7a indicate that as the amount of BS units in the copolymer increases, the exclusion of BS repeating units from the PBAz-rich phase crystals also increases. As the quality of the fractionation increases, melting points of the fractions decrease and the total crystal fraction (as judged by the enthalpy of melting) also decreases. It should be noted that in Figure 5.7a, a change in scale had to be introduced to represent the copolymer with 45 molar % BS.

Figure 5.7b shows the final heating scan after SSA, or SSA fractionation profiles, for neat PBS and PBS-rich copolymers. For all cases presented in Figure 5.7b only PBS or PBS rich crystals are formed (with crystal unit cells very similar to that of neat PBS as will be shown below). For these PBS rich copolymers, the addition of PBAz units lowers their T_g values (see ref. 5). Therefore, apart from the interruption of the linear PBS sequences by BAz repeating units, a plasticization effect also contributes to the melting point depressions. As can be seen in Figure 5.9 below, the copolymers PBS-rich phase experiences a far larger melting point depression with composition than the PBAz-rich phase. From the large changes in the fractionation profiles caused by only 18 mol% BAz addition, it seems the effect of adding BAz to PBS is more significant than adding BS units to PBAz.

The large change in the distribution of SSA thermal fractions for the PBS-rich crystalline phase in the copolymers can be appreciated in Figure 5.8. In order to quantitatively assess the changes in fractionation profile, the relative height (h_r) of each thermal fraction was calculated for the 6 highest melting temperature thermal fractions, employing the following expression (Equation 5.1):

$$h_r = \frac{h_i}{\sum_{i=1}^{n} h_i} \qquad 5.1$$

where h_i is the height of the melting peak of thermal fraction ''i''.

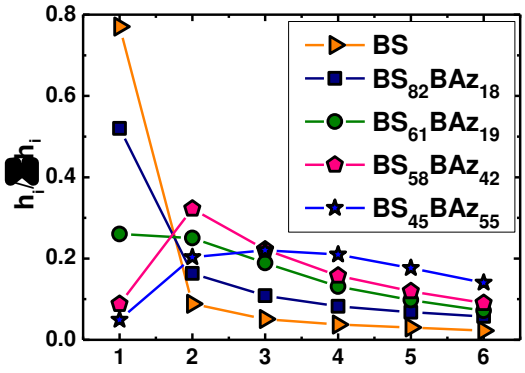

Figure 5. 8. *Distribution of SSA fractions expressed as normalized height values corresponding to the 6 highest temperature melting fractions.*

The results are plotted in Figure 5.8. Fraction 1 starts as the dominant fraction (i.e., that with the maximum relative height) in neat PBS. As BAz units are added to the copolymer, the importance of fraction 1 gradually decreases, at the expense of the increase in the other fractions. The dominant fraction gradually changes from fraction 1 to fraction 2 and finally to fractions 3, as the amount of BAz in the copolymer increases.

The large changes observed in Figure 5.8 indicate that as the amount of BAz in the copolymer increases, the comonomer exclusion to the amorphous regions also increases, suggesting that the amount of comonomer inclusion is relatively small and does not increase very much with composition. These results are consistent with the WAXS results to be presented below.

Figure 5.9 compares the melting temperatures of the highest temperature peak as a function of composition after SSA fractionation, with a trend line of the melting temperatures of samples without SSA. SSA promotes molecular segregation and lamellar thickening during the fractionation periods where unmolten crystals are sequentially annealed. Therefore, SSA should promote the maximum exclusion of non-crystallizable defects to the amorphous regions of the sample. Hence, one would expect that in the present case, SSA would induce more comonomer exclusion as samples that have not been treated with the SSA protocol.

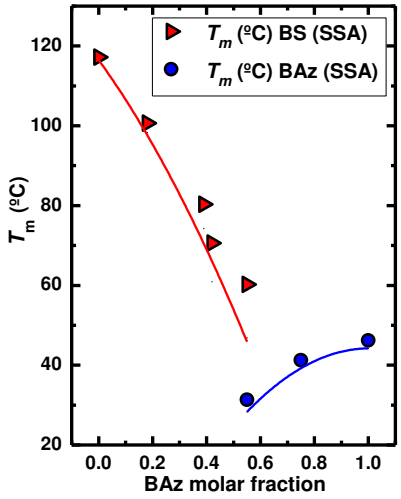

Figure 5. 9. *Highest temperature peak melting values as a function of copolymer composition. Data points correspond to measurements after SSA fractionation (i.e., Tm values of the highest temperature fraction for each sample are shown) and the trend line corresponds to melting peak values of the samples determined during a second DSC scan at 20 ºC/min (without SSA fractionation).*

According to the thermal behavior presented in Figure 5.9, the differences between samples with and without SSA fractionation are not very large. As expected, the melting point values are slightly higher for the samples submitted to SSA fractionation. For copolymers where the random copolymer chains contain a majority of BS repeating units, PBS dominates the copolymer structural behavior, whereas for compositions with more than 55 % BAz, only PBAz like crystals can form according to WAXS (see below).

As demonstrated previously,[12] the $BS_{45}BAz_{55}$ random copolymer is a special material. It is very near the eutectic composition observed in Figure 5.9. The presence of

a eutectic point has also been reported for several isodimorphic copolyesters[12] Furthermore, this is one of the few copolymers where both PBAz and PBS-rich crystalline phases can be formed, and therefore it is a double crystalline random copolyester. During the heating scans separate melting of PBAz and PBS-rich crystalline phases can be clearly observed for samples with or without SSA. Figure 5.7a shows how after SSA, both crystalline components are clearly fractionated indicating a high degree of comonomer exclusion.

The two melting points corresponding to the $BS_{45}BAz_{55}$ random copolymer are also plotted in Figure 5.9 at the corresponding composition. Such double crystalline structure in a random copolymer is difficult to explain without some degree of isodimorphism. Otherwise, a nearly 50/50 random copolymer where total comonomer exclusion is present would be completely amorphous.

5.4.2 Wide Angle X-ray Scattering (WAXS)

Samples for WAXS were prepared in the DSC using the same SSA thermal protocol applied to the samples for the DSC measurements shown in Figure 5.6 and Figure 5.7 but without the final heating scan, in order to preserve the morphology created by SSA fractionation. Then they were loaded in the diffractometer chamber at 25 °C and the WAXS patterns were measured.

Figures 5.10a and 5.10b, and Figures 5.10c and 5.10d, show the diffractograms at 25 °C of the samples without and with SSA fractionation respectively. If the WAXS patterns before and after SSA are compared, no large qualitative differences are appreciated. The WAXS pattern for poly(butylene succinate) corresponds to the most common α form, whose monoclinic unit cell dimensions are reported to be[13-16] a = 0.523 nm, b = 0.908−0.912 nm, c = 1.079−1.090, nm and β = 123.9°. The most intense reflections for PBS appeared at 0.452, 0.404, and 0.392 nm, and they have been indexed in Figure 5.10 as (020/$\bar{1}$11), (021) and (110) planes.[2, 13-17]

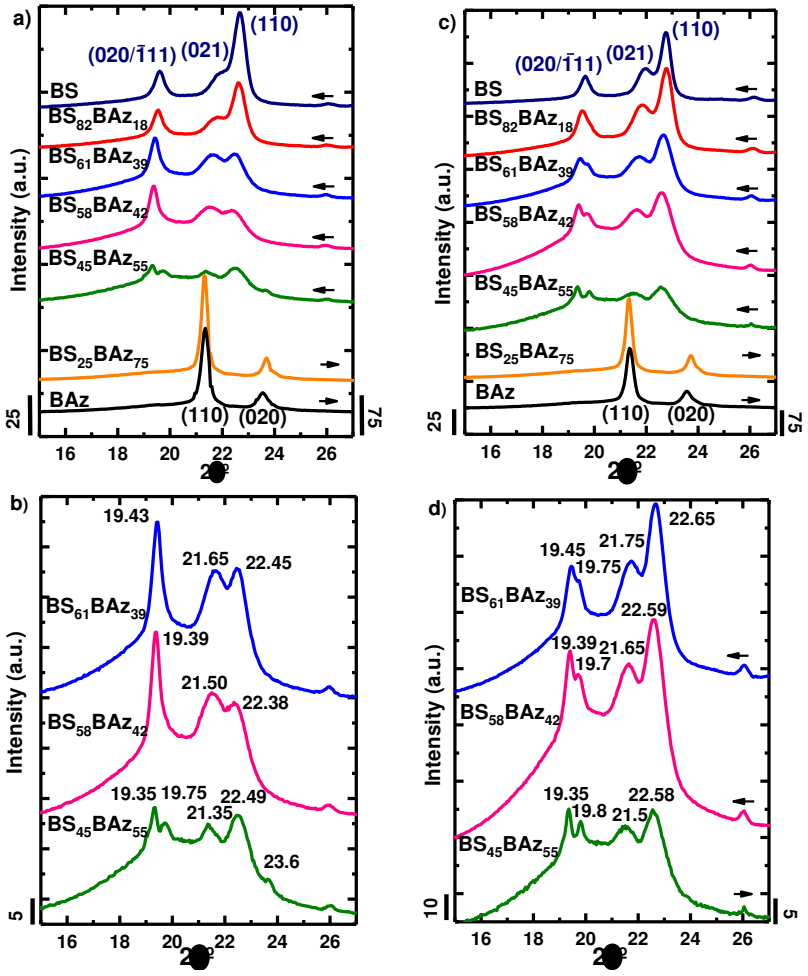

Figure 5. 10. *WAXS diffraction patterns at 25 °C: (a) and (b) before SSA, (c) and (d) after SSA.*

For PBAz, a recent publication[17] has reported that fiber patterns from a melt drawn homopolymer are consistent with an orthorhombic unit cell with the following dimensions: a = 0.496 nm, b = 0.746 nm, and c = 3.65 nm. The most intense WAXS reflections of this homopolymer appeared at 0.416 and 0.377 nm and they have been indexed to (110) and (020) as indicated in Figure 5.10.

The WAXS patterns of Figure 5.10 indicate that at 25 °C, almost all samples contain only one type of crystal. The samples which have more than 58 % BS only display reflections that are consistent with a PBS type unit cell. On the other hand, the BAz and $BS_{25}BAz_{75}$ display a WAXS pattern that is characteristic of neat PBAz. $BS_{45}BAz_{55}$ contains characteristic reflections of both phases, although the WAXS pattern

is completely dominated by PBS reflections. The reason behind this result is that the PBAz phase is partially molten at 25 °C, the temperature at which the WAXS patterns were taken (see Figure 5.6c).

Analysing the WAXS patterns in more detail, the samples after SSA fractionations (Figure 5.10b) show more intense and narrower signals than the samples without SSA fractionation (Figure 5.10a), as a result of the higher crystallinity degree (see below Table 5.2) which was increased considerably as a result of the SSA thermal treatment.

In order to better appreciate differences in the samples before and after SSA, Figures 5.10c and 6d presents close-ups for 3 specific samples. Figure 5.10d shows that a new small signal (appearing at 2θ values of approximately 19.7-19.8°) that is not present in neat BS appears after SSA in the WAXS patterns of $BS_{61}BAz_{39}$ and $BS_{58}BAz_{42}$ but is absent in the samples without SSA (Figure 5.10c).

As the peak indexed as (020/$\bar{1}11$) in neat PBS (Figure 5.10a) is a mixture of (020) and ($\bar{1}11$) reflections,[16] with very close *d* spacings, the new peak that appears at ~19.75° in the copolymer samples (Figure 5.10d) could be assigned to the ($\bar{1}11$) reflection of PBS. It has been reported before,[2, 17] that when the BAz content increases in the copolymer samples, the lattice spacings increases as well. This increase occurs to accommodate the BAz units that are larger in size as compared to the BS units. The (020) plane reflects the intermolecular distances, while the ($\bar{1}11$) is influenced by both the intermolecular distance and repeating length along the chain. If we only consider the expansion along *b* axis (more loosely packed compared with *a* axis), the (020) plane expanses much faster than ($\bar{1}11$) plane. This causes the splitting of the two overlapped peaks. Another reason for the assignment is that the intensity of ($\bar{1}11$) reflection is much weaker compared with the (020) reflection, according to Ichikawa et al.[14] The splitting of the (020) and ($\bar{1}11$) reflections becomes more significant in samples after SSA (Figure 5.10d). Another observation is that the intensity of (110) reflection becomes obviously stronger after SSA. This indicates that the crystallites can rearrange their internal structure during SSA.

Figure 5.11 shows the *d* spacing values of selected diffraction planes for the PBS-rich samples, before (solid line) and after SSA fractionation (data points). The PBS-rich phase in the copolymers exhibits a PBS like unit cell whose size increases when BAz is included in the copolymer.

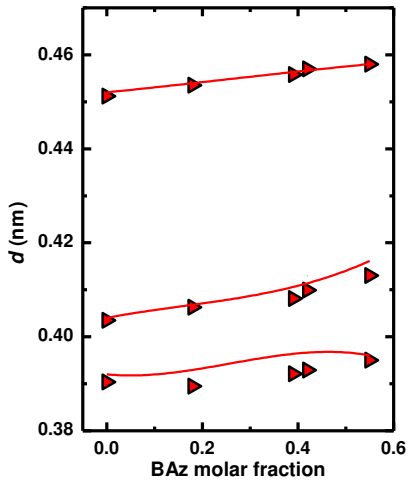

Figure 5. 11. *Experimental diffraction spacings (d) for PBS and PBS-rich crystalline phases as a function of BAz molar content. From bottom to top, data for (110), (021), and (020) planes are presented. Data points correspond to samples after SSA fractionation and solid lines to measurements without SSA fractionation.*

Although the *d* spacing values after SSA are slightly smaller than those in samples without SSA, there are no big differences between *d* spacing before and after SSA. Therefore, it seems that even an SSA fractionation protocol, which usually drives polymeric crystals closer to equilibrium, is not enough to expel all the minority comonomer groups to the amorphous regions. Therefore, the crystal unit cells have to increase slightly their volume (an increase in (020) plane distances indicates a unit cell expansion, as the unit cell dimension b increases) to accommodate the extra PBAz repeating units that coexist with the PBS major component when BAz content increases, supporting the idea of isodimorphic cocrystallization.

5.4.3 Small Angle X-ray Scattering (SAXS)

In order to get information about lamellar sizes, analogous experiments to those performed by WAXS were conducted employing SAXS. Figure 5.12a and Figure 5.12b show the plots of relative SAXS scattering intensities before and after SSA fractionation respectively. All the samples exhibit an intense main maximum that can be interpreted as the long period of the lamellar stacks. Secondary maxima are seen in some cases due to higher order reflections.

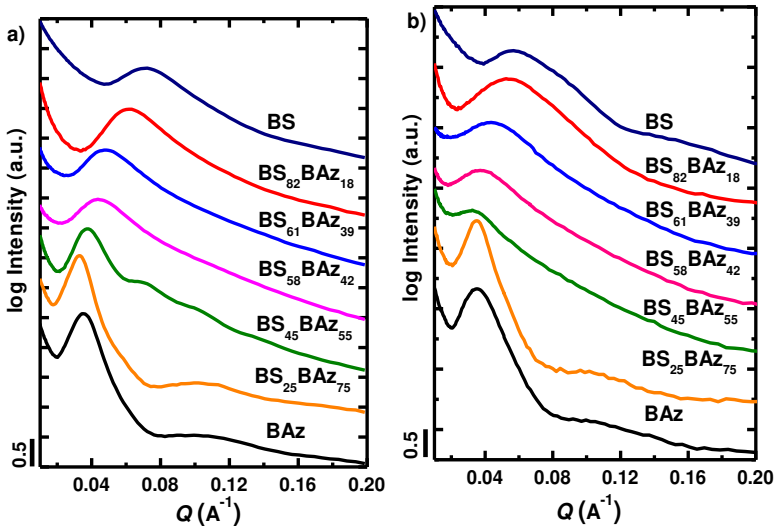

Figure 5. 12. *Intensity as a function of scattering vector for the indicated homopolymers and copolymers. Data taken at 25 °C: (a) before SSA and (b) after SSA.*

The long periods (d^*) corresponding to Figure 5.12 were estimated by equation 5.2 from Lorentz corrected plots (Iq^2 versus q):

$$d^* = (2\pi)/q_{max} \qquad 5.2$$

Figure 5.13 presents how the obtained long periods (d^*) vary as a function of copolymer composition. The qualitative trends before and after SSA are similar. The long period strongly depends on composition. All values to the left of the $BS_{45}BAz_{55}$ copolymer correspond to d^* spacings of PBS and the PBS-rich phase within the copolymers, while of the only two remaining data points correspond to the PBAz-rich

phase and PBAz respectively. Additionally, the long period values to the left of the eutectic point, (i.e., PBS and PBS-rich crystalline phases), increase with BAz content in the copolymers. This behavior indicates that the incorporation of PBAz both in the crystalline unit cell and in the amorphous regions of the PBS rich interlamellar zones has a synergistic effect on the morphology at the lamellar level. On the other hand, when 25 % BS is included in the PBAz rich copolymer, *d** increases. This behavior is related to the incorporation of some BS repeating units inside the PBAz-rich phase lamellae.

SSA fractionation promotes annealing and should therefore induce lamellar thickening. However, the results after SSA in Figure 5.13, do not show significant changes in *d** (only a small increment in some cases for the PBS and PBS-rich samples, while a decrease is seen for the PBAz and PBAz-rich cases). To demonstrate whether the increase of the long period (*d**) comes from the amorphous layer (l_a) or the crystalline layer (l_c), the contribution of each component has to be calculated.

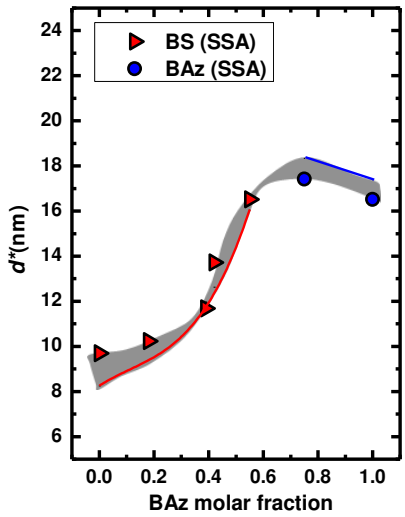

Figure 5. 13. *Long periods (d*) obtained by SAXS as a function of copolymer composition (expressed as BAz molar fraction). Data points correspond to samples after SSA fractionation and solid lines to measurements without SSA fractionation. The shadowed area shows differences in trends before and after SSA.*

The calculation of the crystalline lamellar thickness, l_c, was performed employing the following approximation:

$$l_c = d^* x_v \quad 5.3$$

where x_v is the crystalline volume fraction that was estimated from the following equations.

$$x_v = (x_m \rho)/\rho_c \quad 5.4$$

$$x_m = \frac{\Delta H_m}{\Delta H_{m(100\%)} W} \quad 5.5$$

where x_m is the mass fraction of crystals, ρ is the experimentally determined density of the sample (at 25 °C), and ρ_c is the density of a 100% crystalline sample. The mass fraction of crystals can be calculated from the enthalpy of fusion of the phase under consideration (ΔH_m), the enthalpy of fusion of a 100% crystalline sample and the weight fraction of the phase under consideration (W) employing equation 5.5.

$$l_a = d^* - l_c \quad 5.6$$

Table 5. 2. *Density (±0.0003 g cm^{-3}), normalized crystallization enthalpy (±1 J g^{-1}), mass and volume crystalline fractions (±0.01), long period, and lamellar thickness values (±0.1 nm).*

Before SSA (25 °C)

	ρ (g/cm^3)	ΔH_m (J/g)	X_m	X_v	d^* (nm)	l_c (nm)	l_c' (nm)
BS	1.2447	67	0.32	0.32	8.2	2.6	2.7
$BS_{82}BAz_{18}$	1.1973	67	0.32	0.30	9.4	2.8	2.8
$BS_{61}BAz_{39}$	1.1672	68	0.32	0.30	12.0	3.6	4.1
$BS_{58}BAz_{42}$	1.1399	79	0.38	0.34	12.6	4.3	4.1
$BS_{45}BAz_{55}$	1.1355	73	0.35	0.31	16.1	5.0	--
$BS_{25}BAz_{75}$	1.1224	68	0.45	-	18.3	8.3[a]	6.7
BAz	1.1087	51	0.34	-	17.4	5.9[a]	6.2

After SSA (25 °C)

	ρ (g/cm^3)	ΔH_m (J/g)	X_m	X_v	d^* (nm)	l_c (nm)	l_c' (nm)
BS	1.2770	100	0.48	0.48	9.7	4.7	3.1
$BS_{82}BAz_{18}$	1.2066	101	0.48	0.46	10.2	4.7	2.9
$BS_{61}BAz_{39}$	1.2105	85	0.41	0.39	11.7	4.6	4.2
$BS_{58}BAz_{42}$	1.1672	73	0.35	0.32	13.7	4.4	4.3
$BS_{45}BAz_{55}$	1.1831	77	0.37	0.35	16.5	5.7	--
$BS_{25}BAz_{75}$	1.1041	74	0.49	-	17.5	8.6[a]	6.4
BAz	1.1331	66	0.44	-	16.6	7.3[a]	5.7

[a]These values were calculated using the following approximation: $l_c = d^*x_m$ because ρ_c is unknown for PBAz. The density of the samples was measured at 25 °C.

The density of the samples was measured at 25 °C and the results are listed in Table 5.2. The melting enthalpies reported in Table 5.2 have been normalized to take into account the weight fraction of the crystallizable phase. The enthalpy of fusion of a 100% crystalline sample and the crystalline density of PBS can be found in the literature, $\Delta H_{m(100\%)}$ = 210 J g^{-1} [18] and ρ_c= 1.26 g cm^{-3}.[19] A value for $\Delta H_{m(100\%)}$ of 150 J g^{-1} has been reported[20] for PBAz. However, since the number of repeating units per unit cell is unknown, its density cannot be calculated. The thickness of amorphous layer can be calculated by equation 5.6.

The average lamellar thickness was also calculated by the one-dimensional electron density correlation function K(z).[21]

$$K(z) = \frac{\int_0^\infty I(q)q^2 \cos(qz)\,\mathrm{d}\,q}{\int_0^\infty I(q)q^2\,\mathrm{d}\,q} \qquad 5.7$$

where z is the correlation distance along which the direction of the electron density distribution is measured. $I(q)$ is the 1-dimensional intensity profile. Multiplication of q^2 is carried out to account for the isotropic distribution. In this work, as the measured q range does not reach the Guinier region and Porod region, no extrapolation was carried out.

Figure 5.14 shows a typical correlation function, demonstrating how the crystalline layer thickness $l_c´$ can be estimated. The data obtained from the correlation function analysis ($l_c´$) was included in Table 5.2. It should be noted that multiple oscillations were observed in the K(z) curves of $BS_{45}BAz_{55}$, indicating the failure of the method. This can be explained since that sample cannot be described by a simple two phase model, probably because of the existence of two crystalline phases at 25 °C. It is observed that the lamellar thickness measured by the correlation function analysis is smaller than that calculated by multiplying the long period by the crystal volume fraction.

However, the lamellar thickness calculated by the two methods shows a similar variation with copolymer composition.

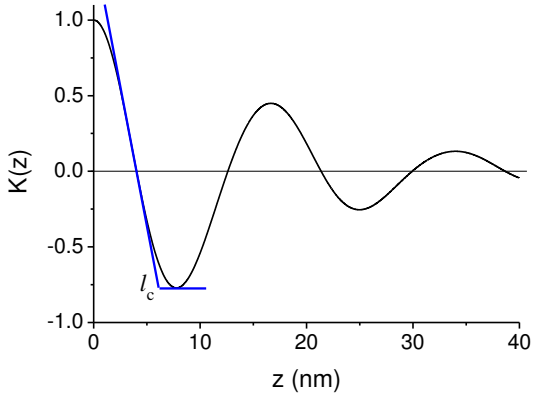

Figure 5. 14. *Example showing the analysis of lamellar structure using electron density correlation analysis. The sample is BAz before SSA. As the crystallinities of the copolymers were believed to be smaller than 0.5, the smaller value was assigned to the crystalline layer thickness.*

Figure 5.15 shows a plot of the calculated crystalline lamellar thickness (l_c) and amorphous layer thickness (l_a) as a function of copolymer composition before and after SSA. To better appreciate the differences, an area between the data points before and after SSA has been shaded. Figure 5.15 demonstrates how the crystalline lamellar thickness values are higher after SSA fractionation for most samples, as expected. However, Table 5.2 shows that for the electron density correlation analysis, similar results are obtained, except for PBAz and $BS_{25}BAz_{75}$. In these two cases the differences are very small before and after SSA and the results may be influenced by the way the values are extracted from the data.

The trends observed in Figure 5.15 can be explained by the compensating effect that the crystalline fraction has on the long period value (reflected in equation 3 and 6). In other words, although the crystalline phase volume is higher, there is also less interlamellar amorphous phase and the values of long period remain almost unchanged before and after SSA (see Figure 5.13). From these results it can be concluded that after SSA thermal fractionation, total exclusion of the minor comonomer units in the crystals is not obtained.

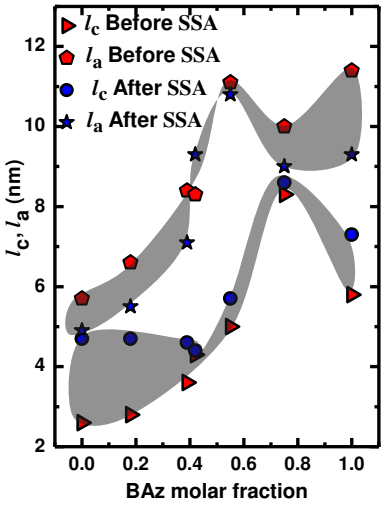

Figure 5. 15. *Crystalline lamellar thickness (l_c) and amorphous layer thickness (l_a) obtained as a function of copolymer composition (expressed as BAz molar fraction). The shadowed areas show differences in trends before and after SSA.*

5.5 Conclusions

This work shows that a low degree of co-crystallization (i.e., comonomer inclusion) occurs in PBS-*ran*-PBAz random copolymers when they are cooled from the melt or subjected to an SSA fractionation protocol. For PBS-rich copolymers, the PBS-rich phase can accommodate a small amount of BAz units within the PBS like crystalline unit cells that are formed. A similar phenomenon occurs with PBAz-rich copolymers. In the case of the $BS_{45}BAz_{55}$ random copolymer (which has a composition near the pseudo-eutectic point), two crystalline phases are formed, each one with a minor content of the second co-unit within the copolymer. After self-nucleation of the PBS-rich crystalline phase, the separate crystallization of both phases can be achieved in this double crystalline $BS_{45}BAz_{55}$ copolymer.

SSA results have demonstrated that comonomer exclusion drives the fractionation ability of the samples. Therefore, the amount of comonomer inclusion is much lower than the amount of comonomer exclusion during crystallization.

Isodimorphism stems from the similarity of the repeating units of PBS and PBAz and it is independent of kinetic factors. This conclusion is reached after determining that the degree of comonomer exclusion remains almost unchanged, even after SSA, a thermal fractionation technique that promotes segregation of molecular defects that interrupt crystallizable sequences.

5.6 References

1. Mincheva, R.; Delangre, A.; Raquez, J. M.; Narayan, R.; Dubois, P., Biobased Polyesters with Composition-Dependent Thermomechanical Properties: Synthesis and Characterization of Poly(butylene succinate-co-butylene azelate). *Biomacromolecules* **2013,** *14*, 890-899.
2. Arandia, I.; Mugica, A.; Zubitur, M.; Arbe, A.; Liu, G.; Wang, D.; Mincheva, R.; Dubois, P.; Müller, A. J., How Composition Determines the Properties of Isodimorphic Poly(butylene succinate-ran-butylene azelate) Random Biobased Copolymers: From Single to Double Crystalline Random Copolymers. *Macromolecules* **2015,** *48*, 43-57.
3. Lorenzo, A. T.; Arnal, M. L.; Sanchez, J. J.; Muller, A. J., Effect of annealing time on the self-nucleation behavior of semicrystalline polymers. *Journal of Polymer Science Part B: Polymer Physics* **2006,** *44*, 1738-1750.
4. Fillon, B.; Wittmann, J. C.; Lotz, B.; Thierry, A., Self-nucleation and recrystallization of isotactic polypropylene (alpha-phase) investigated by differential scanning calorimetry. *Journal of Polymer Science Part B: Polymer Physics* **1993,** *31*, 1383-1393.
5. Müller, A. J.; Arnal, M. L., Thermal fractionation of polymers. *Progress in Polymer Science* **2005,** *30*, 559-603.
6. Balsamo, V.; Müller, A.; Stadler, R., Antinucleation effect of the polyethylene block on the polycaprolactone block in ABC triblock copolymers. *Macromolecules* **1998,** *31*, 7756-7763.
7. Sabino, M.; Feijoo, J.; Müller, A., Crystallisation and morphology of neat and degraded poly (p-dioxanone). *Polymer Degradation and Stability.* **2001,** *73*, 541-547.
8. Michell, R. M.; Müller, A. J.; Deshayes, G.; Dubois, P., Effect of sequence distribution on the isothermal crystallization kinetics and successive self-nucleation and annealing (SSA) behavior of poly(ε-caprolactone-co-ε-caprolactam) copolymers. *European Polymer Journal* **2010,** *46*, 1334-1344.
9. Pérez, R. A.; Córdova, M. E.; López, J. V.; Hoskins, J. N.; Zhang, B.; Grayson, S. M.; Müller, A. J., Nucleation, crystallization, self-nucleation and thermal fractionation of cyclic and linear poly(ε-caprolactone)s. *Reactive and Functional Polymers* **2014,** *80*, 71-82.

10. R. A. Perez-Camargo, A. Mugica, M. Zubitur, A. J. Müller, Advances in Polymer Science 2015, doi: 10.1007/12_2015_326..
11. Müller, A. J.; Michell, R. M.; Pérez, R. A.; Lorenzo, A. T., Successive Self-nucleation and Annealing (SSA): Correct design of thermal protocol and applications. *European Polymer Journal* **2015,** *65*, 132-154.
12. L. Sheng, R. A. Register, *Crystallization in Copolymers* . In Handbook of Polymer Crystallization, E. Piorkowska, G. C. Rutkedge, Eds.; Wiley: Hoboken, NJ, **2013**, 327–346.
13. Ihn, K. J.; Yoo, E. S.; Im, S. S., Structure and Morphology of Poly(tetramethylene succinate) Crystals. *Macromolecules* **1995,** *28*, 2460-2464.
14. Ichikawa, Y.; Kondo, H.; Igarashi, Y.; Noguchi, K.; Okuyama, K.; Washiyama, J., Crystal structures of α and β forms of poly(tetramethylene succinate*). Polymer* **2000**, *41*, 4719-4727.
15. Ichikawa, Y.; Suzuki, J.; Washiyama, J.; Moteki, Y.; Noguchi, K.; Okuyama, K., Strain-induced crystal modification in poly(tetramethylene succinate). *Polymer* **1994,** *35*, 3338-3339.
16. Liu, G.; Zheng, L.; Zhang, X.; Li, C.; Jiang, S.; Wang, D., Reversible Lamellar Thickening Induced by Crystal Transition in Poly(butylene succinate). *Macromolecules* **2012,** *45*, 5487-5493.
17. Diaz, A.; Franco, L.; Estrany, F.; del Valle, L. J.; Puiggali, J., Poly(butylene azelate-co-butylene succinate) copolymers: Crystalline morphologies and degradation. *Polymer Degradation and Stability* **2014,** *99*, 80-91.
18. Papageorgiou, G. Z.; Bikiaris, D. N., Crystallization and melting behavior of three biodegradable poly(alkylene succinates). A comparative study. *Polymer* **2005,** *46*, 12081-12092.
19. Yang, J.; Liang, J. Z.; Li, F. J., Melt Strength and Extensional Viscosity of Low-Density Polyethylene and Poly(butylene succinate) Blends Using a Melt-Spinning Technique. *Journal of Macromolecular Science Part B: Physics* **2012,** *51*, 1715-1730.
20. Papageorgiou, G. Z.; Bikiaris, D. N.; Achilias, D. S.; Papastergiadis, E.; Docoslis, A., Crystallization and biodegradation of poly(butylene azelate): Comparison with poly(ethylene azelate) and poly(propylene azelate). *Thermochimica Acta* **2011,** *515*, 13-23.

21. Strobl, G. R.; Schneider, M., Direct evaluation of the electron density correlation function of partially crystalline polymers. *Journal of Polymer Science: Polymer Physics Edition* **1980,** *18*, 1343-1359.

Chapter 6

Broadband Dielectric Spectroscopy

6.1 Introduction

In this chapter Poly(butylene succinate-*ran*-butylene azelate) random copolyesters (PBS-*ran*-PBAz) were studied using Broadband Dielectric Spectroscopy (BDS) and Differential Scanning Calorimetry (DSC), in order to study the complex development of the amorphous phase.

The crystallinity of polymeric materials affects the properties of the remaining amorphous phase in a complex way. It has been generally found that the glass transition of semicrystalline polymers occurs at higher temperatures than that of the corresponding fully amorphous material, additionally, the glass transition range for these semicrystalline materials is usually much broader.[1] These facts reflect constrains that the crystalline phase exert on the amorphous phase of polymers, which eventually lead to the disappearance of the glass transition for materials with crystallinity around 50% or higher. This result is usually attributed to the presence of amorphous segments forming what has been called the rigid amorphous fraction (RAF),[1] whose motions are severely restricted by the crystallites. In this view, a semicrystalline polymer would be composed by at least 3 fractions: the crystalline one, the RAF and the (mobile) constrained amorphous fraction or CAF. The latter would be responsible for the measurable glass transition by DSC, whereas the melting process and the X-ray diffraction reflections are manifestations of the crystalline phase. The RAF still has local mobility, as proved by its contribution to the secondary relaxations.[2] In addition, in the initial stages of crystallization, the experiments evidence the coexistence of these two amorphous fractions with the unconstrained amorphous fraction (UCAF) which is characteristic of the fully amorphous material.[3, 4]

Taking all this into account, one could expect that the situation encountered in copolymers with crystallizable components is probably more intricate since each of the 3

amorphous fractions described above could be found, each one with a different comonomer concentration. In this chapter, we have investigated this complex case in poly(butylene succinate-*ran*-butylene azelate) isodimorphic copolymers. By analyzing the dielectric relaxation of these materials we have had access to both the local and segmental dynamics. The data analysis provided the distinct contributions of the succinate and azelate groups to the local copolymer relaxation allowing a quantification of the fraction of each component involved in the crystalline phase. On the other hand, the behavior of the dielectric relaxation loss peak above the glass transition temperature strongly suggests that a significant UCAF remains in most of the copolymers despite of the relatively high crystallinity. Interestingly, the segmental dynamics is found to be very sensitive to the details of the crystallization process, indicative of subtle changes induced by crystallization in the remaining amorphous phase.

6.2 Broadband Dielectric Spectroscopy (BDS) Results

6.2.1 BDS of Homopolymers

Figure 6.1 presents isochronal plots of permittivity loss versus temperature at 10^2 Hz for PBS and PBAz homopolymers (denoted BS and BAz). Two peaks are observed for each sample, which correspond to different kinds of molecular motions. On one hand, the α relaxation process, detected at high temperatures is related with the cooperative mobility of relatively large segments of the polymer, those related with the glass transition. On the other hand, the β relaxation, detected at lower temperatures is attributed to local molecular rearrangements occurring in the glassy state.[5] It should be noted that a single β relaxation is observed for semicrystalline PBS, which is at odds with a recently published work where an additional slower β relaxation component was observed.[6] We confirmed that this difference is attributed to the careful drying of the sample used before our dielectric experiments (see Appendix part). For both PBS and PBAz, the dielectric relaxations are related with reorientations of the dipole moments in the ester groups.

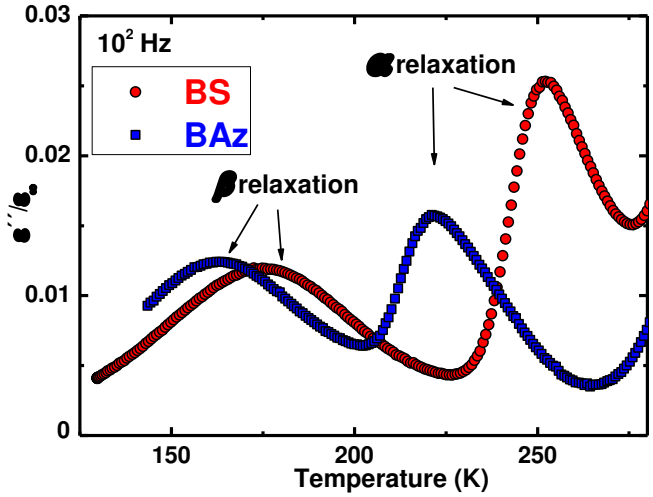

Figure 6. 1. *Isochronal plots of ε´´/ε∞ for BS and BAz homopolymers at 10^2 Hz.*

The isothermal permittivity loss versus frequency for the homopolymers at different temperatures, where the β relaxation can be easily recognized, is shown in Figure 6.2a. The BAz β relaxation peaks have higher intensity as compared to those corresponding to BS. Moreover, the peak frequency, f_{max}, of BAz losses occurs at markedly higher frequencies than those of BS, indicating a faster local dynamics of the former. This could be attributed to the longer aliphatic part of the BAz repeating unit. In order to quantify these differences, the relaxation time from each isothermal plot has been calculated as:

$$\tau = (2\pi f_{max})^{-1} \qquad 6.1$$

The resulting values are presented in Figure 6.2b. For both polymers a clear Arrhenius behavior is found and accordingly the data have been fitted to Arrhenius equation:

$$\tau(T) = \tau_{\infty}\, exp\left[\frac{E_a}{k_B T}\right] \qquad 6.2$$

The resulting fitting parameters are shown in Table 1. The activation energy for BS, as determined from the Arrhenius fit, is 41.1 kJ/mol, which agrees very well with values

previously reported,[7, 8] whereas the value for BAz is 39.2 kJ/mol. No values of activation energy for BAz have been found in literature, but the value obtained here is close to those reported for other aliphatic polyesters.[9-13]

As can be seen in Table 6.1, the values obtained for τ_∞ are far smaller than those corresponding to typical vibrational frequencies, a situation that is often found when analyzing the secondary relaxations of polymers. These extremely low values are indicating that the molecular origin of the relaxation does not correspond to single activated jumps between two equivalent positions of molecular units over an energy barrier, and therefore, a more complex situation should be envisaged. One way of describing such behavior is by using the Eyring equation, where the relaxation time is expressed in terms of the difference in the Gibbs free energy, $\Delta G=\Delta H-T\Delta S$, between the equilibrium and the activated state. This leads to an equation (eq. 6.3) similar to the Arrhenius one, where an entropic term appears in addition to the enthalpic one, i.e.

$$\tau(T) = \frac{h}{k_B T}\, exp\left[\frac{\Delta G}{k_B T}\right] = \frac{h}{k_B T}\, exp\left[-\frac{\Delta S}{k_B}\right] exp\left[\frac{\Delta H}{k_B T}\right] \qquad 6.3$$

where h is Plank's constant and ΔH and ΔS are, respectively, the enthalpic and entropic changes corresponding to the activated state. When the data in Figure 6.2b are described in this way, nearly undistinguishable fitting, from the Arrhenius one, is found and the corresponding parameters are also shown in Table 6.1. As expected the entropic terms take relatively large values. When comparing the values of the entropic terms for the two polymers we found a significantly larger value for BAz, a fact indicative of more complex local arrangements. On the other hand, the enthalpic terms obtained with the Eyring analysis are about 10% smaller than the activation energies obtained from the Arrhenius fitting above but follow the same trend.

To analyze more quantitatively the β relaxations, the main part of the loss peak has been described by a Gaussian-like function:

$$\varepsilon''(f) = \varepsilon''_{max}\ exp\left[\frac{(logf - logf_{max})^2}{w^2}\right] \qquad 6.4$$

The fittings to eq. 4 are shown as solid lines in Figure 6.2a. In this way, the main part of the curves (data around the loss peak) are well described, although some deviations at very high and very low frequencies remains evident.

In the framework of the Eyring description used above, the Full Width at Falf Maximum of this Gaussian description of $\varepsilon''(f)$, $FWHM_{\varepsilon''} = 2\sqrt{ln2}\ w$, can be approximately related to the *FWHM* of the corresponding distributions of the enthalpic and entropic terms in the Eyring equation as:[14]

$$FWHM_{\varepsilon''} - 1.14 = \frac{\log e}{k_B T} FWHM_{\Delta H} - \frac{\log e}{k_B} FWHM_{\Delta S} \qquad 6.5$$

The values of $FWHM_{\varepsilon''}$ obtained at different temperatures are well described by this equation and the so obtained $FWHM_{\Delta H}$ and $FWHM_{\Delta S}$ values, corresponding to the distributions of the enthalpic and entropic terms, are also included in Table 6.1. It is found that the distribution width of the entropic term is markedly larger for BS than for BAz, whereas those of the enthalpic terms are not so quite similar to each other.

Table 6. 1. *Parameters Describing the Temperature Dependence of the β relaxation of the Homopolymers. Typical uncertainty values are indicated in the table head.*

β relaxation	τ_∞(s) ± 30 *(%)*	E_a ± 1 (kJ/mol)	ΔH ± 1 (kJ/mol)	ΔS ± 0.001 (kJ K/mol)	FWHM$_{\Delta H}$ ± 5 (%)	FWHM$_{\Delta S}$ ± 5 (%)
BS	3.4×10^{-16}	41	40	0.046	56	110
BAz	7.3×10^{-17}	39	38	0.06	49	64

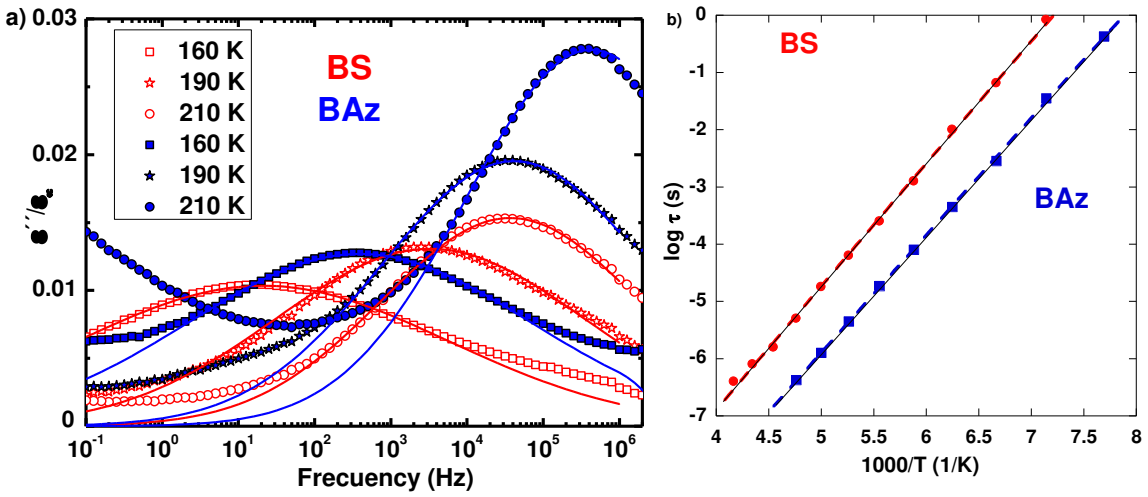

Figure 6. 2. *(a) Dielectric loss spectra versus frequency of both homopolymers at 160, 190 and 210 K. Lines are the descriptions of the main loss peaks in terms of Gaussian like functions (b) Arrhenius plots of β processes for BS and BAz homopolymers. Solid lines are Arrhenius fittings.*

Figures 6.3a and 6.3b show representative isothermal dielectric loss curves in the temperature range relevant for the α relaxation. In these graphs, it can be observed that the α relaxation peaks have lower intensity than those for the β relaxations at the same temperature and this makes difficult an accurate quantitative analysis. The relatively low values of the dielectric losses corresponding to the α relaxation can be attributed to the relatively high crystallinity of the polymers which simultaneously produce a broad relaxation and reduced dramatically the relaxation strength which is proportional to the area below the loss peak.[3] Consequently the quantification of the α relaxation rate has been made by using the isochronal representation of the dielectric losses (see Figure 6.1 as an example). In this representation when selecting low frequencies, the α relaxation is observed as a clear and prominent loss peak a few degrees above T_g, well separated from the secondary relaxation, which is detected at temperatures well below T_g. Moreover, the usually high apparent activation energy of the α relaxation gives rise to a relatively sharp peak. The dramatic differences between the isothermal and isochronal representation of the α relaxation data is a general feature in systems where a broad distribution of relaxation times exist, as it is the case of semicrystalline polymers, polymer networks, polymer

blends, etc. Using the isochronal representation of the dielectric losses at different frequencies, the temperature (T_{max}) at which the α relaxation loss-peak occurs has been determined for both polymers. The results obtained are plotted in Figure 6.3c. In this figure, the equivalent results obtained from raw data of isothermal dielectric relaxation at 250 K for BS and 220 K for BAz are included for comparison purposes (star symbols). In this way, we confirm that the differences between both types of analysis are not large.

In order to describe the temperature dependence of α relaxation, the data in Figure 6.3c were fitted to a Vogel-Fulcher-Tamman-like equation (VFT),

$$f(T_{\max}) = f_{\infty} exp\left(\frac{-B}{T_{max}-T_0}\right) \qquad 6.6$$

where T_0 is the Vogel temperature, B is an energetic term and f_∞ would correspond to a typical vibration frequency. The obtained fitting lines are shown in Figure 6.3c and the parameters are included in Table 6.2. As the α relaxation in BAz is rather close to the β relaxation (see Figure 6.1), the loss peak temperature determined using high frequency data can be influenced significantly by contributions from the β relaxation. Thus, in the fitting of BAz data only the low frequency range has been taken into account, and because that the value f_∞ was taken equal to that found for BS. In this way a good description of the data of BAz is obtained below f=10^4 Hz. Note that at this frequency the β relaxation of BAz is already less than 2 decades faster than the α relaxation (see dotted line in Figure 6.3 c).

Here it is important to recall the connection between the α relaxation and the glass transition. In a semicrystalline polymer mobile dipolar entities exist only in the amorphous phase and the reorientation of the molecular dipoles is essentially blocked below the glass transition temperature. Therefore, a glass transition temperature can be determined from dielectric experiments as the temperature at which molecular mobility is extremely small. The dielectric glass transition temperature values, $T_{g,BDS}$, calculated using

equation 6 as $f(T_{g,BDS})=10^{-3}$ Hz are shown in Table 6.2. As it can be seen, these values are almost the same as those determined for T_g by DSC measurements.

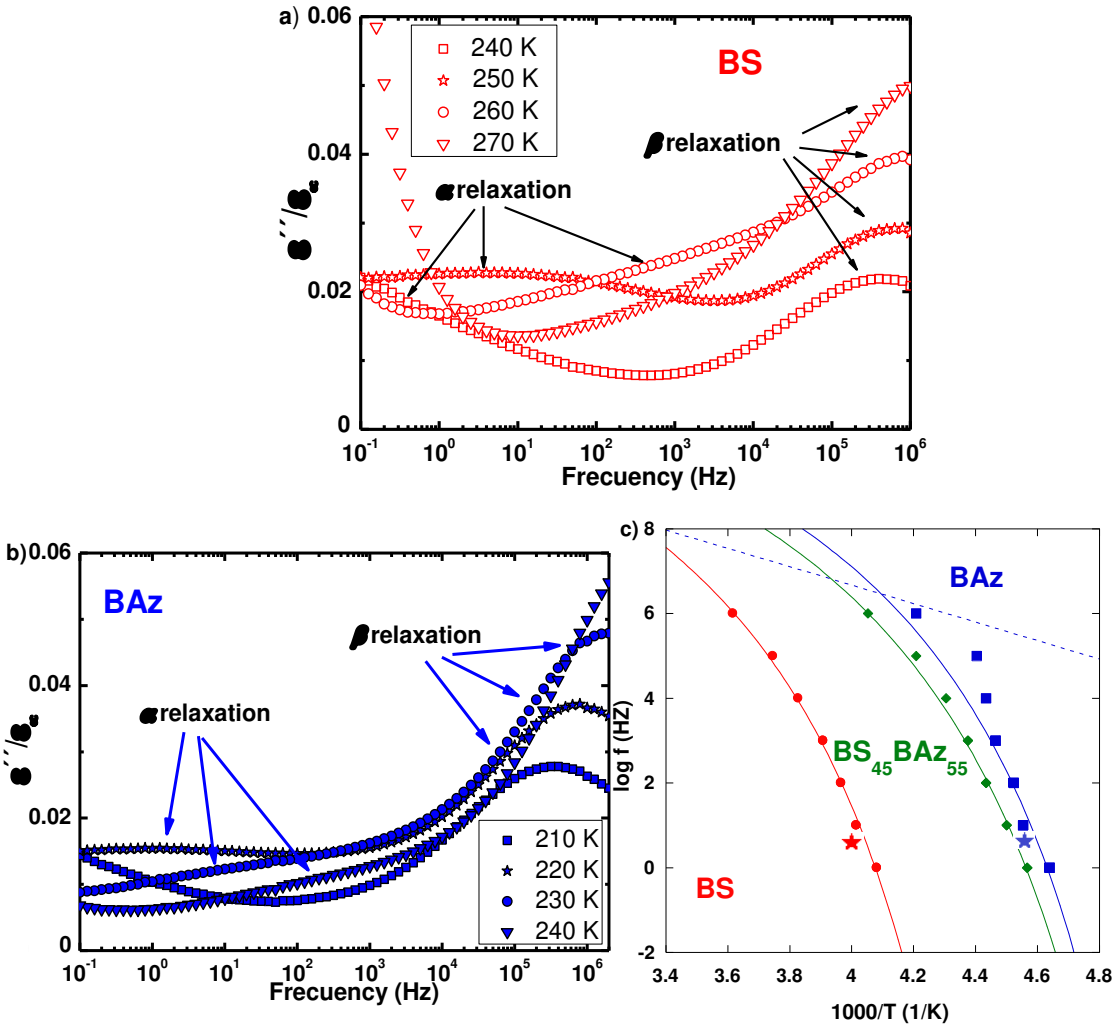

Figure 6. 3. *(a) Dielectric loss spectra versus frequency of BS homopolymer at different temperatures. (b) Dielectric loss spectra versus frequency of BAz homopolymer at different temperatures (c) Arrhenius plot of the peak frequencies of BS, BAz and $BS_{45}BAz_{55}$. Solid lines represent the corresponding VFT fit of α relaxation, dotted line represents the Arrhenius fit of β relaxation for the BAz homopolymer.*

Table 6. 2. *Parameters Describing the Temperature Dependence of the α Relaxation of the Homopolymers and Glass Transition Temperatures Determined by DSC.*

α relaxation	$B \pm 5$ (K)	$T_0 \pm 1$ (K)	f_∞ (Hz)	$T_{g,BDS}$ ± 1 (K)	$T_{g,\ DSC}$ ± 2 (K) DSC$^{(midpoint)}$
BS	1210	207	4.5×10^{13}	238	238
BAz	974	185	(*)4.5×10^{13}	210	210

(*)The value was taken equal to that found for BS because in the fitting of BAz data only the low frequency range was taken into account.

6.2.2 BDS of Copolymers

Analogous measurements have been made for all copolymer samples. Figure 6.4 shows the isochronal plots of $\varepsilon''/\varepsilon_\infty$ at relatively low frequency (10^2 Hz), where α and β relaxation can be easily located, for all copolymer compositions. The results for both homopolymers are plotted for comparison purposes with dotted lines.

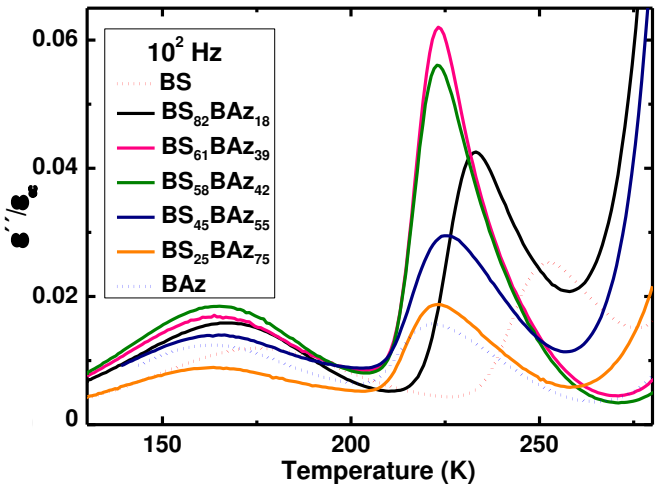

Figure 6. 4. *Isochronal plots of $\varepsilon''/\varepsilon_\infty$ for PBS-ran-PBAz copolymers at 10^2 Hz.*

At first sight, it is obvious that the dielectric behavior of the copolymers is far from monotonous. This evidences the high sensitivity of dielectric relaxations to changes in copolymer composition, which influences simultaneously the structural characteristics (crystallinity) and the mobility of the amorphous phase.

When local dynamics are investigated in semicrystalline polymers, it is found that the dielectric relaxation strength is proportional in a good approximation to the total amorphous fraction.[2, 15] However, polymer crystallinity does not have a large effect (if any) neither on the characteristic time of the relaxation process nor on the shape of the loss curve. Therefore, the data in the β relaxation range can provide quantitative information on the fraction of comonomers involved in the crystallinity of the copolymers investigated.

Figure 6.5 shows the isothermal β dielectric relaxation loss spectra at 160 K for all materials. The dielectric results for both homopolymers are plotted with open symbols, and the lines correspond to the Gaussian description used above. By assuming that most local molecular motions in a copolymer remain largely unaffected with respect to those in the pure polymers, which is in agreement with the already reported results on polybutadienes with different microstructures (ranging from 1,4-polybutadyene to 1,2-polybutadyene),[16] the dielectric β relaxation in the copolymers could be expressed as:

$$\varepsilon''_{BSAz} = (\Phi_m^{BS})\left(\frac{\varepsilon''_{BS}}{1-X_{mBS}}\right)(1 - RF_{BS}) + (1 - \Phi_m^{BS})(\frac{\varepsilon''_{BAz}}{1-X_{mBAz}})(1 - RF_{BAz}) \qquad 6.7$$

where X_m corresponds to mass crystalline fraction of the homopolymer, RF_{BS} and RF_{BAz} accounts for the relative fraction of the corresponding comonomer incorporated in the crystalline phase, and consequently not contributing to the β dielectric relaxation.

Once the β relaxations of the homopolymers were properly described with the Gaussian description presented above, under this assumption, the β relaxation of a copol-

ymer with BS mass fraction Φ_m^{BS} is fully determined by the relative fractions of both comonomers RF_{BS} and RF_{BAz} incorporated in the crystalline phase. Following this method we have look for the suitable values of RF_{BS} and RF_{BAz} that provide the best description of the β relaxation of the copolymers. The resulting values are shown in Table 6.3 as compared with the previously reported copolymer crystallinities obtained by DSC in Chapter 4.[17]

Table 6. 3. *Comonomer Relative Mass Fractions in the Crystalline Phase (± 0.01) Deduced from BDS and Mass Fractions in the Different Crystalline Forms (± 0.01) Determined by DSC.*[17]

	Φ_{mol}^{BS}	Φ_m^{BS}	RF_{BS}	RF_{BAz}	X_{mPBS}	X_{mPBAz}
BS	1	1	0.32	-	0.32	-
$BS_{82}BAz_{18}$	0.82	0.76	0.32	0	0.32	0
$BS_{61}BAz_{39}$	0.61	0.53	0.43	0	0.4	0
$BS_{58}BAz_{42}$	0.58	0.5	0.38	0	0.38	0
$BS_{45}BAz_{55}$	0.45	0.37	0.4	0.28	0.38	0.27
$BS_{25}BAz_{75}$	0.25	0.19	0.1	0.52	0	0.54
BAz	0	0	-	0.33	-	0.33

When comparing the values obtained by DSC and BDS in Table 6.3, it should be noted that DSC determines the total weight fraction of segments incorporated within the crystals of the BS rich phase and/or BAz rich phase respectively, whereas BDS is sensitive to the loss of mobile comonomers irrespectively to the kind of crystals that are formed. In particular, if large co-crystallization takes place, the analysis of BDS and DSC experiments would not provide the same numbers. This is likely the case for $BS_{25}BAz_{75}$, where BDS detects a fraction of BS being involved in the crystallization but no BS like crystallization was detectable by DSC.[17] This result is consistent with the isodimorphic nature of the copolymers, where a small fraction of the minority comonomer is incorporated in the crystalline unit cells of the majority component, as previously demonstrated by WAXS and thermal fractionation in Chapter 4 and 5.[17, 18] Despite the different sensitiv-

ities of DSC and BDS to crystallization phenomena, a remarkable good agreement between the crystallized mass fraction of each comonomer and the amount of the corresponding crystalline phase is found in most of the copolymers. This result is consistent with the already reported fact that the amount of comonomer exclusion is in general much larger than the amount of comonomer inclusion during crystallization of these copolymers.[17, 18]

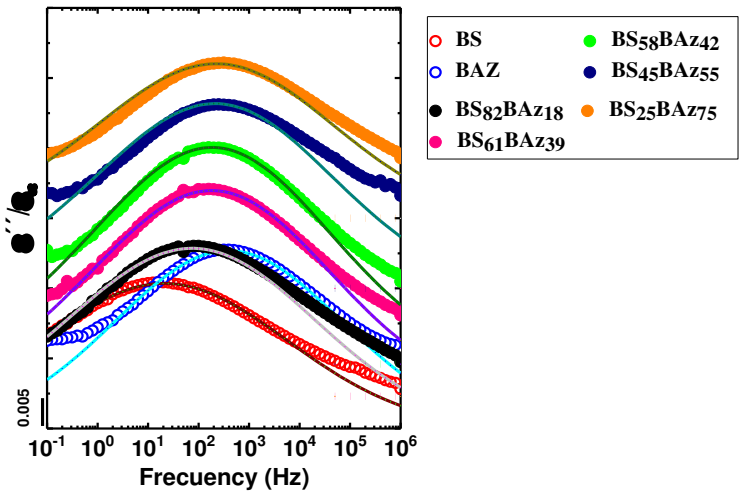

Figure 6. 5. *Calculations of new dielectric loss spectra versus frequency at 160 K. Homopolymers and $BS_{82}BAz_{18}$ are without vertical displacement. For the sake of clarity, losses of the other compositions are vertically shifted and the corresponding zero level displayed as a dotted line.*

Concerning the α relaxation, the situation is more complex, because as aforementioned all the characteristics of the α relaxation are strongly affected by crystallinity, the relaxation strength is dramatically reduced, the relaxation time becomes much longer and the relaxation curves extend over large frequency ranges. Moreover, in crystallizable copolymers the fraction of comonomer involved in the different amorphous fractions RAF, CAF and UCAF cannot be anticipated. As can be seen in Figure 6.4, when increasing the BS fraction in the copolymers with respect to BAz homopolymer, there is a clear increase in the dielectric loss intensity, without much change in the peak position. The former would be related with the decreasing crystallinity of the copolymers, whereas the later

possibly indicates that the more mobile amorphous fraction of the copolymers is rich in BAz comonomers. This trend continues up to the copolymer with the highest BS fraction (82 % molar fraction), where a clear drop in intensity and a peak shift is detected.

The behavior described in the previous paragraph is in qualitative agreement with the output of the analysis of the β relaxation summarized in Table 6.3. For example, see Table 6.4, for $BS_{82}BAz_{18}$ the BS mass fraction within the copolymer in amorphous fractions $\varphi_A^{BS}$is 0.51 and that of BAz (φ_A^{BAz}) is 0.24. Conversely, for $BS_{61}BAz_{39}$ the BS mass fraction in the copolymer in the amorphous fractions (φ_A^{BS}) is 0.30 and that of BAz (φ_A^{BAz}) is 0.47. These differences can explain the quite dramatic changes in the α relaxation between both copolymers. Moreover, as described above the 3 different amorphous fractions (RAF, CAF and UCAF) that can exist in each copolymer sample could present different fractions of the two comonomers, with no clear reasons a priori for any trend.

Table 6. 4. *Total (Φ_m) and Amorphous (φ_A) Mass Fractions of BS and BAz within the Copolymers (± 0.01).*

	$\Phi_m^{BS/BAz}$	φ_A^{BS}	φ_A^{BAz}
BS	0/1	0.68	-
$BS_{82}BAz_{18}$	0.76/0.24	0.51	0.24
$BS_{61}BAz_{39}$	0.53/0.47	0.3	0.47
$BS_{58}BAz_{42}$	0.50/0.50	0.31	0.5
$BS_{45}BAz_{55}$	0.37/0.63	0.22	0.45
$BS_{25}BAz_{75}$	0.19/0.81	0.17	0.39
BAz	0/1	-	0.67

Due to the difficulties mentioned above for the homopolymers, the quantitative analysis of the α relaxation time in the copolymers has also been made by using the isochronal data representations (as those shown in Figure 6.4). In this way, the glass transition temperature determined from BDS has been calculated for the copolymers follow-

ing the same procedure used for the homopolymers, i.e., calculating by means of the VFT fit the temperature at which the peak loss would occur for a frequency of 10^{-3} Hz, see copolymer data in Figure 6.3c as an example. As for BAz, the value of f_∞ was fixed and only the low frequency data (f<10^4Hz) were used in the fitting. The $T_{g,\mathrm{BDS}}$ results are shown in Figure 6.6 as a function of BAz fraction in comparison with glass transition temperatures determined by calorimetry $T_{\mathrm{g,\,DSC}}$.

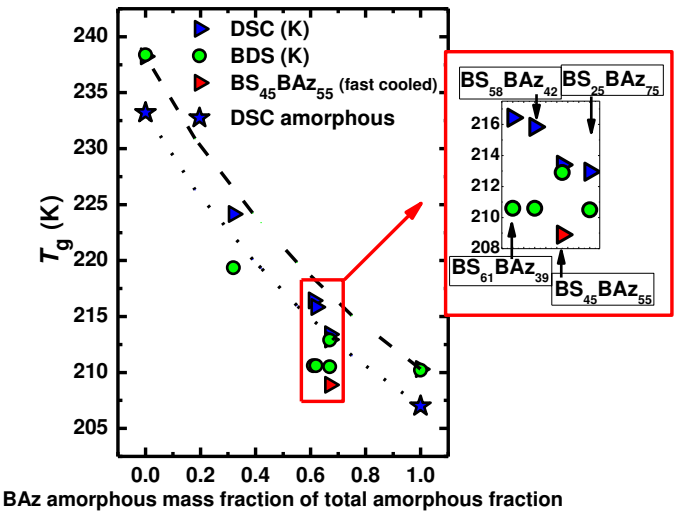

Figure 6. 6. *Glass transition temperatures as a function of weight fraction of amorphous BAz with respect to the total amorphous phase. Dashed line and dotted lines correspond to the Fox equation with the glass transition of semicrystalline and amorphous polymers respectively.*

When selecting the horizontal axes of Figure 6.6 for a mixture of partially crystalline polymers, several circumstances have to be taken into account. On one hand, the crystalline fraction does not participate directly in the glass transition phenomena, although it can have a significant impact in the glass transition temperature of the surrounding amorphous phase. On the other hand, the amorphous regions in semicrystalline polymers tend to have some polymer strands with short range local order packing that

apparently does not contribute to the glass transition as detected by DSC,[19] but can also affect the value of the glass transition temperature. Our choice in Figure 6.6 has been using as horizontal axis the mass fraction of amorphous BAz with respect to the total amorphous phase in the copolymer. These values have been determined from the output of the analysis of the dielectric β relaxation results shown above.

The values of $T_{g,DSC}$ lie close to the prediction of the Fox equation obtained from the values of the $T_{g,DSC}$ of the homopolymers (see dashed line in Figure 6.6). However, significant differences between $T_{g,BDS}$ and $T_{g,DSC}$ are found in most of the copolymers. $T_{g,BDS}$ values are generally 5 K lower than those determined by DSC. Nevertheless, for $BS_{45}BAz_{55}$ (whose amorphous BAz mass fraction with respect to the total amorphous phase is 0.67) a rather good agreement between $T_{g,BDS}$ and $T_{g,DSC}$ is found, as it was also the case for the homopolymers.

As already commented, differences between $T_{g,BDS}$ and $T_{g,DSC}$ can be explained by taking into account the effects of the crystalline regions on the mobility of the remaining amorphous phase. In a recent work on poly(butylene succinate),[6] it has been found that the glass transition temperature of a fully amorphous PBS (blue star symbol in Figure 6.6) is about 6 K smaller than that of crystallized PBS. As far as we are aware, no corresponding value for PBAz has been reported. Thus, in order to obtain a $T_{g,DSC}$ value for amorphous BAz (yellow star symbol in Figure 6.6), a new DSC experiment was performed on a sample of the homopolymer previously cooled at a high rate by quenching the polymer melt in liquid nitrogen. The subsequent heating scan exhibits a clear step in heat flow immediately followed by cold-crystallization peak corroborating that a measurable amount of unconstrained amorphous fraction (UCAF) was obtained in the sample during the fast cooling. The so obtained $T_{g,DSC}$ value is about 3.5 K smaller than that of crystallized PBAz. In line with these results, dielectric experiments on poly(propylene succinate) (PPS)[11] (a polymer belonging to the same family as PBAz and PBS) provided an estimate of the difference in glass transition temperature of about 5 K when comparing data of fully amorphous PPS and those of PPS with 20% crystallinity. It is noteworthy

that these differences are about the same as those observed between $T_{g,BDS}$ and $T_{g,DSC}$ results in most of the copolymers, particularly when BAz is not involved in crystallization, i.e., in the copolymers $BS_{82}BAz_{18}$, $BS_{61}BAz_{39}$, and $BS_{58}BAz_{42}$.

As the BDS values of T_g have been determined from the peak position of the dielectric losses, these values will most probably reflect the segmental mobility in the most mobile amorphous fraction. If only two amorphous fractions would exist in a polymer material (RAF and CAF) the T_g value would reflect the mobility of the CAF, however, in a situation where also an unconstrained amorphous fraction (UCAF) exists,[4] the dominant dielectric signal would correspond to the later. Taking this into account, we have evaluated the prediction of the glass transition temperatures for fully amorphous mixtures of BS and BAz using the Fox equation with the values of T_g for amorphous PBS and PBAz given above (232 K and 207 K respectively). The resulting values for the copolymers are presented in Figure 6.6 as a dotted line. Interestingly, the $T_{g,BDS}$ values of the copolymers lie in general below but close the Fox prediction for fully amorphous copolymers (see Figure 6.6), suggesting that a possible explanation of the differences found between BDS and DSC T_g values would be that in the copolymers where BAz is not involved in the crystallization, a significant amount of UCAF is present, where no relevant effects of the crystalline phase on the molecular motions exist. This phase would present a prominent dielectric relaxation because of the absence of any constrain in the dipole moment reorientation and therefore it would determine the temperature of the loss peak. The stretched high temperature tail in the dielectric loss curves would be due to the CAF contributions. On the contrary, the DSC values are determined from the midpoint of the heat flow jump and they would be sensitive to the molecular motions occurring in the majority CAF, which are slower because of the influence of crystallinity, and the corresponding T_g values would be shifted to higher temperatures.

A similar difference between T_g values is also present for the copolymer with higher BAz content ($BS_{25}BAz_{75}$), a sample containing about 50% of BAz chains in the crystalline phase. In this sample, the low values of the dielectric T_g would be also indicative of

the fact that a significant amount of UCAF is present. Again, the fact that the T_g value from DSC occurs at higher temperature would be explained by the slower motions in the CAF that are not influencing much the position of the dielectric loss peak.

6.2.3 Rate dependence in $BS_{45}BAz_{55}$ copolymer

$BS_{45}BAz_{55}$ is the only copolymer where $T_{g,BDS}$ and $T_{g,DSC}$ nearly coincide and this would mean that no significant UCAF exists in this copolymer, which is congruent with the presence in this copolymer of two distinct crystalline phases each rich in one of the comonomers.[17] In the previous chapter (Chapter 4) it was found that in $BS_{45}BAz_{55}$ copolymer non-trivial differences in the crystalline state appear, depending on the thermal history used during crystallization. When the melted copolymer was cooled-down at relatively high rates, both BS-rich phase and BAz-rich phase crystallization occurs. However, by self-nucleation of the BS-rich phase the crystallization of the BAz-rich phase was strongly reduced due to the fact that BAz crystallization had to occur in the interlamellar domains of BS-rich phase spherulites, (Figure 4.10 in Chapter 4). Trying to determine the influence of the crystallization process on the dielectric relaxation results, new BDS experiments were performed on a $BS_{45}BAz_{55}$ copolymer crystallized using different protocols, namely different cooling rates (10 and 50 K/min) and also promoting BS-rich phase self-nucleation (annealing at 333 K during 5 min). Representative curves obtained after different treatments for $BS_{45}BAz_{55}$ are shown in Figure 6.7a. When comparing the different curves, the strong impact of the way the sample crystallizes on the dielectric relaxation is evident. At low temperatures, the isochronal plots on fast cooled samples display a weaker β relaxation, which implies a higher crystallinity. The quantification of the crystalline fraction of the different comonomers in these samples, see Table 6.5, was obtained following the same procedure described above. In this way, we obtained high values of the BAz fraction in the crystalline phase (RF_{BS} up to 0.39) for the fast cooled sample with only slightly smaller BS fraction in the crystalline phase (RF_{BAz} 0.37 vs 0.40). Similarly, the analysis of the melting process by DSC experiments on samples subjected to similar

thermal histories, shown in Figure 6.7b, also evidenced an increasing BAz crystallinity when the cooling rate is increased.

The previous results show that fast cooling promotes BAz-rich phase crystallization most likely because of the limited development of BS crystals. This is in agreement with the interpretation of the aforementioned DSC experiments involving BS-rich phase self-nucleation, where the opposite situation (good development of the BS crystallinity) takes place and the crystalline relative fraction of BAz decreases from 0.32 to 0.25 (Table 6.5). Thus, when the PBS-rich phase is self-nucleated, it crystallizes to saturation at higher temperatures before the PBAz-rich phase starts to crystallize, and therefore the PBAz-rich crystallization is mainly restricted to the interlamellar domains of PBS-rich phase spherulites which are fully grown and impinged with one another. When considering the corresponding effects on the α relaxation, rather dramatic changes among the experimental data recorded on the same copolymer composition (i.e., $BS_{45}BAz_{55}$) were found after using different cooling rates. Namely, for the samples cooled fast enough (at 10 and 50 K/min) the peak intensity (Figure 6.7a) markedly increases and the peak occurs at significantly lower temperatures. These characteristics suggest that in these crystallization conditions a significant amount of UCAF exists. The new peak position in this copolymer agrees well with that determined for those copolymers with lower BAz amount ($BS_{58}BAz_{42}$ and $BS_{61}BAz_{39}$) but showing no evidence of BAz comonomer crystallization (see Figure 6.6 and the insert showing a close up of the region around the $BS_{45}BAz_{55}$ copolymer data). In agreement with this result, also the glass transition temperature as determined by these new BDS experiments in fast cooled $BS_{45}BAz_{55}$ copolymer samples lies about 5 K below that determined by BDS in the originally measured $BS_{45}BAz_{55}$ copolymer (See Figure 6.6). In spite of that, the value of $T_{g,DSC}$ in the fast cooled $BS_{45}BAz_{55}$ copolymer remains approximately the same, as shown in Figure 6.7c. All this is in line with the idea that in addition to RAF and CAF a significant UCAF would be present in $BS_{45}BAz_{55}$ copolymer when it is cooled rapidly from the melt, whereas, if present, it would not be relevant when slow BS crystallization is allowed to develop before BAz

crystallization can take place. This would be the situation of the sample subjected to self-nucleation procedure and also that of the copolymer cooled down slowly (at a rate smaller than ca. 5 K/min).

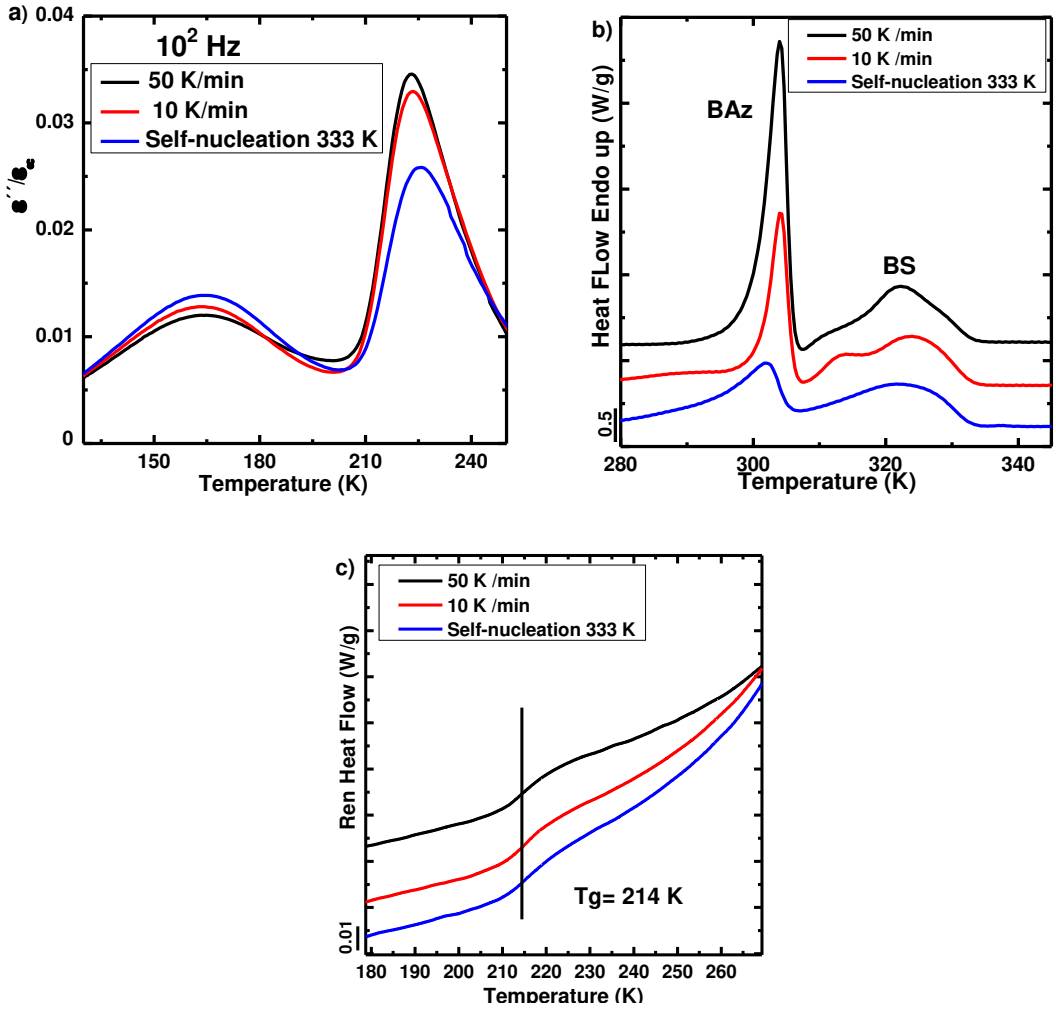

Figure 6. 7. *(a) Isochronal plots of ε´´/ε∞ for $BS_{45}BAz_{55}$ copolymer at different cooling protocols (10^2 Hz) for double crystalline $BS_{45}BAz_{55}$ after being cooled at different rates. And corresponding DSC scans: (b) using a heating rate of 10K/min that exhibits both BS-rich phase and BAz-rich phases melting peaks, (c) using a heating rate of 3 K/min which shows the $T_{g,DSC}$ curves.*

All previous results concerning the glass transition temperature as determined by BDS and DSC manifest the structural complexity of double crystalline random copolymers. In the particular case investigated here each crystalline phase is rich in one of the

comonomers as was evidenced by previous studies. In addition of the crystalline phases, three distinct amorphous fractions (RAF, CAF and UCAF) exist in most copolymers. Two of them, i.e., CAF and UCAF, contribute to the calorimetric *T*g, while UCAF dominates the dielectric relaxation loss peak position defining the dielectric *T*g. Finally, all three amorphous fractions (RAF, CAF and UCAF) contribute to the local dielectric secondary relaxation.

Table 6. 5. *$BS_{45}BAz_{55}$ Mass Fractions in the Crystalline Phase Deduced from BDS (± 0.01) and Mass Fractions in the Different Crystalline Forms Determined by DSC (± 0.01), Using Different Crystallization Protocols.*

Crystallization Protocol	RF_{BS} (BDS)	RF_{BAz} (BDS)	X_{mPBS} (DSC)	X_{mPBAz} (DSC)
50 K/min	0.37	0.39	0.36	0.43
10 K/min	0.37	0.32	0.36	0.33
Self-nucleation 333 K	0.4	0.25	0.33	0.3

As can be seen in Figure 6.6 the data points obtained by DSC when represented as a function of the amorphous BAz content with respect to the total amorphous content of the copolymer lie below the Fox equation predictions obtained using the glass transition temperatures of the semicrystalline homopolymers. A possible explanation for the deviation would be that the RAF is relatively enriched in BS comonomers and consequently the mobile amorphous fractions would be enriched in BAz comonomers. When considering the $T\mathrm{g}_{,\mathrm{BDS}}$ values, the comparison with the Fox equation predictions using the glass transition temperatures of the amorphous homopolymers also show a similar trend, which again suggests that the UCAF would be enriched in BAz comonomer. Moreover, the results obtained in the $BS_{45}BAz_{55}$ copolymer crystallized using different protocols indicate that the amount of the phases/fractions and the comonomer partitioning in each of them can be very sensitive to the sample crystallization details.

6.3 Conclusions

Dielectric relaxation of PBS-*ran*-PBAz random copolymers provides detailed information on the dynamics of the comonomers remaining in the amorphous phase. The characteristics of the more local molecular motions determine the dielectric β relaxation for both homopolymers and copolymers, which is in agreement with previously reported results on polybutadienes with different microstructures.[16] This result allows using the relaxation strength of the dielectric β relaxation to quantify the comonomer fraction involved in the crystalline and amorphous phases, with results in overall good agreement with crystallinity values determined from DSC experiments. This agreement confirms that in these copolymers the amount of comonomer exclusion is much larger than the amount comonomer inclusion during crystallization.

On the other hand, we found that the α relaxation of the copolymers depends not only on the crystalline fraction but also on the details of the crystallization process. In most cases, the peak temperature of the α relaxation determined at low frequencies reflects in general segmental motions that are not much affected by the constrains imposed by the neighboring crystals. The relatively low values of the resulting dielectric glass transition temperatures, when compared with the calorimetric glass transition temperatures, suggest the presence of three distinct amorphous fractions in most of the copolymers. Particularly, there is a significant amount of unconstrained amorphous fraction (UCAF) dominating the dielectric loss peak position. Nevertheless, it seems that there is a majority constrain amorphous fraction (CAF) determining the calorimetric glass transition. Experiments also showed that the multiphase character and the corresponding comonomer fractions can be influenced by the details of the crystallization protocol used. To conclude, it is noteworthy of remark that only by the combination of experimental techniques sensitive to different aspects of the complex structure of random copolymers formed with crystallizable comonomers it is possible to access the details of the structural organization of these extremely complex polymeric materials.

6.4 Appendix

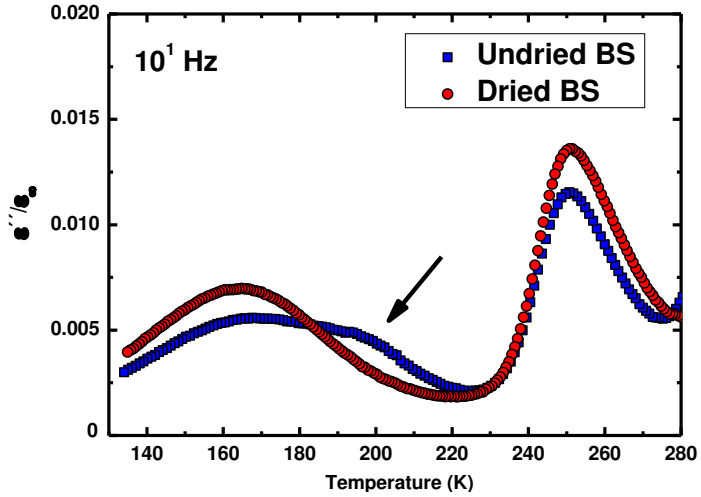

Figure A1. *Isochronal plots of $\varepsilon''/\varepsilon_\infty$ for undried and dried BS homopolymer at 10^1 Hz.*

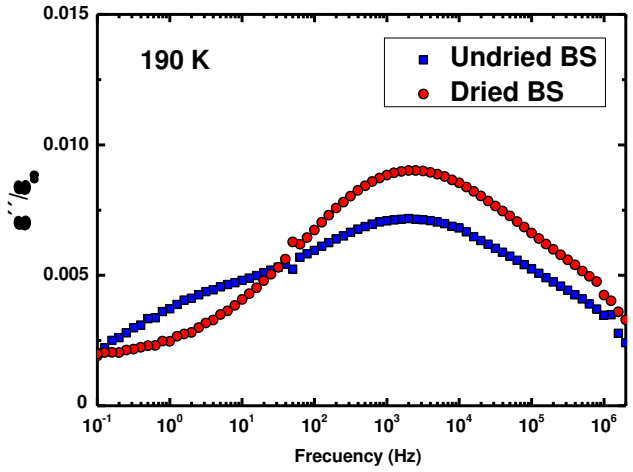

Figure A2. *Dielectric loss spectra versus frequency of undried and dried BS homopolymer at 190K.*

Figure A1 and A2 present, respectively, isochronal and isothermal plots of permittivity losses on undried and high vacuum dried BS samples. In order to obtain the undried BS data, the measurements were carried out on a previously dried sample stored for weeks in a desiccator and without having been subjected to any further drying protocol. After that measurement, the same sample was dried under high vacuum (10^{-5} Torr) overnight and the measurements were repeated. Both samples show a clear dielectric relaxation at low temperature, which is attributed to local dipole reorientation occurring in the glassy state. The dried sample presents a single peak, in agreement with what has been observed in similar homopolymers in literature[11] and in BAz in this work. Moreover, the β relaxation measured in dried BS is similar to that determined in amorphous BS by Charlon et al.[6] which is in line with the general finding that crystallization of polymers does not affect the secondary relaxation except in an amplitude factor.[2, 3, 12, 15] However Charlon et al.[6] observed a double peak structure in the β relaxation of crystallized BS which looks very much the same determined by us in the undried BS. The above results clearly evidence that new relaxation mode at low-frequencies/high-temperature is not an intrinsic characteristic of PBS but would be most likely related to the uptake of water molecules. This finding is against the interpretation given by Charlon et al. in ref (2) where they concluded that the presence of this new relaxation peak is due to the same molecular arrangements of the β relaxation in fully amorphous BS but taking place in a more constrained amorphous environment. Already commented, this interpretation is against the general finding that crystallization of polymers does not affect the secondary relaxation except in an amplitude factor.[2, 3, 12]

6.5 References

1. Schick, C.; Wurm, A.; Mohammed, A., Vitrification and Devitrification of the Rigid Amorphous Fraction in Semicrystalline Polymers Revealed from Frequency Dependent Heat Capacity. In *Polymer Crystallization: Observations, Concepts and Interpretations*, Reiter, G.; Sommer, J. U., Eds.; Springer: Berlin, **2003**, *14*, 252.
2. Coburn, J. C.; Boyd, R. H., Dielectric relaxation in poly(ethylene terephthalate). *Macromolecules* **1986,** *19*, 2238-2245.
3. Alegria, A.; Colmenero, J., Dielectric relaxation of polymers: segmental dynamics under structural constraints. *Soft Matter* **2016,** *12*, 7709-7725.
4. Kummali, M. M.; Alegría, A.; Miccio, L. A.; Colmenero, J., Study of the Dynamic Heterogeneity in Poly(ethylene-ran-vinyl acetate) Copolymer by Using Broadband Dielectric Spectroscopy and Electrostatic Force Microscopy. *Macromolecules* **2013,** *46*, 7502-7512.
5. Hill, A. J.; Tant, M. R., The Structure and Properties of Glassy Polymers. In *Structure and Properties of Glassy Polymers*, American Chemical Society, **1999**, *710*, 1-20.
6. Charlon, S.; Delbreilh, L.; Dargent, E.; Follain, N.; Soulestin, J.; Marais, S., Influence of crystallinity on the dielectric relaxations of poly(butylene succinate) and poly[(butylene succinate)-co-(butylene adipate)]. *European Polymer Journal* **2016,** *84*, 366-376.
7. Tai, H. J., Dielectric spectroscopy of poly(butylene succinate) films. *Polymer* **2007,** *48*, 4558-4566.
8. Yu, L.; Ke, S.; Zhang, Y.; Shen, B.; Zhang, A.; Huang, H., Dielectric relaxations of high-k poly(butylene succinate) based all-organic nanocomposite films for capacitor applications. *Journal of Materials Research* **2011,** *26*, 2493-2502.
9. Starkweather, H. W.; Avakian, P.; Fontanella, J. J.; Wintersgill, M. C., Internal motions in polylactide and related polymers. *Macromolecules* **1993,** *26*, 5084-5087.
10. Tatsumi, T.; Ito, E.; Hayakawa, R., Study of the dielectric β-relaxation in poly(ethylene terephthalate) and ethylene isophthalate terephthalate copolyesters. *Journal of Polymer Science Part B: Polymer Physics* **1992,** *30*, 701-706.

11. Soccio, M.; Nogales, A.; Lotti, N.; Munari, A.; Ezquerra, T. A., The β relaxation as a probe to follow real-time polymer crystallization in model aliphatic polyesters. *Polymer* **2007,** *48*, 4742-4750.
12. Nogales, A.; Ezquerra, T. A.; García, J. M.; Baltá–Calleja, F. J., Structure–dynamics relationships of the α-relaxation in flexible copolyesters during crystallization as revealed by real-time methods. *Journal of Polymer Science Part B: Polymer Physics* **1999,** *37*, 37-49.
13. Dantras, E.; Dandurand, J.; Lacabanne, C.; Caminade, A. M.; Majoral, J. P., TSC and Broadband Dielectric Spectroscopy Studies of the α Relaxation in Phosphorus-Containing Dendrimers. *Macromolecules* **2004,** *37*, 2812-2816.
14. Gambino, T.; Martínez de Ilarduya, A.; Alegría, A.; Barroso-Bujans, F., Dielectric Relaxations in Poly(glycidyl phenyl ether): Effects of Microstructure and Cyclic Topology. *Macromolecules* **2016,** *49*, 1060-1069.
15. Soccio, M.; Nogales, A.; Lotti, N.; Munari, A.; Ezquerra, T. A., Evidence of Early Stage Precursors of Polymer Crystals by Dielectric Spectroscopy. *Physical Review Letters* **2007,** *98*, 037801.
16. Hofmann, A.; Alegría, A.; Colmenero, J.; Willner, L.; Buscaglia, E.; Hadjichristidis, N., Secondary and Segmental Relaxation in Polybutadienes of Varying Microstructure: Dielectric Relaxation Results. *Macromolecules* **1996,** *29*, 129-134.
17. Arandia, I.; Mugica, A.; Zubitur, M.; Arbe, A.; Liu, G.; Wang, D.; Mincheva, R.; Dubois, P.; Müller, A. J., How Composition Determines the Properties of Isodimorphic Poly(butylene succinate-ran-butylene azelate) Random Biobased Copolymers: From Single to Double Crystalline Random Copolymers. *Macromolecules* **2015,** *48*, 43-57.
18. Arandia, I.; Mugica, A.; Zubitur, M.; Iturrospe, A.; Arbe, A.; Liu, G.; Wang, D.; Mincheva, R.; Dubois, P.; Müller, A. J., Application of SSA thermal fractionation and X-ray diffraction to elucidate comonomer inclusion or exclusion from the crystalline phases in poly(butylene succinate-ran-butylene azelate) random copolymers. *Journal of Polymer Science Part B: Polymer Physics* **2016,** *54*, 2346-2358.
19. Shen, X.; Hu, W.; Russell, T. P., Measuring the Degree of Crystallinity in Semicrystalline Regioregular Poly(3-hexylthiophene). *Macromolecules* **2016,** *49*, 4501-4509.

Chapter 7

Isothermal Crystallization

7.1 Introduction

In this chapter, a detailed isothermal study of the nucleation kinetics, spherulitic growth rates and overall crystallization kinetics of PBS-*ran*-PBAz copolymers is performed in a wide composition range in order to demonstrate the dramatic influence of composition on crystallization kinetics. By measuring nucleation, growth and overall crystallization kinetics, it is possible to ascertain which factors determine the final solidification kinetics of the copolymers and assess the influence of composition. In addition, the enthalpy of melting of 100% crystalline PBS and PBAz is also determined by a novel and practical technique: extrapolating real time synchrotron Wide Angle X-ray Scattering (WAXS) isothermal crystallization data and isothermal DSC data.

7.2 Isothermal crystallization

7.2.1 Nucleation kinetics studied by PLOM

Nucleation data obtained by polarized light optical microscopy are plotted in Figures 7.1a, 7.1b, 7.1c, 7.1d and 7.1e. These figures show the nucleation density ρ (N/mm^3) as a function of time for neat PBS-rich copolymers. On the other hand, due to the high nucleation density of the samples which contain only PBAz-rich crystals (i.e., $BS_{25}BAz_{75}$ copolymer and PBAz homopolymer), it was impossible to determine their nucleation kinetics.

The nucleation behavior observed in all samples (e.g., Figures 7.1a, 7.1b, 7.1c, 7.1d and 7.1e) was close to instantaneous. A more detailed analysis indicates that two important parameters affect the nucleation density of PBS-rich copolymers (Figure 7.1f): (a) the chosen isothermal crystallization temperature and (b) the increase of the BAz minor comonomer content.

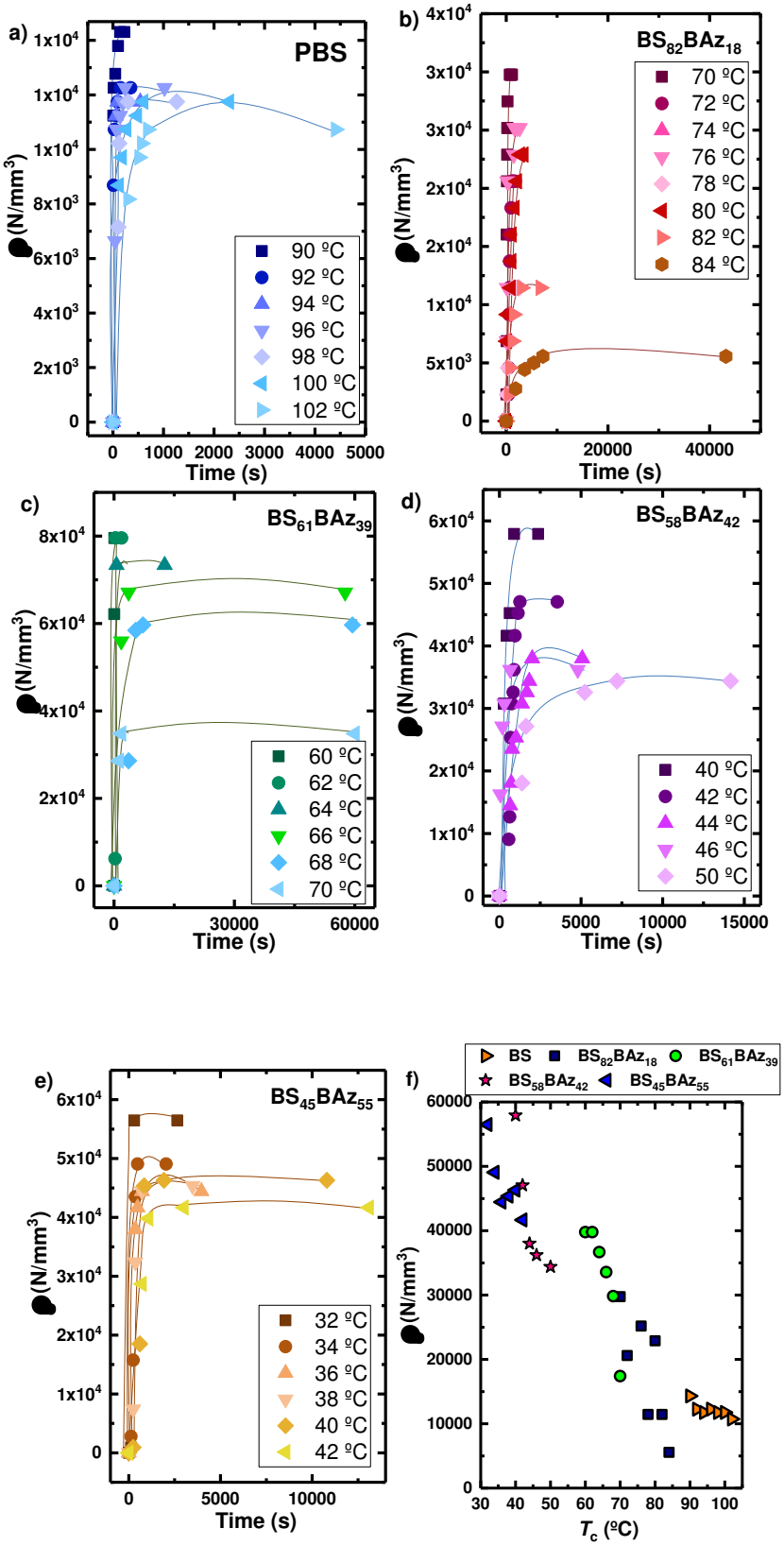

Figure 7.1. *(a), (b),(c) and (d) Nucleation density as a function of time for PBS and $BS_{58}BAz_{42}$ copolymer. (f) Nucleation density at saturation values (long time) as a function of crystallization temperature T_c.*

At lower isothermal crystallization temperatures the nucleation density was higher than that obtained at higher temperatures, due to the increase in the thermodynamic driving force required for nucleation as supercooling increases for any given sample.[1] For example, in the case of PBS homopolymer, when the sample is measured at 90ºC, it only takes 3 minutes to fill the whole microscope field with spherulites. However, when it is measured at 102ºC, more than one hour is needed for the entire field to be completely filled with crystalline superstructures.

On the other hand, the incorporation of BAz comonomer significantly increases the nucleation density for the PBS-rich phase. This can be easily appreciated in Figure 7.1f, where nucleation density increases with the BAz content, and also in PLOM micrographs of PBS-*ran*-PBAz copolymers presented in Figure 7.2. These micrographs were taken, after the samples were cooled from the melt at 5 ºC/min and had impinged on one another completely filling the microscope observation field (therefore, the temperature at which the images were taken varies depending on the crystallization range of the sample).

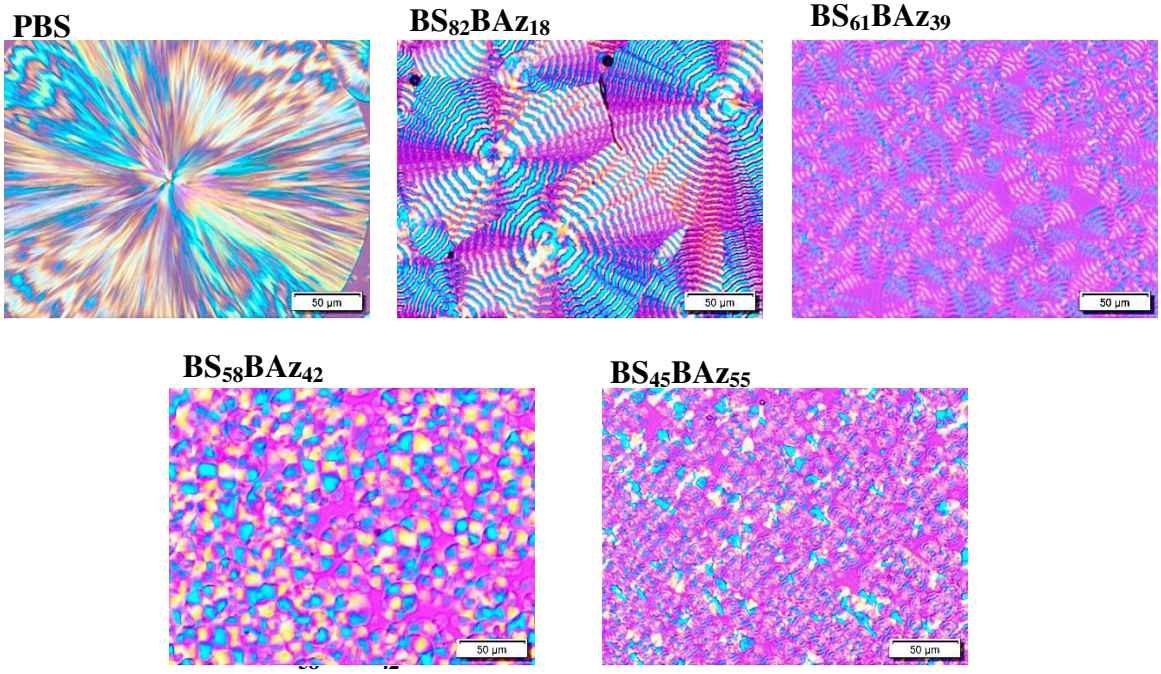

Figure 7.2. *Polarized light optical micrographs of PBS-rich copolymers during non-isothermal crystallization from the melt at 5 ºC/min. Pictures were taken when spherulites completely covered the microscope field under observation.*

The spherulites are negative in all cases with Maltese Cross extinction patterns. Additionally, regular banding was observed in the PBS-rich copolymer spherulites but not in neat PBS, where some highly irregular banding can only be observed near the spherulite edges in Figure 7.2. The addition of miscible "impurities", such as plasticizers and miscible polymeric components is known to induce banding.[2] In the present case, the addition of comonomeric units in a random fashion within the PBS chain also causes a similar effect. The accumulation of the excluded comonomeric units near the lamellar surfaces (it has to be remembered that in these isodimorphic copolymers there are both included and excluded comonomer units within the crystals according to our own previous works in chapters 4,5 and 6) [3-5] may be the determining factor to induce lamellar twisting in the present case.

In the case of the compositions rich in PBAz, although the density of nuclei could not be measured for both samples, the $BS_{25}BAz_{75}$ copolymer and PBAz homopolymer, results showed that the incorporation of BS comonomer affects decreasing the nucleation density, the opposite effect of what occurs in the PBS-rich samples. Figure 7.3 shows polarized light optical micrographs of both samples after cooling from the melt at 5 ºC/min (Figure 7.3a and 7.3b) and also isothermally crystallized at same supercooling temperature (Figure 7.3c and 7.3d). When both compositions are cooled from the melt, much lower nuclei density is appreciated in $BS_{25}BAz_{75}$ copolymer because of the incorporation of the addition of BS comonomer causes an unexpected antinucleation effect. This effect is better appreciated when both are isothermally crystallized at same supercooling temperature, where while PBAz continues showing high nuclei density in the micrograph $BS_{25}BAz_{75}$ copolymer (Figure 7.3d) less and bigger espherulites appear.

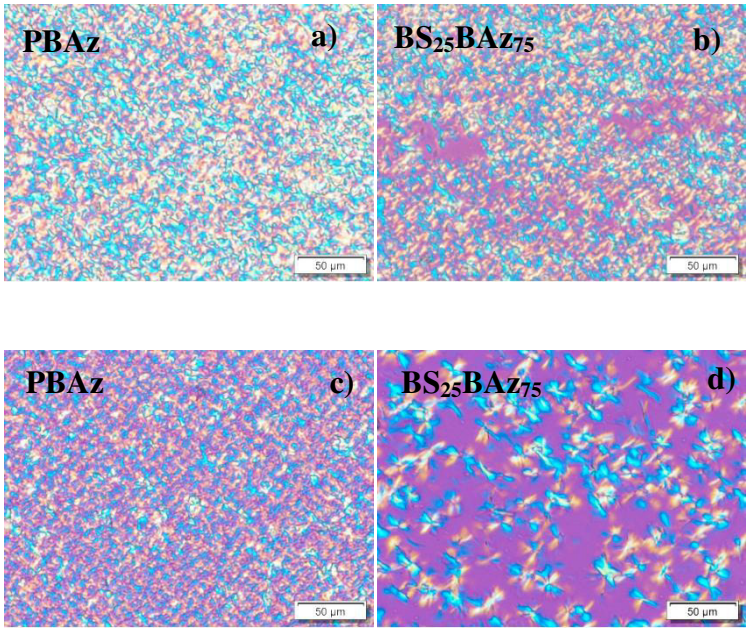

***Figure** 7.3. Polarized light optical micrographs, a) PBAz homopolymer and b) $BS_{25}BAz_{75}$ copopolymer during non-isothermal crystallization from the melt at 5 ºC/min. c) $BS_{25}BAz_{75}$ homopolymer isothermally crystallized at 35ºC and d) PBAz copolymer isothermally crystallized at 24ºC.*

7.2.2 Kinetics of superstructural growth (secondary nucleation) by PLOM

The spherulitic growth rate of PBS and PBS-rich copolymers as a function of the isothermal crystallization temperature is shown in Figure 7.4. As explained before, due to the high nucleation density of some samples only compositions rich in PBS were measured. Experiments were performed by cooling the samples from the melt to a chosen crystallization temperature in the range between 100 and 32ºC. From the slope of plots of radius versus time (which were always linear), spherulitic growth rates, G (µm/min), for each composition was determined at different crystallization temperatures.

Figure 7.4, shows the spherulitic growth rate G (µm/min) as a function of T_c. In this case, only the right side of the typical bell-shape trend caused by the competition between thermodynamic control of secondary nucleation and diffusion was observed.[6] When lower T_c values were employed, both the nucleation and the growth rates were too high and measurements of spherulitic growth before impingement proved impossible.

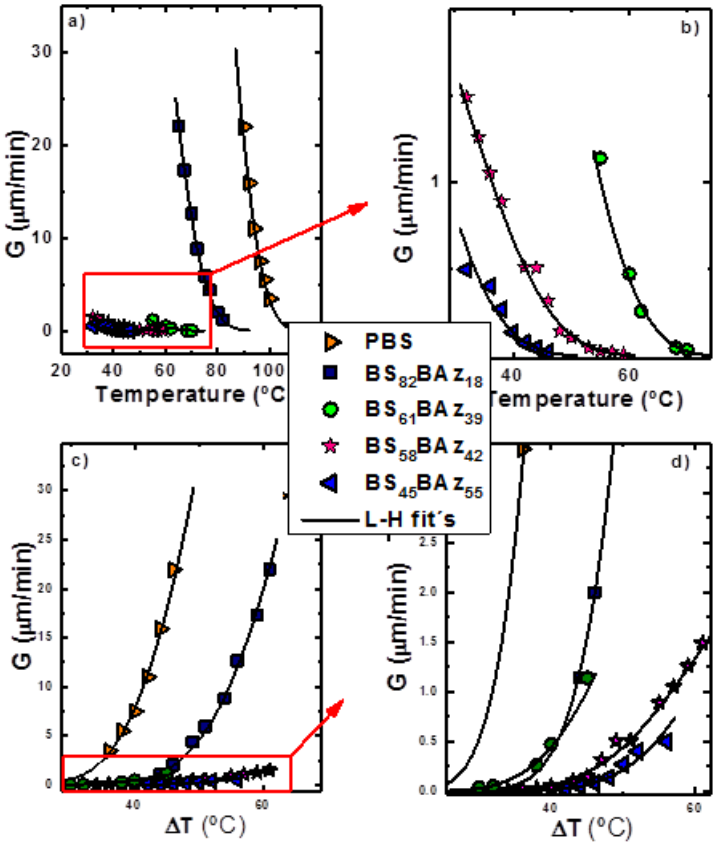

Figure 7.4*. (a) and (b) spherulitic growth rates determined by PLOM for neat PBS and PBS-rich copolymers. The solid lines are the fits to the Lauritzen−Hoffman (LH) theory. (c) and (d) spherulitic growth rates as a function of supercooling.*

The spherulitic growth rate G (µm/min) depends strongly on the copolymer composition, as G dramatically decreases with the increase of BAz-units content. As a result big differences are observed between compositions with only 18 % of BAz content and compositions with more than 39 % of BAz content (see Figure 7.4a and 7.4b). The supercooling required for crystallization also increases with BAz content in the copolymers as a result of the change in equilibrium melting temperature with composition. When G is plotted as a function of supercooling ($\Delta T = T_m^0 - T_c$), using the equilibrium melting temperatures (T_m^0) determined below, in Figure 7.4c and 7.4d, it can be observed that the representation as a function of supercooling shifts the curves in the x-axis "nearly or little" normalizing the differences in crystallization. However, the curves are not superimposed also on the vertical axis, as the kinetic differences between PBS-rich copolymer chains cannot be normalized by T_m^0 thermodynamic variable.

These results indicate that apart from this thermodynamic effect, also kinetic effects affect the chains diffusion of copolymers due to PBS linear sequences are frequently interrupted by BAz repeating units and the thermodynamic driving force required for crystallization has to increase.[3]

Summarizing the results obtained so far, the incorporation of BAz units in the random copolymers with a majority of PBS content causes two opposing trends: an increase in nucleation density and a decrease in spherulitic growth kinetics. The competition between these two factors will determine the overall crystallization rate (that was determined by DSC and will be presented in the next section).

7.2.3 Overall Isothermal Crystallization

To determine the overall crystallization rate of PBS, PBAz and PBS-*ran*-PBAz copolymers, isothermal crystallization experiments were performed by DSC. From DSC experiments, the inverse of the half-crystallization time ($1/\tau_{50\%}$) was determined and plotted against the crystallization temperature, (Figure 7.5a). The $1/\tau_{50\%}$value is the inverse of the time needed to achieve the 50% of the total transformation to the semi-crystalline state during the isothermal crystallization process and provides an experimental measure of the overall crystallization rate which includes both nucleation and growth.

For those compositions rich in PBS, results show that when the BAz comonomer content increases the inverse of the half-crystallization time decreases as well as it occurs with espherulitic growth (G), explained above in the text. However, as in overall crystallization both nuclei density and spherulite growth rate contribute, in this case $1/\tau_{50\%}$ does not decrease as dramatically as G with the increase of BAz-units, and therefore the nucleation density is thought to affect strongly in DSC crystallization

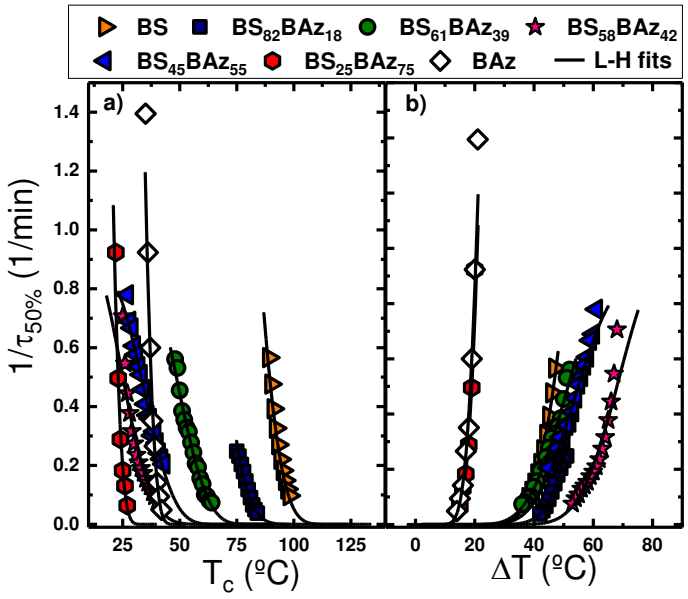

Figure 7.5. *Inverse of half-crystallization time as a function of (a) T_c and (b) supercooling ΔT for indicated PBS-ran-PBAz samples.*

On the other side, it was not possible to measure the nucleation density of both PBAz homopolymer and $BS_{25}BAz_{75}$ by PLOM, but in this case, the half-crystallization time ($1/\tau_{50\%}$) determined by DSC for both samples showed an almost equal behavior. When these results are plotted against supercooling (ΔT) (Figure 7.5b), there are no differences between the pure PBAz and the copolymers, and the curves in the x-axis are shifted normalizing the differences in crystallization temperature exhibited by both compositions. Furthermore, the curves are also superimposed on the vertical axis. Although the micrographs in Figure 7.3 showed that the density of nuclei decreases when 25% of BS content was added in the copolymer, the overall crystallization rate seems not to be affected, indicating that two important behaviors could be affecting the crystallization of PBAz-rich copolymers: (a) the aggregation of BS comonomer has a plasticizing effect in the PBAz-rich phase or (b) the inclusion of this BS-units in the PBAz crystalline region could easily be carried out and the exclusion of these units does not limit that much the crystallinity. This latter behavior would be in overall good agreement with what Wending Sutter equation proposed in (Figure 7.13a), explained below in the text. This theory suggested that the energy barrier needed in order to introduce BS comonomer units in the PBAz-rich crystalline face is much lower than in

the opposite case. In addition, the estimation of the minor comonomer percentage incorporated in PBAz crystals predicted a large amount of comonomer inclusions.

7.2.4 Fitting of DSC Isothermal Data to the Avrami Model

The isothermal experimental data obtained from the DSC measurements were fitted to the Avrami equation.[7-9]

$$1 - V_c\,(t - t_0) = \exp(-k(t - t_0)^n) \qquad 7.1$$

where $V_c(t)$ is the relative volumetric transformed fraction as a function of time, t the experimental time and t_0 is the induction time for crystallization. k is the overall crystallization rate constant and n is the Avrami index, which strongly depends on both the time dependence of the nucleation (n_n) and the crystal growth geometry (n_d). [10] In polymers with spherulitic-type morphology (3D structure), the Avrami index expected is between 3 and 4, while in crystals growing with 2D aggregates, such as axialites, the Avrami values would be between 2 and 3. In both cases, the final value will depend on whether the nucleation event is sporadic or instantaneous.[6, 11, 12]

The fits to the Avrami equation were performed using the Origin plug-in developed by Lorenzo et al.[7], and in Figure 7.6 an example of a representative fit of Avrami model for the $BS_{25}BAz_{75}$ copolymer crystallization at 24ºC is plotted.

Even though Avrami fit estimations were made for all the compositions and at different crystallization temperatures, the result of the $BS_{25}BAz_{75}$ copolymer was taken as an example of a good fit between the Avrami model and the experimental data predicted by DSC isothermal scans. In Figure 7.6c it can be observed how the Avrami equation could perfectly describe the overall crystallization kinetics of the chosen copolymer in the primary crystallization range, i.e., in a conversion range of 3−20%, with a correlation coefficient of 1.000. The fit of the Avrami equation was very good until at least 50% conversion (see Figure 7.6a and Figure 7.6b) and only experienced significant deviations from the experimental data beyond 75% conversion.

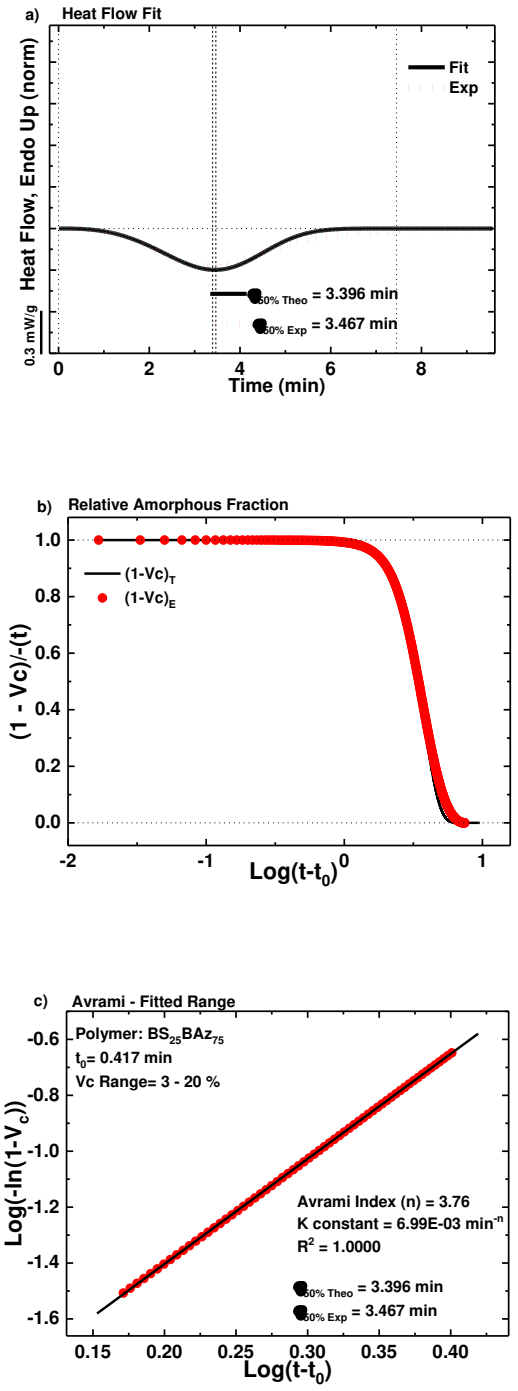

Figure 7.6. *(a–c) The fits to the Avrami equation using the Origin plug-in developed by Lorenzo et al.*[7] *and the experimental data for the* $BS_{25}BAz_{75}$ *copolymer sample.*

Figure 7.7 shows the Avrami index as a function of T_c for all the compositions. Most of the samples exhibited an expected Avrami index value between 2.5 and 4, since by PLOM spherulites were observed for all the samples. In addition, it appears to be a tendency of increasing the Avrami index with temperature, due to a more sporadic nucleation produced at lower temperatures. Nevertheless, some compositions exhibited Avrami index values close to 1.5, a value which agreed well with instantaneously nucleated axialites (or 2D aggregates). This low value could be explained for several reasons. On the one hand, the high nucleation density of the samples. It must be remembered that by adding BAz comonomer units the nucleation density was greatly enhanced, and the samples in which PBS-rich phase crystallizes but with the highest BAz content show the lowest Avrami index values. On the other hand, the low isothermal temperatures, T_c values, used to study the overall crystallization rate by DSC, which produced an even more instantaneous nucleation. In DSC studies, the overall crystallization kinetics can be determined at even lower temperatures than those employed in determining spherulitic growth kinetics, as long as the sample does not crystallized during the cooling step to T_c (at 60 ºC/min).

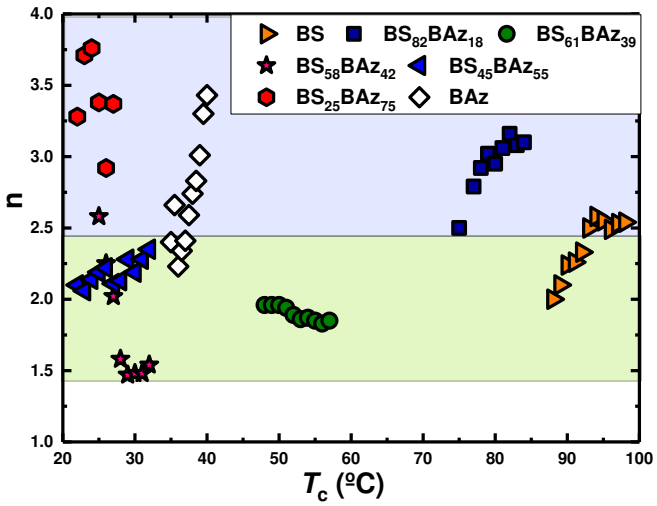

Figure 7.7. *Avrami index as a function of T_c.*

7.2.5 Enthalpy of fusion of the 100% crystalline polymers

The heat of fusion of a 100 % crystalline polymer ($\Delta H^0_{m(100\%)}$) is a required value for the estimation of crystalline fraction of polymers by DSC. In this work, we have reevaluated these values for both PBS and PBAz employing combined DSC and X-ray diffraction (WAXS) measurements.

In order to calculate the $\Delta H^0_{m(100\%)}$ of a polymer, the most commonly used method in the literature is to prepare samples with different crystallinity degrees (applying different cooling rates for instance) and then determine their crystallinities by WAXS. The experimental heats of fusion are determined by DSC and then a plot is made of WAXS crystallinity degree versus enthalpy of fusion and an exptrapolation is made to 100% crystallinity. The difficulty in this method is that it is not easy to prepare fast crystallizing polymer samples (like PBS and PBAz) with different crystallinities. In fact, if the available values from the literature are examined,[13, 14] they were determined by extrapolating 6 measurements only.

In the present work, we propose a new fast method to determine the 100% enthalpy of fusion of a fast crystallizing polymer by making use of real time WAXS measurements at the synchrotron. A sample of each homopolymer was heated to erase its thermal history (at a temperature 30 ºC higher than the melting peak registered by DSC at 10 ºC/min) and then cooled at 50 ºC/min to a selected crystallization temperature. During the isothermal crystallization process, WAXS patterns were obtained every 10 seconds until the sample complete its crystallization process. Employing the WAXS patterns, the crystallinity values were calculated using the relative areas under the crystalline peaks. Before the crystallization starts, just when the sample reaches the desired crystallization temperature after cooling from the melt, the sample is in the melt, so the WAXS pattern at time= 0 corresponds to the amorphous halo that is later used for the crystallinity calculations. Figure 7.8 shows an example of the WAXS patterns observed at different crystallization times at a T_c=34ºC for PBAz homopolymer.

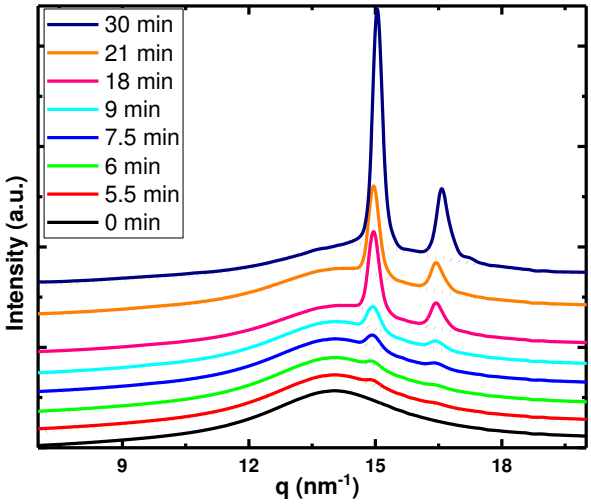

***Figure 7.8**. WAXS patterns for PBAz homopolymer at different crystallization times at 34ºC.*

In Figure 7.9, crystallinity degree values calculated by WAXS are plotted against the crystallization enthalpy values obtained at each measured time from the respective DSC isothermal curve. Both DSC and WAXS measurements were done at 3 different isothermal temperatures for each homopolymer.

The values for the enthalpy of fusion of the 100% crystalline polyester were found to be $\Delta H^0_{m(100\%)}$= 150±10 J/g for PBS and $\Delta H^0_{m(100\%)}$= 137±10 J/g for PBAz. In the case of PBS, this value resulted between $\Delta H^0_{m(100\%)}$= 110 J/g estimated empirically by the group contribution method[15] and the $\Delta H^0_{m(100\%)}$= 210 J/g calculated by Papagerorgiu et al.[14]. In the case of PBAz, the new value resulted lower than $\Delta H^0_{m(100\%)}$= 160 J/g estimated by the group contribution method[15] and also than the $\Delta H^0_{m(100\%)}$=150 J/g calculated by Papagerorgiu et al.[13].

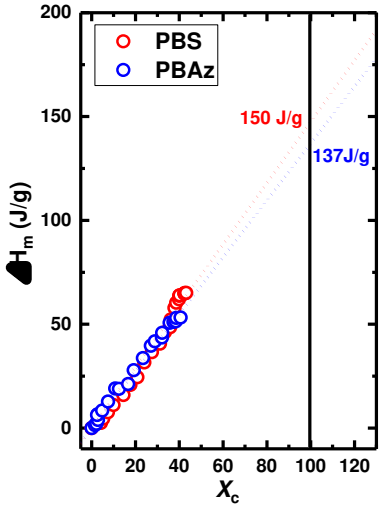

Figure 7.9. *DSC crystallization enthalpy values as a function of crystallinity degrees obtained by WAXS.*

7.2.6 Equilibrium Melting Temperature (T_m^o)

The equilibrium melting temperature T_m^0, is the melting point of lamellar crystals with infinite thickness and negligible surface effects on melting. It represents the first order transition of a hypothetical macroscopic perfect crystal.[16] It is very important to determine this parameter in order to analyze the crystallization growth kinetics, and in the case of copolymers every composition will show a different value of T_m^0, as melting is a function of the nature, type and distribution of comonomer units.[16] In this work, several methods have been used to estimate this value.

The first method used to evaluate T_m^0 was The Thomson−Gibbs approach,[17, 18] which is based on the thermodynamic consideration that the melting temperature of a crystal of finite thickness is smaller than that of a crystal of infinite thickness. The Thomson−Gibbs approach is also considered a good way in order to obtain T_m^0 values of copolymers, since more than one experimental technique is used for its calculation, such as the DSC and SAXS. The method follows equation 7.2:

$$T_m = T_m^\circ \left(1 - \frac{2\sigma_e}{l\Delta H_{m\%100}}\right) \qquad 7.2$$

where T_m^0 is the equilibrium melting point, $\Delta H_{m\%100}$ is the enthalpy per unit volume of a perfect crystal (100% crystalline), and σ_e is the fold surface free energy. Following this equation, experimental values of melting temperature obtained by DSC after isothermal crystallization are represented linearly as a function of the inverse of the lamellar thickness (l), determined by SAXS, and the intersection with the ordinate axis will represent the melting temperature of a crystal of infinite thickness, which is the equilibrium melting temperature of the defect-free crystal (Figure 7.10b).

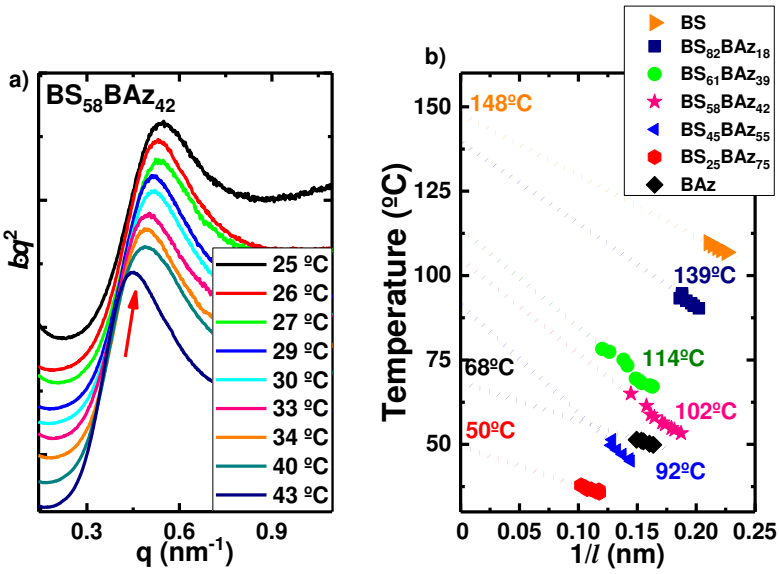

***Figure 7.10**. (a) Lorentz-corrected SAXS profiles, with $I{\cdot}q^2$ as a function of the scattering vector. (b) Representation of the Thomson−Gibbs plots to obtain $T_m{}^o$ for all PBS-ran-PBAz samples.*

For each composition, between 5 and 9 samples were prepared and isothermally crystallized at different temperatures. For that, they were firstly heated to above 30ºC of their melting point during 3 minutes and afterwards cooled down at 60ºC/min (in order to prevent crystallization during cooling) to a chosen crystallization temperature. The samples were left at those temperatures the time required to crystallize and finally quenched to room temperature. Figure 7.10a shows the SAXS measurements performed to $BS_{58}BAz_{42}$ samples after the thermal treatment explained above. All samples exhibit a clear intense maximum that can be interpreted as the scattering caused by lamellar

stacks, and from those q_{max}, values the long periods (d^*) were estimated by equation 7.3 from Lorentz corrected plots ($I \cdot q^2$versus q):

$$d^* = (2\pi)/q_{max} \quad 7.3$$

The calculation of the lamellar thickness (l), was performed employing the approximation $l = x_c \cdot d^*$, where x_c is the crystalline fraction. For that, after the SAXS measurements, DSC heating scans were also performed to the same samples in order to obtain the experimental melting points, melting enthalpies and therefore crystalline fractions.[3] Then applying the Thomson−Gibbs equation,[17, 18] the inverse of lamellar thickness values were plotted versus the experimental melting points of the isothermally crystallized samples (Figure 7.10b), and from the intercept the equilibrium melting temperatures (T_m^0) were determined, (see Table 7.1).

The second method used to estimate T_m^0 values was the Hoffman-Weeks plot,[19] which involves the extrapolation of a linear region of melting temperatures (T_m) observed experimentally at various crystallization temperatures (T_c), to the thermodynamic equilibrium line $T_m = T_c$.[20, 21] From the intercept T_m^0 is calculated.

Figure 7.11a shows an example of the DSC heating scans after the previous isothermal crystallization at different temperatures for $BS_{82}BAz_{18}$ copolymer. Despite the fact that two peaks were observed at low temperatures, only the peak which varies when the T_c increases was taken into account, since the second peak occurs after a recrystallization process during the heating scan and did not reflect the melting of the isothermally formed crystals. In addition, the extrapolation of melting temperatures (T_m) to the thermodynamic equilibrium line $T_m = T_c$ of all compositions is observed in Figure 7.11b, and T_m^0 values of the intercept showed in Table 7.1.

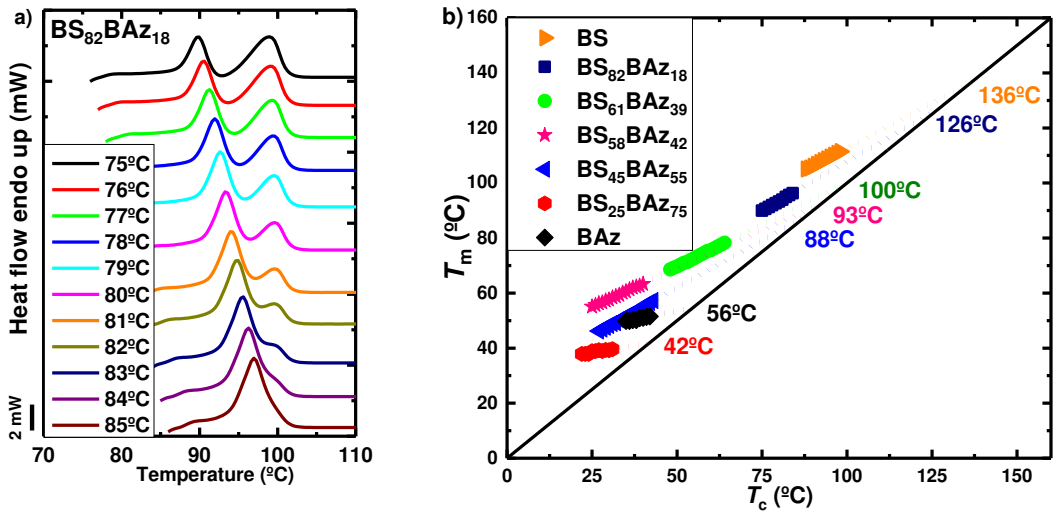

Figure 7.11. (a) DSC heating scans after a previous isothermal crystallization at different temperatures in $BS_{82}BAz_{18}$ copolymer. (b) Hoffman–Weeks plots for all compositions (the black line represents the thermodynamic equilibrium line T_m=T_c).

Table 7.1 and Figure 7.12 reports the T_m^0 obtained by both methods. For comparison purposes, we compare in both Table 7.1 and Figure 7.12 the end melting temperatures determined by DSC on non-isothermally crystallized samples (previously cooled from the melt at 20 ºC/min and then heated at the same rate). These are the temperatures where the endothermic signal of the DSC trace finally disappears and joins the DSC base line, i.e., when all traces of crystallinity disappear. These values represent the melting points of the thickest possible lamellae in the material, even if they had reorganized during the heating DSC scans.

Table 7.1 and Figure 7.12 also show the end melting temperatures determined during the final heating DSC scans of samples submitted to Successive Self-nucleation and Annealing (SSA) thermal fractionation obtained from a previous work [4]). The final melting temperature after SSA treatment[22] represents the melting of even thicker lamellae as this method promotes successive annealing.

Hoffman-Weeks and Gibbs-Thomson methods give extrapolated values that theoretically represent the fusion of infinite crystals, without surfaces or defects and with extended chains. Therefore they should always be greater than any experimental value. In general terms, this expectation is corroborated in Table 7.1 and Figure 7.12.

Table 7.1. *Experimentally obtained end melting temperatures ($T_{m(end)}$) and equilibrium melting temperatures, T_m^0 (ºC), obtained by different techniques.*

	$T_{m(end)}$ from DSC scans	$T_{m(end)}$ from SSA	T_m^0 Hoffman-Weeks (HW)	T_m^0 Gibbs-Thomson (GT)	$T_{m(SSA/GT)}^0$
BS	118	119	136	148	148
$BS_{82}BAz_{18}$	100	102	126	139	129
$BS_{61}Baz_{39}$	79	82	100	114	107
$BS_{58}BAz_{42}$	68	68	93	102	104
$BS_{45}BAz_{55}$	58	61	88	92	92
$BS_{25}BAz_{75}$	41	43	42	50	57
BAz	46	48	56	68	68

The T_m^0 determined by Hoffman-Weeks for pure PBS (136 ºC) is similar to previously reported values (125-134ºC)[14, 23-25], and the T_m^0 measured by Gibbs-Thomson (148ºC) is also similar to reported values in the literature that have employed the same method (146.5 ºC).[14, 24] In the case of PBAz, only values obtained from Hoffman-Weeks extrapolation were found in literature,[13, 26] 53ºC and 67ºC respectively which agree very well with the calculated in this work.

In the case of the extrapolated T_m^0 values for the copolymers, determined by both GT and HW methods, a significant scattering of the data as a function of composition can be seen in Figure 7.12, which is a consequence of both experimental errors and extrapolation errors.

In order to get a smoother trend with composition, we have performed a reasonable approximation which is also reported in Figure 7.12. In the case of homopolymers, the T_mº data is usually considered more reliable than in the case of copolymers.[11] If the data related to PBS in Table 7.1 is examined, the differences between SSA experimental melting point and the highest Tmº values obtained by GT is

29 ºC. In other words, the ideal crystals have an equilibrium melting temperature which is 29 ºC higher than the apparent or experimentally determined melting temperature of the thickest possible crystals that can be prepared by SSA. Therefore, we have assumed that the 29 ºC difference can also hold for the PBS rich copolymers phase and we have added this constant value to the experimentally determined SSA value in order to estimate Tmº(SSA/GT) values that have a smoother trend with copolymer composition and are in fact not far from the values determined by GT method as reported in Table 7.1. For PBAz-rich phases, the added factor was 20 ºC in correspondence with the difference between SSA experimental melting point and the highest Tmº values obtained by GT.

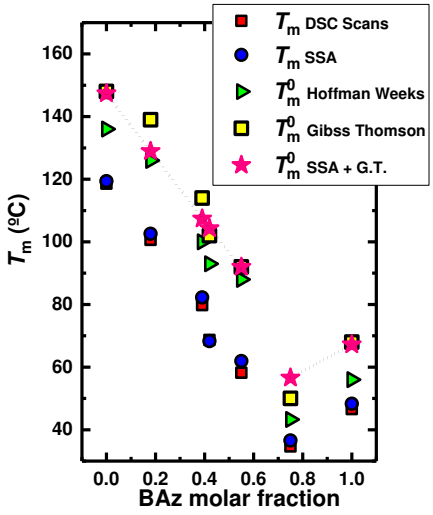

***Figure 7.12**. Experimentally obtained end melting temperatures $T_{m(end)}$ and equilibrium melting temperatures, T_m^o(ºC), versus BAz molar content.*

7.2.7 Study of co-units cocrystallization by comparing the equilibrium melting point with theoretical exclusion-inclusion models

Several theories have been developed in order to explain copolymer crystallization and the partitioning of co-units between the crystalline and amorphous phase in random copolymers by using the experimental estimations of the equilibrium melting points. Those models account for the effect of exclusion and inclusion in copolymer crystals, or the effect of composition on competition for cocrystallization when inclusion occurs.

Those which assume comonomer exclusion from the crystal into the amorphous phase, are Flory[27] and Baur[28] exclusion theories. The Flory theory was the first to treat the issue of crystallization of random copolymers. Neglecting the enthalpy of mixing for the two comonomer units, the equilibrium melting point of a copolymer containing a concentration x_B of non-crystallizable comonomer can be expressed as:

$$\frac{1}{T_m^0} - \frac{1}{T_{m(X_B)}} = \frac{R}{\Delta H_m^0} \ln (1 - X_B) \qquad 7.4$$

where T_m^0 and ΔH_m^0 are the homopolymer equilibrium melting temperature and heat of fusion, and R is the universal gas constant.

Baur improved the Flory expression on the basis of the concept of "hindered equilibrium" introduced by Kilian:[29]

$$\frac{1}{T_m^0} - \frac{1}{T_{m(X_B)}} = \frac{R}{\Delta H_m^0} [\ln(1 - X_B) - \langle \xi \rangle^{-1}] \qquad 7.5$$

Where, $\langle \xi \rangle = [2X_B(1 - X_B)]^{-1}$ is the average length of crystallizable homopolymer sequences in the melt.

Subsequent theoretical works accounted for the inclusion of the comonomer B in crystals of the A repeating unit. Sanchez and Eby[30] suggested that when the B comonomer was partially included into the crystal of A, it could act as a defect and modify the equilibrium melting point according to:

$$\frac{1}{T_m^0} - \frac{1}{T_{m(X_B)}} = \frac{R}{\Delta H_m^0} \ln (1 - X_B + X_B e^{-\varepsilon/RT}) \qquad 7.6$$

where $x_B e^{-\varepsilon/RT}$ is the equilibrium fraction of B repeat units that are able to crystallize, and ε is the excess free energy of a defect created by the incorporation of one B unit into the crystal.

Then Wendling and Suter[31] proposed a more thorough treatment of the problem to account for isodimorphic behavior, employing the new parameter to calculate the

defect Gibbs free (ε). This model takes into account the energy required by minor comonomer repeating units to introduce in the crystal lattice and also assumes that the free energy penalty paid to accommodate a defect in the crystal decreases while the amount of included comonomer increases:

$$\frac{1}{T_m^0} - \frac{1}{T_{m(X_B)}} = \frac{R}{\Delta H_m^0} \ln(1 - X_B) \left[\frac{\varepsilon X_{CB}}{RT} + (1 - X_{CB}) ln \frac{1 - X_{CB}}{1 - X_B} + X_{CB} ln \frac{X_{CB}}{X_B} + \langle \xi \rangle^{-1}\right] \quad 7.7$$

where X_{CB} is the concentration of the B unit in the crystal. If there is an equilibrium comonomer inclusion, the concentration of comonomer B unit in the crystal is given by:

$$X_{CB}^{eq} = \frac{X_B e^{-\varepsilon/RT}}{1 - X_B + X_B e^{-\varepsilon/RT}} \quad 7.8$$

And when X_{CB} in equation 7.7 is substituted by equation 7.8 gives a simplified equation following equilibrium inclusion model, equation 7.9:

$$\frac{1}{T_m^0} - \frac{1}{T_{m(X_B)}} = \frac{R}{\Delta H_m^0} \ln \ln \left(1 - X_B + X_B e^{-\varepsilon/RT}\right) - \langle \xi \rangle^{-1} \quad 7.9$$

where:

$$\langle \xi \rangle^{-1} = 2(X_B + X_B e^{-\varepsilon/RT}) \cdot \ln \left(1 - X_B + X_B e^{-\varepsilon/RT}\right) \quad 7.10$$

The case of complete exclusion and of uniform inclusion can be obtained as particular solutions to this equation.

Figure 7.13a shows the results after employing Flory, Baur, Sanchez-Eby and Wendling-Suter models to determine the equilibrium melting temperatures of PBS-*ran*-PBAz polyesters in comparison to the Tmº (SSA/GT) previously described. As can be seen, the Flory and Sanchez-Eby models did not fit the experimental values since they lead to an overestimation of the equilibrium melting points. Regarding Baur, its prediction seems to be more realistic for PBS rich compositions. Previous works in Chapter 6 showed that in these copolymers the amount of comonomer exclusion was much larger than the amount of comonomer inclusion during crystallization, and

therefore good agreement should be found between experimental and Baur calculated data. However, a good fit for the PBAz-rich compositions was not found.

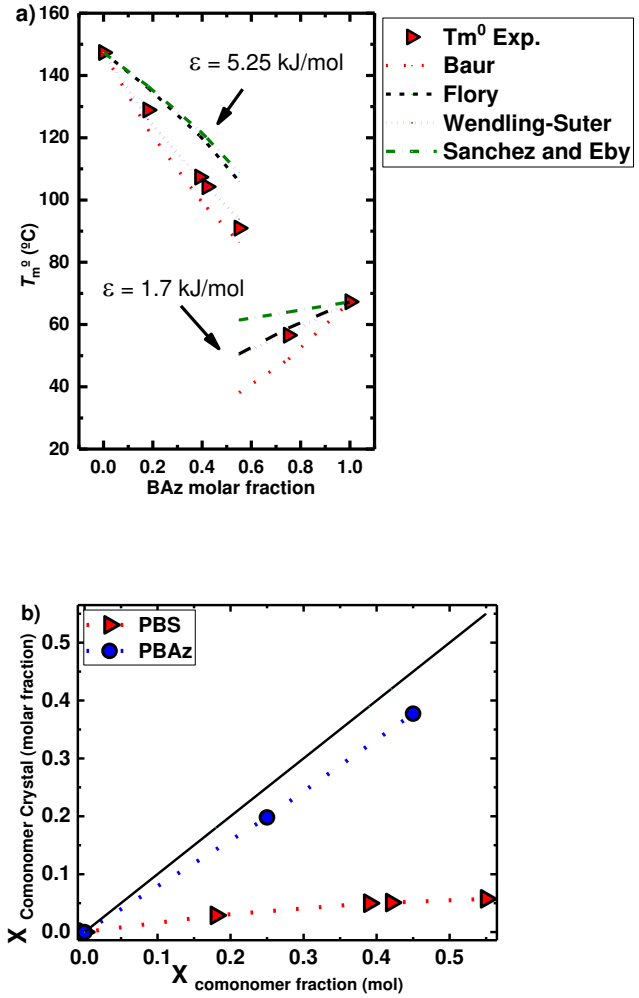

Figure 7.13. *(a) Comparison of the experimental equilibrium melting temperatures with the theoretical melting temperatures predicted by the different equations; ε = 5.25 for PBS-rich phase and ε =1.7 for PBAz-rich phase. (b) Equilibrium concentrations of the minor comonomer units in the crystal of the homopolymer corresponding to the major comonomer, as a function of copolymer composition.*

The Wendling-Suter model showed the best fit to the experimental data for lower comonomer content and allowed to calculate the defect Gibbs free (ε) energy. ε was calculated from the function ε/RT which was determined as an adjustable parameter and was constant regardless of the comonomer composition. In case of including BAz comonomer units in PBS-rich crystals, the best fit was found for ε =5.25

kJ/mol, in the limiting case where $X_{CB} = 0$. On the other hand, when the average defect free energy in the case of incorporation of BS repeating units into the PBAz-rich crystal, the best fit was found for $\varepsilon = 1.7$ kJ/mol. The low value of ε in the case of incorporation of BS units in the PBAz crystal indicates that BS units are much easier to include within PBAz crystal unit cells. This result together with the Baur´s failed fit, would lead to the conclusion that the comonomer inclusion in PBAz-rich phase would be larger than expected, and therefore it would be in good agreement with the results obtained from the isothermal crystallization in PBAz-rich compositions (Figure 7.5b), which showed that when $(1/\tau_{50\%})$ values are plotted against supercooling (ΔT), the curves in the x-axis and vertical axis are superimposed.

The Wendling-Suter model results were further used in order to estimate the percentage of the minor comonomer units which were practically incorporated in both cases PBS and PBAz the crystals. Using Eq. 7.8 the equilibrium concentration of minor comonomer repeat units in the crystal was calculated and plotted as a function of minor comonomer fraction in Figure 7.13b. On the one side, in case of PBS-rich compositions, despite the comonomer concentration in crystals increases with increasing the comonomer composition, it continues being small and much lower than the copolymer concentration corresponding to uniform inclusion, i.e. $X_C = X$. And in the other side, for PBAz-rich compositions, a large amount of comonomer inclusions was predicted.

7.3 Conclusions

Two very different behaviors were found when analyzing the isothermal crystallization of PBS-ran-PBAz random copolymers. On the one hand, the incorporation of BAz-units greatly affected the crystallization of the PBS-rich compositions, increasing the density of nuclei and slowing down the crystallization rate due to the difficulty of incorporating units of this minor comonomer. On the other hand, a totally different behavior was found in PBAz-rich compositions, where the incorporation of BS-units not only did not affect the crystallization of this copolymer a lot, but also an antinucleating effect could be appreciated. The thermodynamic analysis of the equilibrium melting point depression corroborated both effects, concluding that in the case of PBS-rich compositions only a small portion of BAz comonomer units were able to introduce into the PBS crystals, and in the case of PBAz-rich compositions great inclusion of BS-units was observed. The extent of comonomer inclusion in the crystal lattice controls the crystallization behavior of isodimorphic copolymers, affecting for instance the shape of the pseudo-eutectic curves, the degree of crystallinity and the rate of crystal formation.

Techniques such as WAXS, SAXS and DSC were successfully used in order to calculate the equilibrium melting temperature of this random copolymers and the less known heat of fusion of 100 % crystalline polymer value.

7.4 References

1. Ebdon, J. R., Introduction to polymers, R. J. Young and P. A. Lovell Chapman and Hall, London. *Polymer International* **1992,** *27*, 207-208.
2. Crist, B.; Schultz, J. M., Polymer spherulites: A critical review. *Progress in Polymer Science* **2016,** *56*, 1-63.
3. Arandia, I.; Mugica, A.; Zubitur, M.; Arbe, A.; Liu, G.; Wang, D.; Mincheva, R.; Dubois, P.; Müller, A. J., How Composition Determines the Properties of Isodimorphic Poly(butylene succinate-ran-butylene azelate) Random Biobased Copolymers: From Single to Double Crystalline Random Copolymers. *Macromolecules* **2015,** *48*, 43-57.
4. Arandia, I.; Mugica, A.; Zubitur, M.; Iturrospe, A.; Arbe, A.; Liu, G.; Wang, D.; Mincheva, R.; Dubois, P.; Müller, A. J., Application of SSA thermal fractionation and X-ray diffraction to elucidate comonomer inclusion or exclusion from the crystalline phases in poly(butylene succinate-ran-butylene azelate) random copolymers. *Journal of Polymer Science Part B: Polymer Physics* **2016,** *54*, 2346-2358.
5. Arandia, I.; Mugica, A.; Zubitur, M.; Mincheva, R.; Dubois, P.; Müller, A. J.; Alegría, A., The Complex Amorphous Phase in Poly(butylene succinate-ran-butylene azelate) Isodimorphic Copolyesters. *Macromolecules* **2017,** *50*, 1569-1578.
6. Gedde, U. W.; *Polymer physic, Chapman & Hall: London*. 1995.
7. Lorenzo, A.; Arnal, M.; Albuerne, J.; Müller, A., DSC isothermal polymer crystallization kinetics measurements and the use of the Avrami equation to fit the data: Guidelines to avoid common problems. *Polymer Testing* **2007**, *26*, 222-231.
8. Reiter, G.; Strobl, G. R., *Progress in understanding of polymer crystallization*. Springer: Berlin, **2007**.
9. Avrami, M., Granulation, Phase Change, and Microstructure Kinetics of Phase Change. III. *Journal of Chemical Physics* **1941**, *9*, 177-184.
10. Müller, A. J.; Balsamo, V.; Arnal, M. L., Nucleation and Crystallization in Diblock and Triblock Copolymers. In *Block Copolymers II*, Abetz, V., Ed. Springer Berlin Heidelberg, **2005**, 1-63.
11. Mandelkern, L., *Crystallization of Polymers: Volume 2: Kinetics and Mechanisms*. Cambridge University Press, **2004**.
12. Schultz, J. M., *Polymer Crystallization: The Development of Crystalline Order in Thermoplastic Polymers*. American Chemical Society, **2001**.

13. Papageorgiou, G. Z.; Bikiaris, D. N.; Achilias, D. S.; Papastergiadis, E.; Docoslis, A., Crystallization and biodegradation of poly(butylene azelate): Comparison with poly(ethylene azelate) and poly(propylene azelate). *Thermochimica Acta* **2011,** *515*, 13-23.
14. Papageorgiou, G. Z.; Bikiaris, D. N., Crystallization and melting behavior of three biodegradable poly(alkylene succinates). A comparative study. *Polymer* **2005,** *46*, 12081-12092.
15. Van Krevelen, D. W.; Te Nijenhuis, K., *Calorimetric Properties*. **2009**, 109-128.
16. Mandelkern, L., *Crystallization of Polymers: Volume 1: Equilibrium Concepts*. Cambridge University Press, **2002**
17. Hoffman, J., D, Theoretical Aspects of Polymer Crystallization With Chain Folds: Bulk Polymers. Soc. Plastics Trans. **1964**, *4*, 315-362.
18. I. Lauritzen Jr, J.; D. Hoffman, J., *Theory of formation of polymer crystals with folded chains in dilute solution*. **1959**, *31*, 1680-1681.
19. D Hoffman, J.; J Weeks, J., *Melting Process and Equilibrium Melting Temperature of Poly(chlorotrifluoroethylene)*. **1962,** *66*A.
20. Hoffman, J. D.; Davis, G. T.; Lauritzen, J. I., The rate of crystallization of linear polymers with chain folding. *Treatise on solid state chemistry*, **1976**, 497-614.
21. Hoffman, J. D.; Miller, R. L., Kinetic of crystallization from the melt and chain folding in polyethylene fractions revisited: theory and experiment. *Polymer* **1997,** *38*, 3151-3212.
22. A. J. Müller, Z. H. H., M. L. Arnal, J. J. Sánchez, Successive self-nucleation/annealing (SSA): A novel technique to study molecular segregation during crystallization. *Polymer Bulletin*, **1997**,*39*, 465-472.
23. Ye, H.-M.; Tang, Y.-R.; Xu, J.; Guo, B.-H., Role of Poly (butylene fumarate) on Crystallization Behavior of Poly (butylene succinate). *Industrial & Engineering Chemistry Research* **2013,** *52*, 10682-10689.
24. Gan, Z.; Abe, H.; Kurokawa, H.; Doi, Y., Solid-state microstructures, thermal properties, and crystallization of biodegradable poly (butylene succinate)(PBS) and its copolyesters. *Biomacromolecules* **2001,** *2*, 605-613.
25. Zheng, Y.; Tian, G.; Xue, J.; Zhou, J.; Huo, H.; Li, L., Effects of isomorphic poly (butylene succinate-co-butylene fumarate) on the nucleation of poly (butylene succinate) and the formation of poly (butylene succinate) ring-banded spherulites. *CrystEngComm,* **2018**, *20*, 1573-1587.

26. Diaz, A.; Franco, L.; Puiggali, J., Study on the crystallization of poly(butylene azelate-co-butylene succinate) copolymers. *Thermochimica Acta* **2014,** *575*, 45-54.
27. Flory, P. J., Theory of crystallization in copolymers. *Transactions of the Faraday Society* **1955,** *51*, 848-857.
28. Baur, V. H., Einfluß der sequenzlängenverteilung auf das schmelz‐ende von copolymeren. *Macromolecular Chemistry and Physics* **1966,** *98*, 297-301.
29. Wendling, J.; Suter, U. W., A New Model Describing the Cocrystallization Behavior of Random Copolymers. *Macromolecules* **1998,** *31*, 2516-2520.
30. Sanchez, I.; Eby, R., Thermodynamics and crystallization of random copolymers. *Macromolecules* **1975,** *8*, 638-641.
31. Wendling, J.; Gusev, A.; Suter, U.; Braam, A.; Leemans, L.; Meier, R. J.; Aerts, J.; Heuvel, J. v.; Hottenhuis, M., Crystal Morphology and Thermodynamics of Poly (ethylene-4, 4 '-biphenyl dicarboxylate) and Related Copolymers with Ethylene-2, 6-naphthalene Dicarboxylate. *Macromolecules* **1999,** *32*, 7866-7878.

Chapter 8

Conclusions and Publications

8.1 Conclusions

A summary of the main conclusions is present below:

i. Isodimorphic behavior of copolymers was corroborated since despite being random all compositions are able to crystallize, their melting temperature goes through a eutectic point when plotted as a function of composition and WAXS results showed that small but reproducible changes are produced in the crystalline unit cell of the dominant crystalline phase upon inclusion of comonomer units.

ii. Regulating the composition of isodimorphic random copolymers is a valuable tool to tailor their properties in an unusually wide temperature ranges such us melting temperature, crystallization degree, crystallization rate and nucleation density.

iii. In the case of the double crystalline $BS_{45}BAz_{55}$ copolymer, the self-nucleation process of the PBS-rich phase separated the crystallization of both phases, corroborating the double crystalline behavior which was also studied by WAXS, SAXS, PLOM, and AFM.

iv. SSA (successive self-nucleation and annealing), a thermal fractionation technique that promotes segregation of molecular defects that interrupt crystallizable sequences, was successfully used to fractionate PBS-*ran*-PBAz. This thermal treatment allows a more thorough examination of the isodimorphic nature of the copolymers, and small-angle X-ray scattering (SAXS) and WAXS analysis of the samples before and after SSA fractionation concluded that the degree of comonomer exclusion remained almost unchanged, corroborating the isodimorphic behavior of the copolymers.

v. The study of the dielectric relaxation of PBS-*ran*-PBAz random copolymers provided detailed information on the dynamics of the comonomers remaining in the amorphous phase. And the results of these measurements led us to quantify

both the comonomer fraction involved in the crystalline phase as well as the amorphous phase.

vi. Regarding to the isothermal crystallization of this copolymers, the incorporation of BAz-units greatly affected the crystallization of the PBS-rich compositions, increasing the density of nuclei and slowing down the crystallization rate. Opposite effect occurs in the case of incorporating BS-units in PBAz-rich crystalline phases, where apart from the crystallinity rate is not affected an antinucleating effect is also appreciated.

vii. In this isodimorphic copolymers, when the percentage of comonomer inclusion was calculated, results concluded that only a small portion of BAz comonomer units were able to introduce into the PBS crystals, while a great inclusion of BS-units in PBAz-crystals was observed.

8.2 Publications made during the PhD Period

i. Arandia, I.; Mugica, A.; Zubitur, M.; Arbe, A.; Liu, G.; Wang, D.; Mincheva, R.; Dubois, P.; Müller, A. J. How Composition Determines the Properties of Isodimorphic Poly(butylene succinate-ran-butylene azelate) Random Biobased Copolymers: From Single to Double Crystalline Random Copolymers. *Macromolecules* **2015**, *48*, 43−57.

ii. Arandia, I.; Mugica, A.; Zubitur, M.; Iturrospe, A.; Arbe, A.; Liu, G.; Wang, D.; Mincheva, R.; Dubois, P.; Müller, A. J. Application of SSA thermal fractionation and X-ray diffraction to elucidate comonomer inclusion or exclusion from the crystalline phases in poly(butylene succinate-ran-butylene azelate) random copolymers. *Journal of Polymer Science Part B: Polymer Physics* **2016**, *54*, 2346−2358.

iii. Arandia, I.; Mugica, A.; Zubitur, M.; Mincheva, R.; Dubois, P.; Müller, A. J.; Alegría, A. The Complex Amorphous Phase in Poly(butylene succinate-*ran*-butylene azelate) Isodimorphic Copolyesters. *Macromolecules* **2017**, *50*, 1569−1578.

iv. Pérez-Camargo, R.A.; Arandia, I.; Safari, M.; Cavallo, D.; Lotti, N.; Soccio, M.; Müller, A.J. Crystallization of isodimorphic aliphatic random copolyesters: Pseudoeutectic behavior and double-crystalline materials. *European Polymer Journal* **2018**, *101*, 233-247.

Summary

Resumen

Con el objetivo de reducir la dependencia del petróleo y evitar la acumulación de residuos plásticos, teniendo en cuenta el gran aumento del uso de los plásticos de un solo uso en muchas áreas como el envasado, el desarrollo de nuevas alternativas más ecológicas se ha intensificado. El objetivo de estas alternativas es utilizar materiales que cubran todas las necesidades de acuerdo con la aplicación requerida, y al mismo tiempo puedan sufrir degradación por estímulos ambientales después de su vida útil, como es el caso de los bioplásticos.

Entre estos bioplasticos, la familia de poliésteres alifáticos es una de las más atractivas debido a su biodegradabilidad y biocompatibilidad. Debido al interés que han generado, se han publicado numerosos trabajos de investigación relacionados con poliésteres alifáticos biodegradables. Desafortunadamente, este tipo de biopolímeros no suelen cumplir todos los requisitos mecánicos necesarios y además se caracterizan por una alta cristalinidad que limita su velocidad de biodegradación. Por lo tanto, para adaptar estas propiedades, se ha realizado la síntesis de copoliésteres aleatorios con comonómeros biobasados para obtener copolímeros al azar versátiles. La copolimerización se ha utilizado para limitar su grado de cristalización y mejorar sus propiedades físicas, y así poder extender sus aplicaciones en el mercado de polímeros biodegradables. Adicionalmente, algunos trabajos han mostrado que a través de la variación de la composición del copolímero, las propiedades térmicas pueden controlarse sin una pérdida significativa de las propiedades cristalinas.

Entre los polímeros más estudiados están los poliésteres termoplásticos alifáticos. Con el fin de controlar la hidrofobicidad, la cristalinidad y la degradación actualmente se investigan la formación de copolímeros al azar que puedan ser fácilmente sintetizados, ya que la copolimerización y las mezclas son maneras versátiles de aumentar la cantidad de polímeros biodegradables. Por ello la preparación de nuevos poliésteres ofrece una gran oportunidad para aumentar la gama de materiales degradables e incluso para generar un conjunto de productos con propiedades fácilmente ajustables. Recientemente se han desarrollado diferentes tipos de copolímeros de poli(butilén succinato) (PBS) para aumentar la biodegradabilidad, disminuir los costes, aumentar la oferta comercial e incluso modificar las propiedades finales. Este es el caso de los copolímeros poli(butilénsuccinato-*ran*-butilénazelato), PBS-*ran*-PBAz, utilizados para este trabajo y cuya estructura química se muestra a continuación, la figura 1:

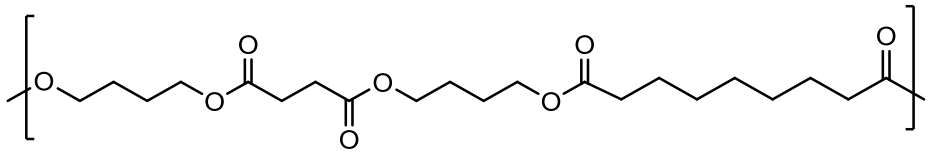

Fig. 1. *Estructura química del poli(butilénsuccinato-ran-butilénazelato), PBS-ran-PBAz.*

El poli(butilén succinato) (PBS) utilizado en este proyecto, es un material de interés debido a su relativo bajo coste de producción, buenas propiedades térmicas, mecánicas y fácil procesabilidad. De hecho, el PBS junto con la polilactida y los polihidroxialcanoatos son algunos de los poliésteres más relevantes utilizados como polímeros verdes. Además, es significativo que el PBS es un derivado del ácido succínico, que normalmente se produce mediante acción microbiana en el ciclo del ácido tricarboxílico metabólico utilizado para la producción de energía.

El ácido azelaíco, copolimerizado con el poli(butilen succinato) para este trabajo, se diferencia del PBS en que tiene siete metilenos en el grupo ácido mientras que el ácido succínico sólo dos, por lo tanto es un comonómero ideal para el presente estudio. Además, se puede conseguir por ozonólisis del doble enlace alqueno del ácido oléico y la posterior oxidación y reducción. Por lo tanto, estos copolímeros se pueden derivar a partir de fuentes renovables.

El estudio del comportamiento de cristalización de los copolímeros al azar es muy importante debido a su fuerte correlación con la velocidad de biodegradación, propiedades mecánicas y aplicaciones. Para este propósito, el proyecto de investigación titulado: Crystallization and Morphology of Poly(butylene succinate-ran-butylene azelate) Random Isodimorphic Copolymers, se ha desarrollado en la Universidad del País Vasco (UPV/EHU) en el departamento de Ciencia y Tecnología de Polímeros de la Facultad de Química.

Para poder estudiar la estructura, morfología y cristalización de estos copolímeros primeramente debemos saber cómo pueden cristalizar los copolímeros al azar constituidos por dos unidades cristalizables, ya que pueden mostrar un comportamiento de cristalización diferente dependiendo de la compatibilidad de los dos componentes en las redes cristalinas. Las unidades de comonómero pueden ser excluidas totalmente y permanecer en la fase amorfa o se puede observar la cocristalización si las unidades de comonómero son similares en estructura química, longitud de unidad de repetición y / o conformación de la cadena de cristal. Se han reportado dos casos de comportamiento de cocristalización: isomorfismo o isodimorfismo.

En el caso de los polímeros isomórficos, se caracterizan por la formación de solo una fase cristalina que contiene ambas unidades cristalinas. En este caso, estas unidades deben cumplir requisitos estrictos moleculares como tener una estructura similar e incluso una conformación molecular que permita su inserción en la estructura cristalina resultante con una distorsión mínima. En el caso de los polímeros isodimórficos, se observan dos fases cristalinas. En cada una de las fases predomina la estructura cristalina de un tipo de unidad repetitiva pero con inclusión de un cierto porcentaje de unidades repetitivas del segundo componente. El aumento de la concentración del comonómero minoritario en cada fase cristalina reduce la temperatura de fusión y la cristalinidad de los copolímeros. El isodimorfismo implica que al menos una de las dos fases cristalinas incorpore el componente minoritario correspondiente en su red cristalina. Los requisitos en este caso son menos estrictos, y en consecuencia el isodimorfismo se observa con más frecuencia en la cristalización de copolímeros al azar que el isomorfismo.

Con el fin de estudiar la estructura y cristalización de los copolímeros isodimórficos PBS-*ran*-PBAz, se ha realizado este trabajo de tesis que se encuentra dividido en 8 capítulos. El primero muestra una introducción general así como la revisión de los antecedentes y el estado actual de las estrategias seguidas para el estudio de los copolímeros PBS-*ran*-PBAz. En el segundo capítulo, a modo de introducción teórica, se exponen los principales fundamentos teóricos en relación a la morfología y cinética de cristalización, con el fin de ayudar a un mejor entendimiento de la investigación que se ha realizado. Y en el tercer capítulo se presentan los materiales utilizados y sus principales propiedades. En este capítulo, además se incluyen las principales técnicas instrumentales y las condiciones empleadas en la experimentación.

Los capítulos 4, 5, 6 y 7 muestran los resultados de los diferentes experimentos realizados a lo largo del trabajo. Resumiendo, en el cuarto capítulo de este trabajo se ha estudiado la estructura, cristalización no isotérmica y morfología de los copolímeros PBS-*ran*-PBAz sintetizados previamente por Mincheva et al. Para ello hemos utilizado las técnicas de Calorimetría Diferencial de Barrido (DSC), Difracción de Rayos X a Altos Ángulos (WAXS) y Difracción de Rayos-X de Ángulo Pequeño (SAXS), y los hemos correlacionado los resultados con los obtenidos de Microscopía Óptica de Luz Polarizada (PLOM) y Microscopía de Fuerza Atómica (AFM). Nuestros resultados muestran que los copolímeros pueden considerarse isodimórficos en tales condiciones debido a que aunque los copolímeros sintetizados son al azar, como se demuestra por RMN, todas las muestras son capaces de cristalizar y sus temperaturas de cristalización y fusión dependen mucho de la composición. Las medidas de WAXS demostraron que aparte de una composición alrededor del punto eutéctico, todos los otros copoliésteres al azar se caracterizaban por una única cristalización con reflexiones del componente más abundante, y que se producen cambios pequeños pero reproducibles en la celda unitaria de la fase cristalina dominante tras la inclusión de unidades de comonómero. Este ligero aumento de volumen se da para acomodar las unidades repetitivas adicionales que coexisten con el componente principal como resultado del isodimorfismo. A su vez, los resultados de WAXS, SAXS, PLOM, AFM y SAXS para el copolímero doblemente cristalino $BS_{45}BAz_{55}$, sugieren que cuando el material se enfría desde el fundido, primeramente se forman esferulitas ricas en PBS creando una plantilla (o "template") para la morfología del copolímero. Al enfriar más la muestra, la fase rica en PBAz cristaliza formando lamelas mucho más pequeñas

que se apilan dentro de las regiones interlamelares de las esferulitas ricas en PBS y los dos tipos de lamelas coexisten dentro de estas esferulitas mixtas inusuales.

En el quinto capítulo de este trabajo se han utilizado las técnicas de Autonucleación y Autonucleacion y Recocido Sucesivo (SSA), llegando a la conclusión de que el isodimorfismo se debe a la similitud de las unidades repetitivas de PBS y PBAz y es independiente de los factores cinéticos. Esta conclusión se alcanza después de determinar que el grado de exclusión del comonómero permanece casi sin cambios incluso después de SSA, una técnica de fraccionamiento térmico que promueve la segregación de defectos moleculares que interrumpen las secuencias cristalizables. El estudio de autonucleación fue a su vez de gran ayuda para entender la cristalización del copolímero doble cristalino $BS_{45}BAz_{55}$, ya que cuando este material se enfría desde el fundido a una velocidad de 10 ºC/min, la cristalización de las dos fases se produce de manera coincidente, y después del proceso de autonucleación de la fase cristalina rica en PBS, se puede lograr la cristalización separada de ambas fases.

En el sexto capítulo se muestran los resultados de las medidas dieléctricas realizadas a estos copolímeros. La cristalinidad de los materiales poliméricos afecta las propiedades de la fase amorfa remanente de una manera compleja. Las restricciones que la fase cristalina ejerce en la fase amorfa de los polímeros suele conducir a la dificultad de medición de la transición vítrea para materiales con cristalinidad de alrededor del 50% o más mediante DSC. Este resultado generalmente se atribuye a la presencia de segmentos amorfos que forman lo que se ha denominado la fracción amorfa rígida (RAF), cuyos movimientos están severamente restringidos por los cristales. En vista de esto, un polímero semicristalino estaría compuesto por al menos 3 fracciones: la cristalina, el RAF y la fracción amor-

fa móvil o MAF. Este último sería responsable de la transición vítrea medible por DSC, mientras que el proceso de fusión y las reflexiones de difracción de rayos X son manifestaciones de la fase cristalina.

Al analizar la relajación dieléctrica de estos materiales, hemos tenido acceso tanto a la dinámica local como a la segmentaria. El análisis de datos proporcionó las distintas contribuciones de los grupos succinato y azelato a la relajación del copolímero, permitiendo una cuantificación de la fracción de cada componente involucrado en la fase cristalina. La buena concordancia entre los valores determinados a partir de las medidas dieléctricas y la cristalinidad obtenida a partir de los experimentos con DSC demuestra que el grado de exclusión de comonómero en estos copolímeros al azar durante la cristalización es mucho mayor que la inclusión del comonómero. Además, el comportamiento de cristalización de estos copolímeros en diferentes protocolos de enfriamiento mostró que la relajación no solo depende de la fracción cristalina sino también de los detalles del proceso de cristalización en estos copolímeros multifásicos complejos.

En el séptimo capítulo y último de resultados hemos realizado estudios isotérmicos detallados de la cinética de nucleación, velocidad crecimiento esferulítico y cinética de cristalización global de los copolímeros PBS-*ran*-PBAz en un amplio rango de composición para demostrar la influencia dramática de la composición sobre la cinética de cristalización. Al medir la nucleación, el crecimiento y la cinética de cristalización global podemos determinar qué factores afectan a la cinética de solidificación final de los copolímeros y evaluar la influencia de la composición. Además, determinamos la entalpía de la fusión del PBS y PBAz 100% de cristalinos mediante un procedimiento novedoso y práctico: extrapolando datos de cristalización isotérmica de WAXS a tiempo real con los datos de

DSC isotérmicos. También se ha hecho uso de varias teorías de exclusión e inclusión para explicar la cristalización de copolímeros y la partición de counidades entre la fase cristalina y la fase amorfa en copolímeros al azar usando las estimaciones experimentales de las temperaturas de fusión en equilibrio ($T_m°$). Para ello se han calculado los valores de $T_m°$ de todos los copolímeros mediante las ecuaciones de Gibbs-Thomson y Hoffman-Weeks, e introducidos en la ecuaciones de las teorías mencionadas anteriormente. De dichas teorías se ha estimado el porcentaje de las unidades de comonómero minoritario que estaban incorporadas en las fases cristalinas ricas en PBS y PBAz, concluyendo que en el caso de composiciones ricas en PBS, a pesar de que la concentración de comonómero en los cristales aumenta al aumentar la composición de comonómero, continúa siendo pequeña y muy inferior a la concentración de comonómero correspondiente a la que sería la inclusión total, a diferencia de las composiciones ricas en PBAz, para las cuales se predijo una gran cantidad de inclusiones de comonómero de PBS.

Finalmente, en el octavo capítulo se presentan las conclusiones generales a las que se ha llegado tras el desarrollo de la presente investigación. En este capítulo, además se incluyen los artículos científicos a los que ha dado lugar el presente trabajo.